

Seismic response of high-rise zipper braced frame structures with outrigger
trusses

Zhi Chen

A Thesis
in
The Department
of
Building, Civil & Environmental Engineering

Presented in Partial Fulfillment of the Requirements
for the Degree of Master of Applied Science (Civil Engineering) at
Concordia University
Montreal, Quebec, Canada

April 2012

© Zhi Chen, 2012

CONCORDIA UNIVERSITY
School of Graduate Studies

This is to certify that the thesis prepared

By: Zhi Chen

Entitled: Seismic response of high-rise zipper braced frame structures with
outrigger trusses

and submitted in partial fulfillment of the requirement for the degree of

Mater of Applied Science (Civil Engineering)

complies with the regulations of the University and meets the accepted standards with respect to originality and quality.

Signed by the final examining committee:

| | | |
|-------|------------------|------------|
| _____ | Dr. O. Pekau | Chair |
| _____ | Dr. R. Sedaghati | Examiner |
| _____ | Dr. L. Lan | Examiner |
| _____ | Dr. L. Tirca | Supervisor |

Approved by

Chair of Department or Graduate Program Director

_____ 20 _____

Dean of Faculty

ABSTRACT

Seismic response of high-rise zipper braced frame structures with outrigger trusses

Zhi Chen

Concentrically braced frame (CBF) structures provide high stiffness and moderate ductility, while they are prone to damage concentrated within a single floor. To overcome this drawback, researchers have proposed to add a vertical member to the CBF system, labeled a “zipper column”, with the aim to involve the buckling and/or yielding of several braces. Thus, the zipper column members are designed to transfer the unbalanced forces caused by buckling of braces in chevron configuration along the building height. By employing the zipper braced frame system (ZBF), the damage is more uniformly distributed over the height. However structures taller than 8-storey are prone to lateral drift amplification due to the higher mode effects. In this study, in order to control the lateral drift, it is proposed to add a set of outrigger trusses over one floor, at the roof level, and if necessary at another floor among those located at the mid-height.

Accordingly, the purpose of this study is two-fold: i) to investigate the inelastic behavior of the 12- and 16-storey ZBF building structures with elastic zippers located in a high risk seismic zone and ii) to study the behavior of ZBF structures when outrigger trusses are added.

Nonlinear time-history analyses conducted in Drain-2DX software are considered in this study to analyze the behavior of the 12- and 16-storey buildings without and with outrigger trusses that are subjected to 21 ground motions equally divided in three ensembles: crustal, subduction and near-field. Outcomes of the study show that buildings located in a high risk seismic zone (Victoria, B.C.) exhibit less seismic damage when outrigger trusses are added to the ZBF system.

ACKNOWLEDGE

Since the fall of 2006, I started my journey in Concordia. During the time of my undergraduate and graduate studying, I received a lot of support from the people and institutions here. I know there will be never enough for me to express how grateful I feel, but I will try my best to address my appreciation here.

I want to send the greatest gratitude to my supervisor, Dr. Lucia Tirca. The research work and this thesis would not reach this far without her support in both my life and study. It was my pleasure to meet her in my last year of undergraduate and become her student during the graduate studying. In these four years, she is not only guiding me in the path of learning, but also passes to me her enthusiasm and attitude of work for my engineering career. Her instruction, encouragement, and inspiration will always guide me in my life.

It was also my pleasure to meet a lot of wonderful graduate students here, like Liang Chen, Juan David Morales Ramírez, Cristina Caprarelli, Nicolae Danila, Geli Guo, Evan Irvine, Gurinderbir Singh Sookh, and all the people in my office: Farzad Ghodoosi-Pour, Arash Rahmatian, Omer Salem Yagob, and Farah Deeba. Thanks for being my family here in Canada such that I didn't miss my beloved country China so much, and the memory of being with them will be always precious to me.

At last, to my family, all my achievements in my life are all because of their support and the endless love.

献给在遥远家乡的父母和在身边一直陪伴我的妻子

我的每一点收获都离不开你们无私的爱与支持

*(To my parents and my wife, each of my achievements is because of your unconditional
love and support)*

TABLE OF CONTENTS

| | |
|--|--------------|
| TABLE OF CONTENTS | vii |
| LIST OF FIGURES | xi |
| LIST OF TABLES | xviii |
| CHAPTER ONE: Introduction | 1 |
| 1.1 Generalities | 1 |
| 1.2 Objectives and Scope | 5 |
| 1.3 Methodology | 5 |
| 1.4 Thesis organization | 7 |
| CHAPTER TWO: Literature Review..... | 9 |
| 2.1 Past studies on the Design of Concentrically Braced Frames with Zipper Columns | 9 |
| 2.1.1 <i>Generalities</i> | 9 |
| 2.1.2 <i>Tension Zipper strut approach</i> | 12 |
| 2.1.3 <i>Weak Zipper strut approach</i> | 14 |
| 2.1.4 <i>Strong Zipper strut approach</i> | 15 |
| 2.1.5 <i>Suspended Zipper strut approach</i> | 19 |
| 2.2 Past studies on high-rise buildings with outrigger and belt truss system | 21 |
| 2.2.1 <i>Need for High-rise buildings</i> | 21 |
| 2.2.2 <i>Generalities regarding the outrigger and belt systems</i> | 22 |

| | | |
|---|--|----|
| 2.2.3 | <i>Analytical method of finding the optimum outrigger truss location.....</i> | 26 |
| 2.2.4 | <i>Graphical method of optimum location of outrigger and belt truss system</i> | 29 |
| 2.2.5 | <i>The concept of virtual outrigger system with belt truss.....</i> | 31 |
| 2.3 | Studying the use of computer program -----Drain-2DX..... | 34 |
| CHAPTER THREE: Design Methodology of Zipper Braced Frame and Outrigger | | |
| Trusses | | |
| 3.1 | Design methodology of Zipper braced frame structure | 37 |
| 3.1.1 | <i>Calculation and distribution of seismic forces</i> | 37 |
| 3.1.2 | <i>Design of braces in chevron configuration</i> | 39 |
| 3.1.3 | <i>Design of beams and columns in concentrically braced frame.....</i> | 39 |
| 3.1.4 | <i>Design of zipper columns</i> | 41 |
| 3.2 | The influence of pattern load selection on the preliminary design of zipper columns..... | 43 |
| 3.3 | Design methodology of outrigger trusses | 55 |
| 3.3.1 | <i>Calculation of rotations in outrigger belted braced frame</i> | 56 |
| 3.3.1.1 | <i>Rotations of the braced frame</i> | 57 |
| 3.3.1.2 | <i>Rotations of outriggers.....</i> | 60 |
| 3.3.2 | <i>Compatibility of rotations.....</i> | 64 |
| 3.4 | Preliminary design of zipper braced frame structure and outrigger truss | 65 |
| 3.4.1 | <i>Building description</i> | 66 |
| 3.4.2 | <i>Preliminary design of zipper braced frame</i> | 66 |

| | | |
|--|--|-----------|
| 3.4.3 | <i>Preliminary design of outrigger truss</i> | 70 |
| 3.5 | Design summary | 74 |
| CHAPTER FOUR: Nonlinear Time-History Analysis of ZBF Building Structures with and without Outrigger Trusses | | 77 |
| 4.1 | Zipper braced frame & Outrigger truss modeling..... | 78 |
| 4.2 | Selection and scaling procedure of ground motions | 80 |
| 4.2.1 | <i>Ground motion selection</i> | 80 |
| 4.2.2 | <i>Scaling ground motions</i> | 84 |
| 4.3 | Numerical analyses using Drain-2DX | 89 |
| 4.3.1 | <i>Modeling in Drain-2DX</i> | 89 |
| 4.3.2 | <i>Drain 2DX results</i> | 90 |
| CHAPTER FIVE: Comparative Study of Time-History Response of ZBF Building Structures with and without Outrigger Trusses under various Ground Motions | | 96 |
| 5.1 | Seismic response of the 12-storey ZBF building..... | 98 |
| 5.2 | Seismic response of the 12-storey ZBF-RT building | 104 |
| 5.3 | The behavior of roof outrigger trusses added to the 12-storey building..... | 109 |
| 5.4 | Seismic response of the 16-storey ZBF building..... | 115 |
| 5.5 | Seismic response of the 16-storey ZBF-RT building | 120 |
| 5.6 | The behavior of outrigger trusses added to the roof floor level of the 16-storey building..... | 126 |

| | | |
|--|--|------------|
| 5.7 | Seismic response of the 16-storey ZBF-M&RT building..... | 126 |
| 5.8 | The behavior of outrigger trusses added to the roof and the 8 th floor level of the 16-storey building..... | 132 |
| 5.9 | Summary of comparative study of seismic response of ZBF with and without outrigger trusses..... | 135 |
| CHAPTER SIX: Conclusions and Future Work..... | | 139 |
| 6.1 | Conclusions..... | 139 |
| 6.2 | Future work..... | 142 |
| REFERENCE | | 143 |

LIST OF FIGURES

| | |
|--|----|
| Figure 2.1 Chevron braced frame behaviour (Bruneau, et al., 2005) | 10 |
| Figure 2.2 Expected behaviors and performance of zipper frame (Nouri, Imani Kalesar, & Ameli, 2009) | 12 |
| Figure 2.3 Behavior of zipper braced frame system with weak zipper column (Tirca & Tremblay, 2004): a) zipper yields in tension; b) zipper buckles in compression | 15 |
| Figure 2.4 Behavior of zipper braced frame system with strong zipper columns (Tirca & Tremblay, 2004) brace buckling initiated a) at the base; b) at the roof. | 16 |
| Figure 2.5 Transfer mechanisms and lateral load distributions adopted to design the zippers when brace buckling initiating at the: a) upper floors; b) lower floors (Tirca & Tremblay, 2004) | 17 |
| Figure 2.6 Behaviour of ZBF with suspended zipper strut (Yang, Leon, & DesRoches, 2008) | 20 |
| Figure 2.7 A tall building with conventional outrigger trusses (R.S.Nair, 1998)..... | 24 |
| Figure 2.8 Forces transfer in conventional outrigger trusses (R.S.Nair, 1998) | 25 |
| Figure 2.9 Deformed shapes of CBF in High-rise building with outrigger trusses (Buyukozturk & Gunes, 2004)..... | 25 |
| Figure 2.10 Analytical Model for studying the optimum location of a single outrigger truss (Taranath B. , 1974) | 27 |

| | |
|--|----|
| Figure 2.11 Optimum locations for different outrigger trusses locations, a) single truss, b) two trusses, c) three trusses, d) four trusses (Taranath B. , 2010) | 29 |
| Figure 2.12 Optimum locations for outriggers: a) single outrigger, b) two outriggers, c) three outriggers, d) four outriggers (Bryan Stafford Smith, 1991)..... | 31 |
| Figure 2.13 “Virtual” outrigger building with a belt truss (R.S.Nair, 1998) | 32 |
| Figure 2.14 Forces transferred by using belt trusses as virtual outriggers (R.S.Nair, 1998) | 33 |
| Figure 3.1 The distribution of seismic forces | 38 |
| Figure 3.2 Vertical distribution vectors of lateral forces with different k (Chen, 2011) .. | 45 |
| Figure 3.3 Lateral force distribution vectors (Chen, 2011) | 45 |
| Figure 3.4 Load pattern LP-ST: a) buckling initiates at top; b) buckling initiates at bottom (Chen, 2011) | 46 |
| Figure 3.5 Load pattern LP-SP: a) buckling of braces initiates at top; b) buckling of braces initiates at the bottom (Chen, 2011)..... | 51 |
| Figure 3.6 Free body diagram of outrigger belted braced frame (Hoenderkamp & Bakker, 2003) | 57 |
| Figure 3.7 Individual segment of the braced frame (after (Hoenderkamp & Bakker, 2003) | 58 |
| Figure 3.8 Outrigger bending and shear deformations of the ZBF with outrigger truss .. | 61 |

| | |
|--|----|
| Figure 3.9 Individual panels of the outrigger truss (after (Hoenderkamp & Bakker, 2003)) | 62 |
| Figure 3.10 Rigid body rotations of outriggers (Hoenderkamp & Bakker, 2003) | 63 |
| Figure 3.11 Plan view of the studied building | 66 |
| Figure 3.12 Computer model of the 12- and 16-storey ZBF system with outrigger trusses | 67 |
| Figure 3.13 Axial force envelopes developed in zippers of the 12- and 16-storey building without outriggers under load patterns: LP-ST; LP-SP; LP-T and LP-P | 68 |
| Figure 4.1 Model of the ZBF system in Drain 2DX | 80 |
| Figure 4.2 Model of the ZBF system equipped with outrigger trusses in Drain 2DX | 80 |
| Figure 4.3 Design and scaled acceleration response spectrum for the 12-storey ZBF building | 85 |
| Figure 4.4 Design and scaled response spectrum of the selected accelerograms for 12storey ZBF-RT building | 86 |
| Figure 4.5 Design and scaled response spectrum of the selected accelerograms for the 16-storey ZBF building | 86 |
| Figure 4.6 Design and scaled response spectrum of the selected accelerograms for 16-storey ZBF-RT building | 86 |
| Figure 4.7 Design and scaled response spectrum of the selected accelerograms for 16-storey ZBF-M&RT building | 87 |

| | |
|---|-----|
| Figure 4.8 Axial force in zipper columns obtained from nonlinear time-history analyses of 12-storey building with and without outrigger trusses: a) Crustal, b) Subduction, c) Near-field | 91 |
| Figure 4.9 Axial force in zipper columns obtained from nonlinear time-history analyses of 16-storey buildings with and without outrigger truss: a) Crustal, b) Subduction, c) Near-field | 92 |
| Figure 4.10 Computed interstorey drift for 12-storey building with and without outrigger truss, a) Crustal; b) Subduction; c) Near-field | 93 |
| Figure 4.11 Computed interstorey drift for 16-storey building with and without outrigger truss, a) Crustal; b) Subduction; c) Near-field | 94 |
| Figure 5.1 Selected records ranked on descended PGV/PGA ratio: a) crustal; b) subduction; c) near-field..... | 97 |
| Figure 5.2 Time-history response of brace buckling and beam hinging for 12-storey building without outrigger truss under motions C2, C4, and C6 | 100 |
| Figure 5.3 Time-history response of brace buckling and beam hinging for 12-storey building without outrigger truss under motions N1, N6, and N7 | 101 |
| Figure 5.4 Time-history response of brace buckling and beam hinging for 12-storey building without outrigger truss under motions S2, S4, and S7 | 103 |
| Figure 5.5 Time-history response of brace buckling and beam hinging for 12-storey building with roof outrigger trusses under motions C2, C4, and C6 | 106 |

| | |
|--|-----|
| Figure 5.6 Time-history response of brace buckling and beam hinging for 12-storey building with one outrigger truss under motions N1, N6, and N7..... | 107 |
| Figure 5.7 Time-history response of brace buckling and beam hinging for 12-storey building with one outrigger truss under motions S2, S4, and S7..... | 109 |
| Figure 5.8 Outrigger truss configuration 1 and axial loads developed in the outrigger diagonals under the gravity component..... | 110 |
| Figure 5.9 Outrigger truss configuration 2 and the axial loads developed in the outrigger diagonals under the gravity component..... | 111 |
| Figure 5.10 Time-history axial load in outrigger truss elements: a) exterior panel T1-e and b) interior panel T1-i under ground motion C2 | 112 |
| Figure 5.11 Time-history axial load in outrigger truss elements: a) exterior panel, T1-e and b) interior panel T1-i under ground motion S4..... | 113 |
| Figure 5.12 Time-history axial load in outrigger truss elements: a) exterior pane T1-e and b) interior pane T1-i under ground motion N6..... | 114 |
| Figure 5.13 Deformed shape of the 12-storey ZBF-RT under ground motion C2 | 114 |
| Figure 5.14 Time-history response of brace buckling and beam hinging for 16-storey building without outrigger truss under motions C2, C4, and C6..... | 117 |
| Figure 5.15 Time-history response of brace buckling and beam hinging for 16-storey building without outrigger truss under motions N1, N6, and N7 | 118 |

| | |
|---|-----|
| Figure 5.16 Time-history response of brace buckling and beam hinging for 16-storey building without outrigger truss under motions S2, S4, and S7 | 120 |
| Figure 5.17 Time-history response of brace buckling and beam hinging for 16-storey building with roof outrigger trusses under C2, C4, and C6 | 122 |
| Figure 5.18 Time-history response of brace buckling and beam hinging for 16-storey building with outrigger truss under motions N1, N6, and N7 | 124 |
| Figure 5.19 Time-history response of brace buckling and beam hinging for 16-storey building with outrigger truss under motions S2, S4, and S7 | 125 |
| Figure 5.20 Time-history axial load in outrigger truss elements: exterior pane T1-e and interior pane T1-i under motion C2 | 127 |
| Figure 5.21 Time-history response of brace buckling and beam hinging for 16-storey building with two outrigger trusses under C2, C4, and C6..... | 130 |
| Figure 5.22 Time-history response of brace buckling and beam hinging for 16-storey building with two outrigger trusses under N1, N6, and N7 | 131 |
| Figure 5.23 Time-history response of brace buckling and beam hinging for 16-storey building with two outrigger trusses under S2, S4, and S7 | 132 |
| Figure 5.24 Time-history axial load in diagonals of roof outrigger under ground motion C2: a) top exterior pane T1-e and b) top interior pane T1-I | 133 |
| Figure 5.25 Time-history axial load in in diagonals of mid-height outrigger under ground motion C2: a) mid-height exterior pane T3-e, and mid-height interior pane T3-i | 134 |

Figure 5.26 Summary of interstorey drifts in 12-storey ZBF under all considered ground motions..... 137

Figure 5.27 Summary of interstorey drifts in the 16-storey ZBF under all considered ground motions 138

LIST OF TABLES

| | |
|---|----|
| Table 3.1 Sequential Triangular distribution vectors for assessing the compressive force in zippers of 12-storey building | 47 |
| Table 3.2 Sequential Triangular distribution vectors for assessing the tensile force in zippers of 12-storey building | 48 |
| Table 3.3 Sequential Triangular distribution vectors for assessing the compression force in zippers of 16-storey building | 49 |
| Table 3.4 Sequential Triangular distribution vectors for assessing the tensile force in zippers of 16-storey building | 50 |
| Table 3.5 Sequential Parabolic distribution vectors for assessing the compressive force in zippers of 12-storey building | 52 |
| Table 3.6 Sequential Parabolic distribution vectors for assessing the tensile force in zippers of 12-storey building | 53 |
| Table 3.7 Sequential Parabolic distribution vectors for assessing the compressive force in zippers of 16-storey building | 53 |
| Table 3.8 Sequential Parabolic distribution factors for assessing the tensile force in zippers of 16-storey building | 54 |

| | |
|---|----|
| Table 3.9 Phase I: Member sections of the 12-storey building..... | 68 |
| Table 3.10 Phase I: Member sections of the 16-storey building..... | 69 |
| Table 3.11 Zipper column sections for 12- and 16-storey buildings | 71 |
| Table 3.12 Design parameters of outrigger truss | 73 |
| Table 3.13 Outrigger truss sections for 12- and 16-storey buildings..... | 74 |
| Table 3.14 Member sections of the 12-storey building | 75 |
| Table 3.15 Member sections of the 16-storey building | 76 |
| Table 3.16 Seismic design and buildings characteristics..... | 76 |
| Table 4.1 Ground motion characteristics | 83 |
| Table 4.2 The fundamental periods of 12- and 16-storey ZBF with different configurations of outrigger trusses..... | 85 |
| Table 4.3 Scaling factors of selected ground motions for analyzing the 12-storey buildings | 87 |
| Table 4.4 Scaling factors of selected ground motions for analyzing the 16-storey building | 88 |

CHAPTER ONE

Introduction

1.1 Generalities

Concentrically braced frame (CBF) in chevron configuration is a cost-effective system for resisting lateral loads. This structural system is usually employed for low- and mid-rise steel framed buildings. Braces in chevron configuration provide support for the CBF beams at the brace to beam intersection point. However, under strong seismic excitations, this configuration shows a concentration of damage within a single floor and the tendency of storey mechanism formation. For instance, extensive damage was found in CBF buildings during Tohoku earthquake on March 2011 (Lignoset al, 2011), Christchurch earthquake on 2010 (Bruneauet al, 2010), Loma Prieta earthquake (1989), Northridge earthquake (1994), Kobe earthquake in 1995 (Tremblay, Bruneau, & Wilson, 1996)and other events. In light of this, frequent damage was observed in braced frames where braces were proportioned to resist tension only, where connections were weaker than the braces attached to them, where braces framed directly into columns, and where braces were inclined principally in one direction. Under strong ground motions, braces in compression have buckled, and in consequence lose their buckling resistance strength. After buckling of braces occurred, beams were deflected downward as a result of the

combined action of the gravity loading and the unbalanced force developed at the braces to beam intersection point due to the difference between the tensile and post-buckling capacity of brace members. In this case, strong floor beams are required to stabilize the system when the unbalance vertical load transferred from braces to beams has increased due to the attaining of the post-buckling strength in the compressive brace. Thus, due to this behavioural characteristic, the chevron bracing system shows a limited efficiency in terms of distributing the lateral loads over the building height.

In Canada, the limitation of the number of stories for the CBF structures was imposed since 1995 (see National Building Code edition 1995, NBCC 95) and was defined as a function of ductility factor and the characteristic of the seismic zone. In the 2005 edition of NBCC, this limitation was changed from the number of stories to the height of the building. In spite of this limitation, researchers have shown that the system is still prone to storey mechanisms under seismic ground motions. This drawback pointed out by Khatib et al. (1988). Typically, in the CBF structures, excessive storey drifts is concentrated within a few stories and large ductility demand is required.

To address the above concern, Khatib et al (1988) proposed a modified CBF system labeled CBF with zipper columns. By definition, the zipper column is a vertical member, added to a CBF system in chevron configuration, in order to link together all brace-to-beam intersecting points. As a result, all compressive braces will be forced to

buckle almost simultaneously while only a few tensile braces will yield. When ground motion reversed, braces that acted previously in tension buckle in compression, while the zipper column transfers the unbalanced load upwards or downwards depending on ground motion signature. This new structural system is able to force almost all braces to buckle or yield and a large amount of energy is dissipated in the system. In the past decade, several researchers have conducted studies in this topic as follows:

- Sabelli (2001) proposed design criteria for CBF with weak zipper strut. In this design method, zipper columns are allowed to buckle and to yield, while braces behave in inelastic range;
- Tremblay and Tirca (2003) proposed design criteria for CBF system with strong zipper column. In this light, zipper columns were designed to behave in elastic range, allowing braces to buckle simultaneously upwards or downwards (Tirca & Tremblay, 2004);
- Leon and Yang (2003, 2008) developed a similar system labeled CBF with suspended zipper strut. A truss system was added at the top floor while top floor braces were designed to respond in elastic range. Yielding is allowed to occur in the zipper column.
- Tirca and Chen (2012) and Chen (2011) have refined the initial design method proposed by Tremblay and Tirca (2003). The system is labeled CBF with elastic zipper columns.

Experimental studies have been only performed for the CBF with suspended zipper strut. Meanwhile, the analytical studies have been conducted by using Drain-2DX software which is a nonlinear computer program for static and dynamic analysis of plane structures.

The research carried out in the field of zipper braced frame is mostly focused on low- and mid-rise buildings. However, along with the increase in building height and stories number, undesired effects, such as excessive lateral deformation due to the activation of higher modes could drive the building near collapse. To overcome this drawback, an outrigger truss system(s) are proposed to be added to the elastic ZBF system. In this regard, the stiffness is increased, the strength is increased and the deformability diminishes. Thus, the purpose of this research is to address the behavior of ZBF structures taller than the recommended code limitation. This study is developed for 12- and 16-storey building structures, while the influence of higher modes on the seismic response of zipper frame structures is discussed. In addition, the efficiency of adding outrigger trusses at the top floor of the 12- and 16-storey building located in Victoria, B.C., which is a high risk seismic zone, is emphasized. If the lateral deformation cannot be reduced below the code limit, a second pair of outrigger trusses is proposed to be added at the mid-height of the 16-storey building. In this research, nonlinear time-history dynamic analyses of 12- and 16-storey ZBF buildings with and without outrigger trusses were conducted by using the Drain-2DX computer program. The proposed design method for the ZBF with outrigger

trusses is in agreement with the CAN/CSA-S16-09 standard and National Building 2005 (NBCC2005). In addition, the applied seismic detailing should comply with the S16-09 standard provisions for moderately ductile CBFs.

1.2 Objectives and Scope

The aim of this research project is two-fold:

- To investigate the inelastic behavior of the 12- and 16-storey ZBF building structures with elastic zippers located in a high risk seismic zone;
- To emphasize the influence of adding outrigger trusses to the zipper braced frame building structure.

1.3 Methodology

In order to achieve the above objectives, the following methodology is proposed:

- Design the gravity system (gravity columns and beams), the seismic force resisting system (braces, columns, and beams of braced frame in chevron configuration) by using seismic forces from the response spectrum analysis of the buildings. The seismic design process should comply with the CSA/ S16 2009 provisions for moderately ductile CBF system. By considering the capacity design approach and the two scenarios proposed for zipper column design in tension and compression, the design of the elastic ZBF system (E-ZBF) is completed. The assumptions made for the aforementioned two main scenarios are: a) the first brace buckles at the

ground floor level, buckling of braces propagates upwards and the transferred unbalance force subjects the zipper column in tension and b) the first brace buckles at the roof floor level, buckling of braces propagates downwards and the unbalanced force transferred into zipper column subjects zippers to act in compression. In addition, for zipper column design and by considering insights from previous studies, four lateral load distribution patterns of internal forces developed in braces are considered in this study. Thus, the employed lateral load distribution patterns are: the sequential triangular (LP-ST) and sequential parabolic (LP-SP) pattern as well as the triangular (LP-T) and the parabolic (LP-P) pattern. Regarding the estimation of the maximum tensile and compressive force triggered in zippers under the aforementioned scenarios, it is considered that zipper columns should be designed to withstand the probable tensile and compressive force developed in braces. For high-rise buildings located in western Canada, in high risk seismic zone (e.g. Victoria, B.C.) , an additional system composed of outrigger trusses is added either at the top floor level only or at the top and mid-height floor. In addition, the design of outrigger trusses consists of applying the compatibility method of rotations between the laterally deflected zipper braced frame and outrigger segments.

- For design validation, selection of ground motions compatible with the uniform hazard spectrum for Victoria, British Columbia location is required, as well as a minimum number of 7 ground motions. Because Victoria region is affected by

shallow crustal and subduction (Cascadia subduction fault) earthquakes, two ground motions ensembles are selected such as: 7 crustal ground motions and 7 subduction ground motions. In this study, for comparison purpose, a third ensemble of 7 near-field ground motions with forward directivity was selected. All selected accelerograms were scaled to fit the uniform hazard spectrum over the period of interest $0.2T_1 - 1.5T_1$, where T_1 is the fundamental period of the building, in agreement with ASCE/SEI -07 provisions.

- In this study, modal response spectrum and nonlinear time-history analyses were involved by employing the ETABS and Drain-2DX software, respectively.
- To comply with the lateral deformation criterion, outrigger trusses, designed to perform in elastic range, were added to the computer model. As a result, the stiffness of the system was increased, lateral deflection was reduced, and zipper columns were able to hold the system in elastic range, while braces are performing in the plastic range.

1.4 Thesis organization

This thesis is organized in six chapters. The first chapter presents the introduction of research generalities, objectives, methodology, and thesis organization. The second chapter summarizes the literature review on the past studies conducted on zipper frame structure and outrigger trusses, as well as the accuracy of the computer model developed in

Drain-2DX environment. The third chapter contains the design process of gravitational resisting system (gravity columns and beams), lateral resisting system (braces, columns, and beams of concentrically braced frame), zipper columns, and outrigger trusses based on the previous study conducted by Tremblay and Tirca (2003), Tirca and Chen (2012), and Hoenderkamp and Bakker (2003). The fourth chapter presents the selection of ground motion ensembles, the scaling process of the selected ground motions, and the seismic response of the 12- and 16-storey zipper braced frame with and without outrigger trusses under time-history nonlinear analyses by using Drain2DX. The computer output such as axial forces in zipper columns and lateral interstorey drift of buildings with and without outrigger trusses is provided in Chapter 5, as well as a detailed discussion regarding the behavior of the studied building structures under different ground motions. Finally, in the sixth chapter, conclusions and the recommendations of the future work are presented.

CHAPTER TWO

Literature Review

2.1 Past studies on the Design of Concentrically Braced Frames with Zipper Columns

2.1.1 Generalities

As one of the widely used seismic load resisting systems in Canada, chevron braced frame is able to provide high stiffness and moderate ductility by allowing the braces to buckle and/or yield in order to dissipate the input energy during ground motion excitations, while all other structural members such as: beams, columns, and connections behave in elastic range. However, under severe ground motion excitations, it is very likely to have storey mechanisms occurred, especially when the beams in concentrically braced frame is not designed to overcome the unbalanced forces generated by buckled braces.

When lateral forces applied, braces elements initially provide both tensile and compressive resistance to balance the lateral effect. Generally, for brace members, the tensile capacity is greater than the compression capacity. When reaching its compressive capacity, the brace member buckles, and a plastic hinge is developed at its mid-length. As a result, a large displacement occurred. At this stage, since the brace section is fully plastic, its axial capacity reduces to accommodate a larger moment developed at the plastic hinge

location. Meanwhile, due to the loss in compression capacity of brace, the lateral force is transferred to the tensile brace, while a large unbalanced force is developed at the brace to beam intersection point. Nevertheless, beams sections in CBFs should be designed to accommodate plastic hinge formation at their mid-span. Most likely, the beam will buckle and the weak storey mechanism is formed as illustrated in Figure 2.1. In this stage, the failure of one floor causes the failure of the entire system. As is shown in the graph of Figure 2.1, where the base shear, V , versus interstorey drift is depicted, the capacity of the system to withstand shear force diminishes while the lateral deformation is substantially increased.

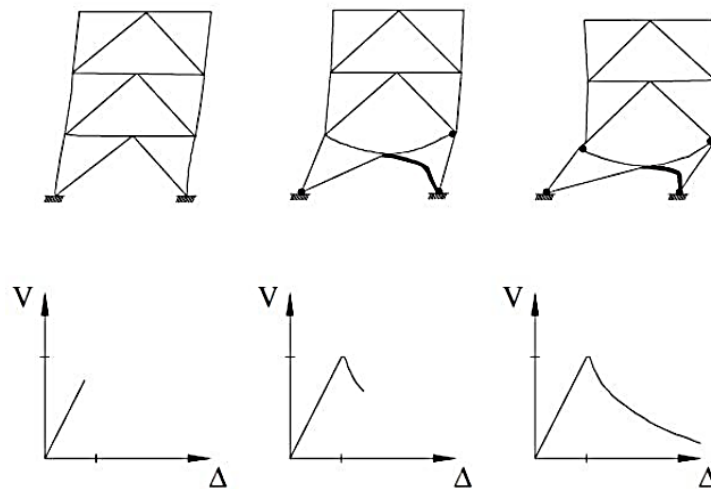


Figure 2.1 Chevron braced frame behaviour (Bruneau, et al., 2005)

In order to avoid the problems of beam failure, different studies have been carried out by researchers such as Khatib and Mahim (1988), Sabelli (2001), Tremblay and Robert (2001), and others. To avoid this type of failure, it was proposed to use strong beams, de-

signed to carry the unbalanced force generated after buckling of brace occurred. However, according to this strategy, the braced frame system is still likely to form weak storey mechanism.

To overcome the above design difficulty, (Khatibet al, 1988) proposed to link all beam-to-brace intersection points of adjacent floors and to transfer the unbalanced load to the vertical member called “zipper column”. In this way, the zipper members can behave either in tension or in compression and should be able to withstand the “zipper mechanism” formation, which implies buckling of braces successively. This unbalanced force transferred to the “zipper column” pushes the zipper in tension if the first buckled brace is located at first floor and buckling of braces progress upward or pushes the zipper in compression, if the brace of the roof floor buckles and buckling is propagated downward. Therefore, after brace buckled and the unbalance force is transferred to the zipper column, this member is able to re-distribute the transferred force to the braces located on the verge of buckling either at the floors above or below depending on the direction of brace buckling propagation. In this regard, the damage concentrated at one floor is spread along the structure height, involving more braces to sustain the remaining lateral loads after redistribution.

Thus, the zipper configuration is expected to improve the seismic performance of CBF systems and to overcome the problem of unbalance forces developed in chevron

braced frames. This proposed system is able to maintain a more uniform damage distribution over the structure height and to develop a stable hysteresis behavior. In addition, besides offering a relatively good performance level in terms of storey drift and energy dissipation under earthquake excitations, the requirement of stiff beams should be avoided.

In the Commentary of AISC Seismic Provisions for Structural Steel Building (AISC 2002), the zipper steel frame system is recommended as a configuration which is able to improve the post-elastic seismic performance of chevron braced system. In Figure 2.2, the expected behavior and performance of zipper frame when the first brace buckles at ground floor level and zipper is loaded in tension is shown.

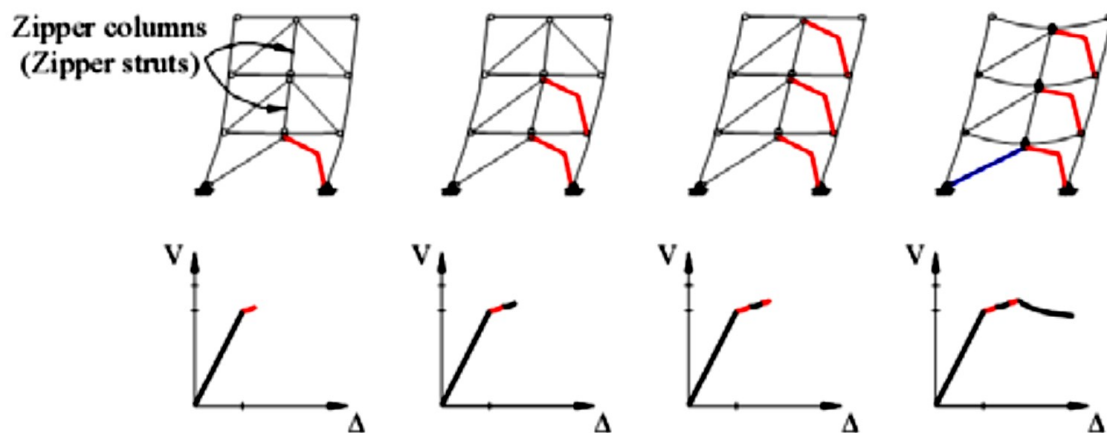


Figure 2.2 Expected behaviors and performance of zipper frame (Nouri, Imani Kalesar, & Ameli, 2009)

2.1.2 Tension Zipper strut approach

According to Khatib and Mahin (1988), the zipper effect is triggered when the structure is deflected in the shape of the first vibration mode. The brace member at the ground floor

buckles firstly and triggers tensile forces in the above zipper column, which causes the upper floor brace to buckle. The same process is gradually propagated upwards. Nevertheless, based on this design approach, zipper columns are proportioned to carry only tensile forces, which means that always the first buckled brace is at the ground floor. In addition, in order to have the zipper braced frame system deflected in the first mode, it requires braces on one half-span of the braced frame to buckle, then, after ground motion reversed sign, the remaining half-span braces will buckle. In this case, the tensile forces in zipper columns can be calculated as the summation of all vertical components of the unbalanced loads resulted from internal forces developed in braces.

Moreover, corresponding to the limitations of tension zipper strut, Khatib and Mahin (1988) pointed out several questions regarding the system design and behaviour:

- “What happen if the buckling of braces initiates from other stories instead of the first storey?”
- “Could the zipper elements be activated in compression instead of tension?”
- “What if the structure is not in a first mode deflected shape when the zipper effect is activated?”
- “How to proportion the braces to maximize the effectiveness of zipper effect?”
- “How to choose the relative stiffness of the zipper elements and beams?”

To date, several researchers proposed versions of ZBF systems by trying to fit the response of the above questions in the proposed design guidelines: Sabelli (2001), Tremblay and Tirca (2003), Yang and Leon (2003).

2.1.3 Weak Zipper strut approach

To prevent the formation of weak storey mechanism and pursuit a uniform drift distribution along the building height, a design method called “weak zipper strut approach” is proposed by R. Sabelli (2001). According to his proposal, the design of brace members should follow the same code requirements as provided for CBF’s braces. He recommended that the compressive and tensile capacity of zipper columns must reach the strength of braces located at the level below. Moreover, the inelastic demand in both cases when zipper columns act in tension and compression should be considered in design.

After applying the weak zipper strut approach in a 3- and a 6-storey zipper braced frames, R. Sabelli (2001) concluded that by having zipper column installed, the interstorey drift demand is more uniformly distributed than that in a chevron braced frames with strong beams. Between the two studied frames, the 3-storey zipper frame shows better seismic performance than the 6-storey frame, and match the expected behavior of zipper braced frame. Brace members have buckled at all floor levels and drifts are nearly equal developed at each floor. On the other hand, for the 6-storey frame, several discrepancies have been observed. Instead of deflecting on the first mode, the deformed shape of the

6-storey frame approximated the shape of the second mode of vibration. In addition, there are significant buckling and tension yielding observed in zipper columns of the 6-storey frame, which was judged inconsistent with the expected performance of zipper braced frame. The behavior of a chevron braced frame with weak zipper columns is shown below in Figure 2.3.

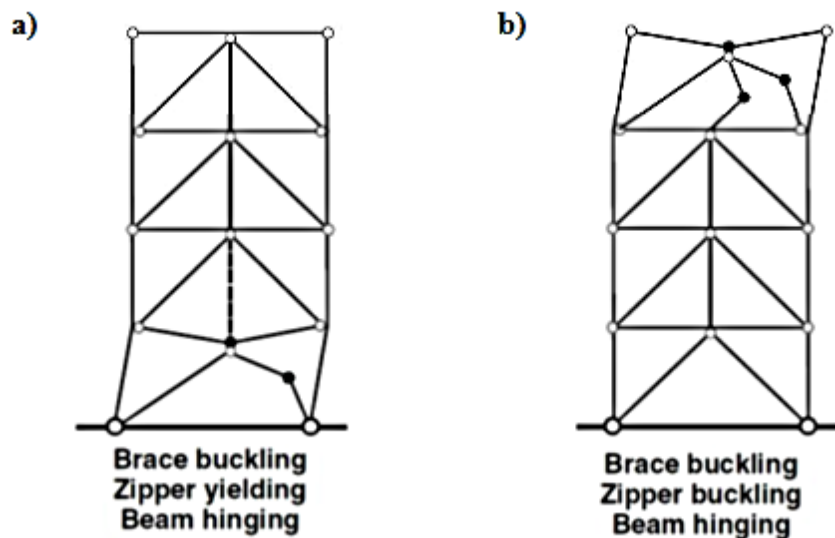


Figure 2.3 Behavior of zipper braced frame system with weak zipper column (Tirca & Tremblay, 2004): a) zipper yields in tension; b) zipper buckles in compression

2.1.4 Strong Zipper strut approach

To limit the inelastic behavior within braces, Tremblay and Tirca (2003) proposed another design method with the aim of maintaining the zipper columns to behave elastically under severe ground motions. Based on the proposed method, a 4-, 8- and 12-storey zipper braced frames have been designed and studied. The results regarding the inelastic behavior of aforementioned braced frames have shown that the zipper mechanism can be developed

either in tension or in compression, and these two critical scenarios can be treated separately. For the scenario of zipper acting in tension, the brace buckling initiates at the bottom storey and propagates upward in the frame. Therefore, zipper columns are subjected to tensile forces due to unbalanced vertical forces resulted from the subsequent buckling of braces as shown in Figure 2.4 a). On the other hand, for the scenario of zipper acting in compression, the first brace buckled at the top floor, and then propagates downward. In this case, the unbalance vertical forces are transmitted from braces to the mid-span of the beams, and eventually transferred to zipper columns as compression forces (Figure 2.4 b).

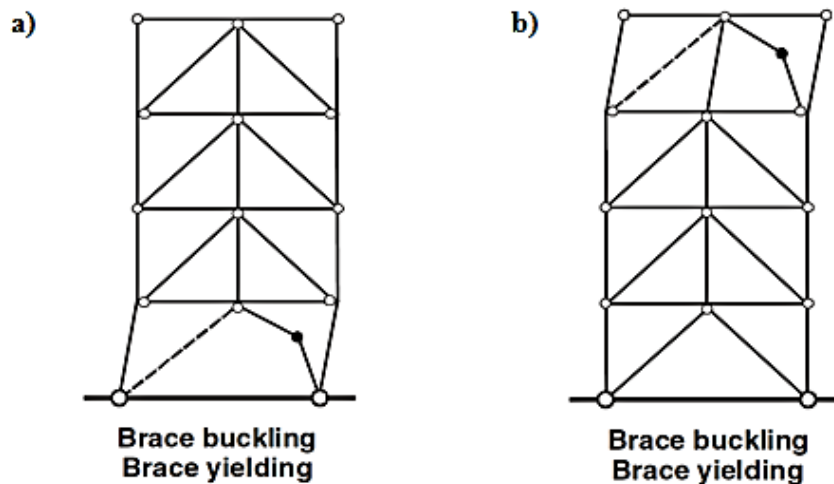


Figure 2.4 Behavior of zipper braced frame system with strong zipper columns (Tirca & Tremblay, 2004) brace buckling initiated a) at the base; b) at the roof.

Under these scenarios, zipper columns are designed to carry the unbalance load generated due to the buckling of brace members. Therefore, two scenarios have been proposed: zipper in tension when brace buckles initiated at the ground floor and zipper in compression when braces buckles initiated at the top floor of the structure. In both cases,

the zipper struts are designed to carry either the maximum tensile force or compressive force which is expected to be transferred and is depended on the buckling/post-buckling and tensile capacity of braces. In Figure 2.5, the two buckling scenarios are shown under the sequential triangular load pattern distribution.

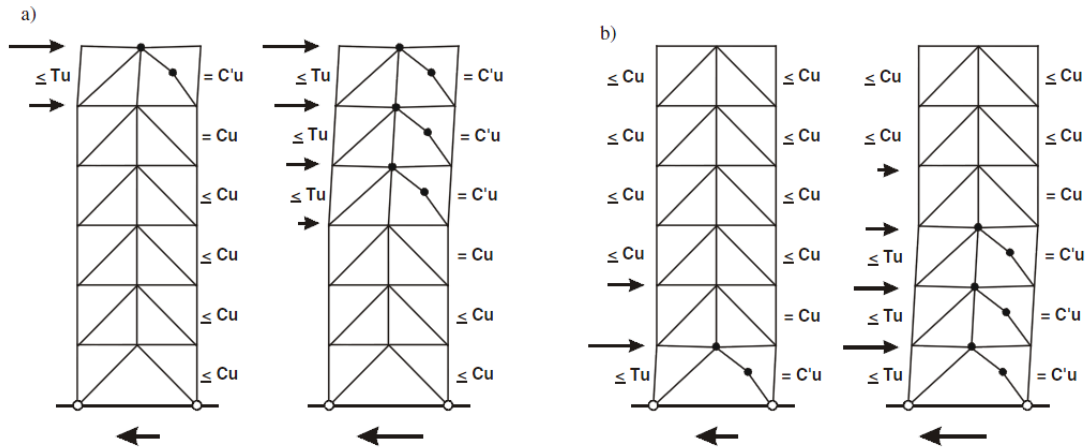


Figure 2.5 Transfer mechanisms and lateral load distributions adopted to design the zippers when brace buckling initiating at the: a) upper floors; b) lower floors (Tirca & Tremblay, 2004)

Under the circumstance of zipper columns behaving in elastic stage (strong zipper), the design method proposed by Tremblay and Tirca (2003) is able to estimate the maximum tensile and compressive force envelop developed in zipper columns under various ground motion excitations.

Furthermore, several assumptions have been made in this research to make the detail calculations of the maximum compressive forces in zipper columns feasible. Some of them follow Khatib and Mahin's assumptions when the idea of zipper frame was arisen. The applied assumptions are listed below:

- The applied lateral load is assumed to vary linearly from a maximum value reached at the roof level to zero at the level below the studied level (triangular shape);
- Plastic hinges are assumed to form at the mid-length of the beams where the buckled braces are connected;
- Braces are assumed to maintain their probable compressive strength, C_u on the verge of buckling, and their strength will drop to the post-buckling capacity, C_u' right after the buckling occurs;
- It is also assumed that the compressive force transmitted downward through the zipper column of the studied level is carried completely by the compressive braces at the level below. Therefore, when the zipper column of the studied level reaches its maximum compressive force, the compression brace at the floor below will be upon buckling, i.e. the compressive force in the brace reaches its probable compressive capacity, C_u , as shown in Figure 2.5 a).

Meanwhile, to calculate the maximum tensile forces in the zipper columns, T_z , the following assumptions are made:

- The lateral load is assumed to vary linearly from a maximum value at the first floor (when the tensile force developed in the brace of the first floor is smaller or equal to the probable yielding force, T_u , the corresponding force in the compressive brace reaches the probable post buckling load C_u' and all braces belonging to the tier under study reach a force $\leq C_u$) to zero at the floor located above the study level.

- Plastic hinges form at the mid-span length of the beams located above the buckled braces;
- The zipper column of each storey is designed to carry the cumulated difference of the tensile force developed in the brace versus the probable post-buckling force C_u' on the subjected storey (Figure 2.5 b).

To summarize, the proposed method is able to estimate the zipper column loads and their elastic seismic behaviors. Under crustal ground motions, inelastic responses are observed in all studied structures. However, under the near-field and Cascadia (subduction) ground motions, dynamic instability may occur in the 12-storey building after the formation of a full zipper mechanism. This study has underlined the requirements of future research and the validation of the proposed design method against different pattern loads distribution over the building height, beside the considered sequential triangular pattern.

2.1.5 Suspended Zipper strut approach

Simultaneously with the research carried out by the aforementioned researchers, Roberto Leon and Yang (2003) from Georgia Institute of Technology, have proposed a modified zipper braced frame called “suspended zipper frame”. The modified system consists of a zipper frame system with a hat truss located at the top floor level. The purpose of having this modification is to keep the top level braces behaving in elastic range and to avoid the formation of a full-height zipper mechanism. In this approach, the failure is defined when the partial- height zipper mechanism is formed.

In a suspended zipper frame, the top level braces remain in elastic range, while all other compression braces in other stories have buckled. The function of the suspended zipper columns is to transfer the unbalanced vertical loads developed due to the braces buckling at floors below and to support the beams at their mid-span. As a result, beams can be designed to form plastic hinge at mid-span. Therefore, significant savings in the amount of steel is made for sizing beams to perform in the plastic range. Meanwhile, the system has a clear force path which makes a capacity design for all the structural members straight forward. The configuration and expected behavior of suspended zipper frame is shown in Figure 2.6.

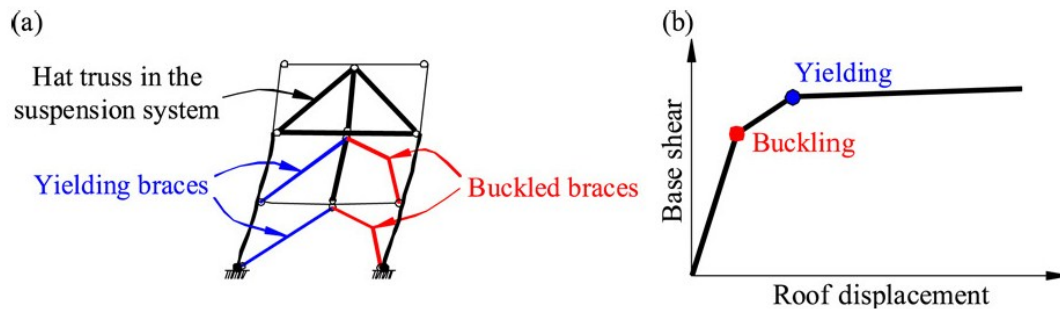


Figure 2.6 Behaviour of ZBF with suspended zipper strut (Yang, Leon, & DesRoches, 2008)

In their research, Leon and Yang aimed to prevent the formation of full-height mechanism, and especially they focused on the case of brace buckling at lower stories. During the process of forming partial-height zipper mechanism, the hat truss helps to redirect the unbalanced forces into the exterior columns which transfer the forces back to the base.

The loading path of suspended zipper braced frame is well defined. Because the zipper struts transfer all the unbalanced forces to the top storey, the members of the hat truss are designed to behave elastically and thus, larger sections are required. In addition, along with the increase of the number of stories, the amount of forces carried by the hat truss can be substantially increased. In that case, the cross-sections of hat truss members became unacceptable large, which creates construction challenges and decreases the cost-efficiency of the system. Therefore, the suspended zipper frame structure is limited by the height of the building or in other words, by the number of stories.

2.2 Past studies on high-rise buildings with outrigger and belt truss system

2.2.1 Need for High-rise buildings

The design of high-rise buildings relies on many factors such as economics, aesthetics, technology, municipal regulations, and politics. Among them, the economic aspect is always the primary governing factor. Along with the economic demand and the world-wide architectural trend, an innovative high rise building structural system is needed. In this light, some innovative structural systems are: tubes, mega-frames, core-and-outrigger systems, artificially damped structures, mixed steel-concrete systems and others (Ali & Moon, 2007).

2.2.2 Generalities regarding the outrigger and belt systems

The outrigger truss system was applied in the Place Victoria Office tower in Montreal in 1965. Since then, the outrigger concept has been widely used in the design of high rise buildings. In outrigger structures, “outriggers” are used to connect exterior columns at the outboard of the building to the lateral load resisting core which can be either shear wall or braced frame. This approach mobilizes the axial strength and stiffness of exterior columns to provide (Taranath B. , 1975) resistance to the overturning moment caused by lateral forces. Meanwhile, by adding outrigger trusses the overall stiffness of the structure increases. However, the conventional outrigger trusses have disadvantages such that space-planning limitations and the requirement of developing special details for connecting these trusses to the structural system.

The development of outrigger braced frame system started in the ‘70s. Thus, Taranath (1974) examined the optimum location of a single belt truss added to the structural system with the aim to reduce the building’s drift under the wind load and has presented a simple method of analysis. He also concluded that the optimum location of the belt truss is at 0.445 times the building height measured from the top. McNabb et al (1975) verified Taranath’s (1974) procedure and recommended the optimum location of two outrigger trusses. He investigated the controlling factors of drift reduction in outrigger structure and stated that the optimum locations for two outriggers added to the braced frame system should be 0.312 and 0.685 times the building height, respectively, measured from the top

of the building. Later on, Smith et al. (1991) proposed simple approximate guidelines for determining the location of the outriggers for preliminary analysis of outrigger braced frames.

In the above investigations, it is assumed that under the wind loading, the flexural rigidity of the core and axial rigidity of the perimeter columns are uniform along the building height, and the lateral force is also uniformly distributed along the building height. However, years before, Rutenberg et al (1987) found that the above mentioned parameters are not uniform along the building height, when a structure with outrigger trusses is considered. Later on, Hoenderkamp et al (2003) presented a simple method of analysis and recommended it to be used for the preliminary design of high-rise braced frame with outrigger trusses under lateral loading. Further, Hoenderkamp et al (2008) investigated the optimum location of the second outrigger by considering the location of the first outrigger truss at the top floor. All of the above studies clearly show that the location of the outriggers has a significant contribution regarding drift.

Traditionally, the outrigger trusses directly connect the earthquake resisting core (shear wall or braced frame) to the adjacent and exterior columns as is shown in Figure 2.7. In this example illustrated by R.S. Nair (1998), two sets of double split-X outrigger trusses developed over three storey levels and located at the mid- and top-height of the building are added to connect the core to the exterior columns.

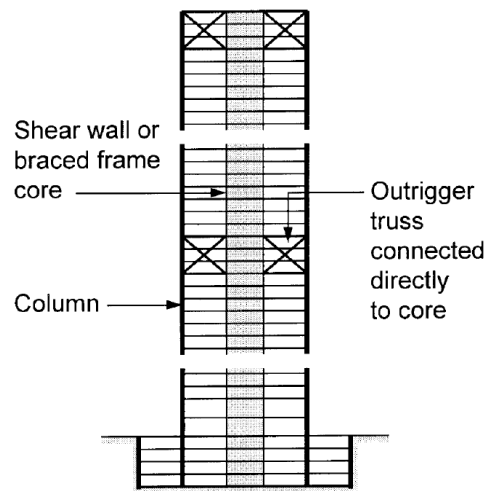


Figure 2.7 A tall building with conventional outrigger trusses (R.S.Nair, 1998)

Depending on the design demand, the height and location of the outrigger truss can be various. Thus, shallower and deeper trusses can be used in different configurations and the number of outriggers over the height of the building can also vary from one to three or even more, depending on building height and wind or earthquake forces.

In order to enhance the lateral resisting performance, the subjected building has to possess enough stiffness that can be achieved by minimizing the overturning moment caused by lateral loads. As illustrated in Figure 2.8, when lateral loads are applied to the structure, the outrigger trusses restrain the rotation of the core and convert part of the overturning moment developed in the core as a vertical couple which triggers axial forces in the exterior columns. This behavioural characteristic is illustrated by Buyukozturk and Gunes (2004) as well and is shown in Figure 2.9. Therefore, the input energy from the lateral load will be then dissipated by shortening and elongation of the columns as well as

deformation of trusses. This effect will reduce the bending moment (overturning moment) in the shear wall or braced frame from the outrigger level to the base, and it will eventually reduce the horizontal deflections of the structure.

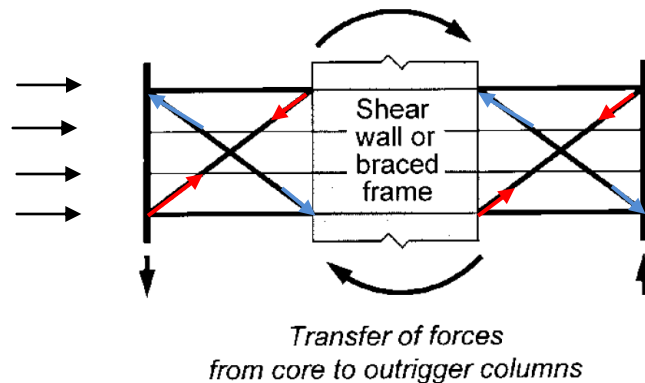


Figure 2.8 Forces transfer in conventional outrigger trusses (R.S.Nair, 1998)

However, regarding the use of conventional outriggers, several shortcomings have been pointed out by (R.S.Nair, 1998):

- The space occupied by the diagonal trusses implies functional limits at the floors at which the outrigger trusses are located.

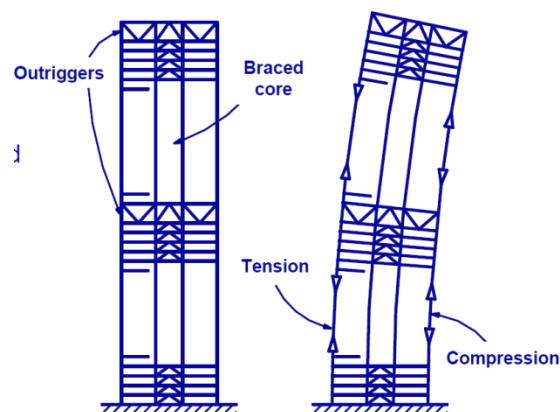


Figure 2.9 Deformed shapes of CBF in High-rise building with outrigger trusses (Buyukozturk & Gunes, 2004)

- Conventional outrigger trusses placed inside the structure normally have an impact in the architectural space.
- Connections of the outrigger trusses to the shear wall require special design, which may end with designing a complicated mechanism.
- In most cases, under gravity load, the shortening of the core and the exterior columns is not equal. By adding outrigger trusses, these are able to restrain the difference of shortening between the core and the exterior columns, while are overcoming larger stresses. For structural system design, stiff and large cross-sections are required which implicitly cause the loss of cost-efficiency characteristic.

2.2.3 Analytical method of finding the optimum outrigger truss location

As noted above, Taranath (1974, 1975) has proposed a simplified method of analysis for the outrigger braced frame structures. He assumed that belt or outrigger trusses have infinite bending stiffness. In addition, he found an optimum location for the belt or outrigger trusses and concluded that finding this location is a significant factor which influences the reduction of the lateral drift.

In order to study the optimum location of belt trusses belonging to an outrigger braced frame, Taranath (1974) made an analytical model, which is illustrated in Figure 2.10. The outrigger truss was located at a distance x from the top, and a compatibility method was applied to find the optimum location of this single truss configuration.

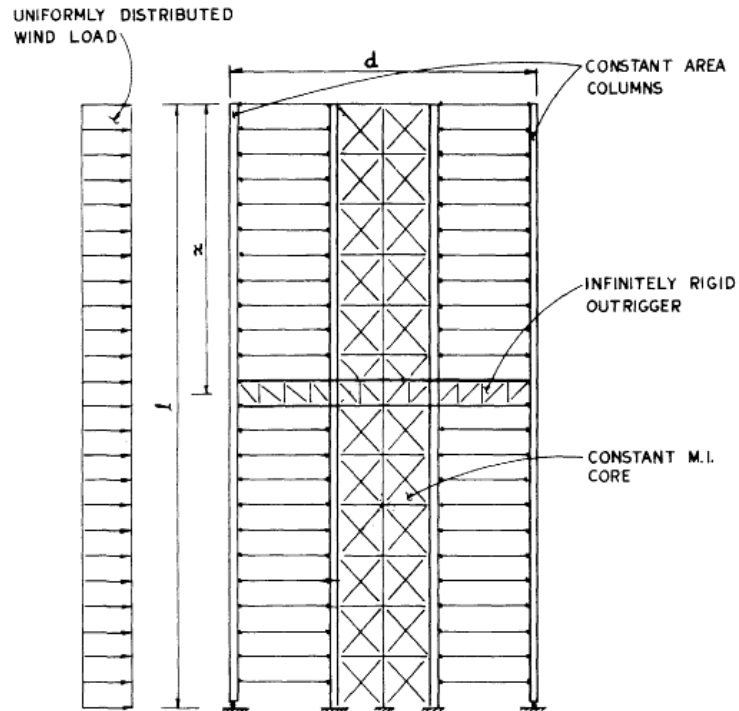


Figure 2.10 Analytical Model for studying the optimum location of a single outrigger truss (Taranath B. , 1974)

The method consists of matching the rotation of lateral resisting core with that of the exterior gravity columns. From the compatibility relation, the restoring moment M_x at the location of the outrigger is evaluated. Furthermore, the deflection of the lateral resisting core at the top floor level due to the restoring couple is calculated and maximized using the principles of calculus. The solution of the mathematic derivation gives an optimum value of x at which the deflection of the lateral resisting core is minimized, and this location x is defined as the optimum location for single outrigger truss configuration in terms of drift control. Thus, the optimum location was found as being $x = 0.445L$ which means that the

best location for adding the outrigger truss is at 0.445 times the building height measured from the top.

Furthermore, Taranath (2010) gave some recommendations for the optimum locations of a single and more outrigger trusses shown in Figure 2.11 by using the principle of minimizing the interstorey drift:

- The optimum location of a single outrigger truss is not at the top level. The reduction in drift by adding a top truss can be about 50%. On the other hand, the reduction in drift by having the truss at the mid height is about 75%. However, combining the serviceability and architectural requirements, the benefits of placing the truss at the top are still preferable.
- For a two-outrigger structure, there are a few options regarding the optimum location. Practically, the optimum drift reduction can be achieved when the outriggers are added at locations completely different from the theoretical optimum locations under various circumstances. Therefore, the engineer and architect may have alternative options in choosing the outrigger locations. Theoretically, Taranath mentioned that the optimum location for two outriggers is: $1/3$ and $2/3$ of the building heights. For a three-outrigger structure, the optimum locations should be at the one-quarter, one-half, and three-quarter heights, and so on. Generally, for an economical design,

the outriggers should be placed at $(1/n+1)$, $(2/n+1)$, $(3/n+1)$, $(4/n+1)$, ..., $(n/n+1)$ height locations, where n is the number of outrigger trusses.

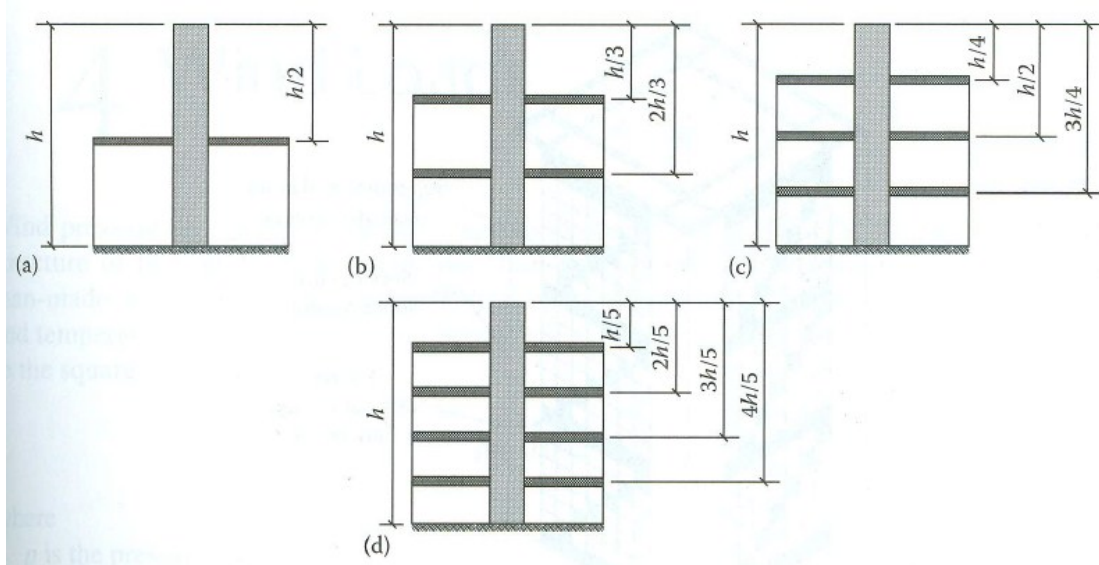


Figure 2.11 Optimum locations for different outrigger trusses locations, a) single truss, b) two trusses, c) three trusses, d) four trusses (Taranath B. , 2010)

2.2.4 Graphical method of optimum location of outrigger and belt truss system

Based on the same compatibility method in which the rotations of the lateral resisting core at the outrigger levels are matched with the rotations of the corresponding outriggers, Bryan Stafford (1991) developed a graphical method in order to find the optimum location of outrigger and/or belt truss systems.

According to Stafford (1991), the number of compatibility equations is related to the degree of redundancy. He considered that a single outrigger structure has one degree of redundancy; a two outrigger case is twice redundant, and so on. The compatibility equations state the equivalence of the rotation of the lateral resisting core to the outriggers.

Meanwhile, the rotation of the lateral resisting core is expressed in terms of its bending deformation, and the rotation of the outriggers is represented by the axial deformation of exterior columns and the bending deformation of outriggers.

Following a similar concept, Stafford (1991) developed a set of non-dimensional parameters α and β which expressed the core-to-column and core-to-outrigger rigidities, respectively. Involving the relation of lateral deflection of outriggers, the above two parameters can be combined into a single parameter, ω . The parameter ω is non-dimensional and represents a characteristic structural parameter for a uniform structure with flexible outriggers. He also states that with all other structural properties remaining constant, there is a reduction in ω as the outrigger's flexural stiffness increased, and that ω increases as the axial stiffness of the column increased. Therefore, for a range of values of ω , the results of optimum location can be graphically plotted. Thus, for any configuration of outrigger structure having specific element properties, ω can be calculated and used for determining the optimum location for the outriggers in terms of minimizing lateral drift. The graphs of ω vs. outrigger locations for different number of outrigger configuration are given in Figure 2.12.

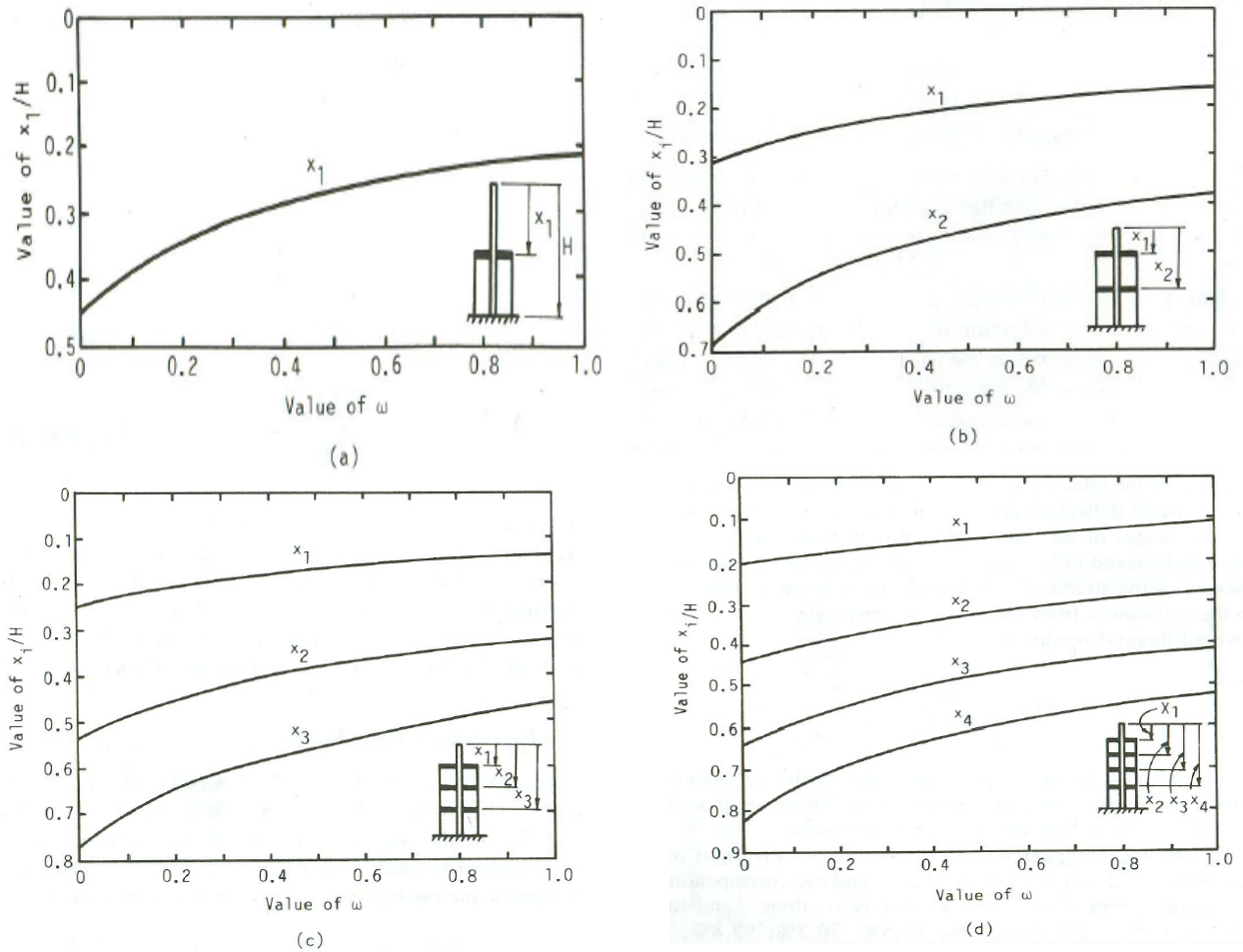


Figure 2.12 Optimum locations for outriggers: a) single outrigger, b) two outriggers, c) three outriggers, d) four outriggers (Bryan Stafford Smith, 1991)

2.2.5 The concept of virtual outrigger system with belt truss

With the aim of eliminating the aforementioned drawbacks of conventional outrigger systems, Stafford Smith, M Cruvellier, and MJ Nollet (1996) proposed a modified design of outrigger system called “Virtual outrigger truss” (offset outrigger truss). Unlike the conventional outrigger concept, which has the outrigger trusses connected to the core and the outboard columns in order to transfer the overturning moment from the lateral resisting core to exterior columns in the form of vertical couple, in the “virtual” outrigger system,

the same process is achieved without considering outrigger trusses as the connection between the core and exterior columns.

The basic idea behind the virtual outrigger concept is to make use of floor diaphragms in company with perimeter belted trusses. The floor diaphragms are typically very stiff and strong in their own plane and are designed to transfer moment in the form of a horizontal couple from the core to trusses. Then, the belt trusses convert the horizontal couples into vertical direction and uniformly distribute the vertical couples in the exterior columns on the perimeter of the structure. Eventually, the exterior columns transfer the vertical couples to the base.

Figure 2.13 shows an elevation view of the same building illustrated in Figure 2.10, except that in this case, there are belt trusses on the perimeter to increase the building stiffness, while the core is in the middle part of the building.

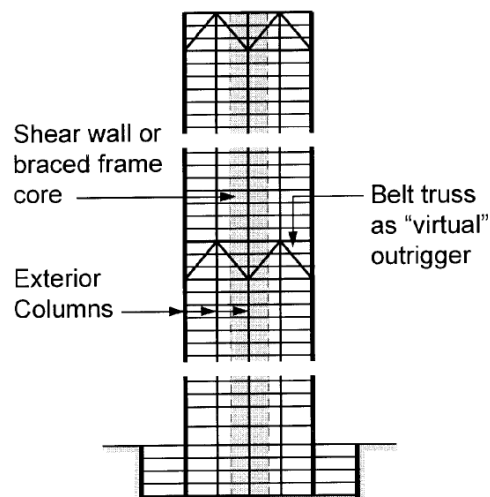


Figure 2.13 "Virtual" outrigger building with a belt truss (R.S.Nair, 1998)

The process of converting part of the overturning moment developed in the core, into a vertical couple and transferred to the exterior columns is shown in Figure 2.14. Both top and bottom flanges of the belt trusses participate to constrain the rotation of the core; therefore, part of the bending moment generated in the core is converted into a horizontal couple and carried by the floor diaphragm (Figure 2.14a). After that, this horizontal couple is then converted by the belted truss into vertical forces and is transferred to the exterior columns (Figure 2.14b).

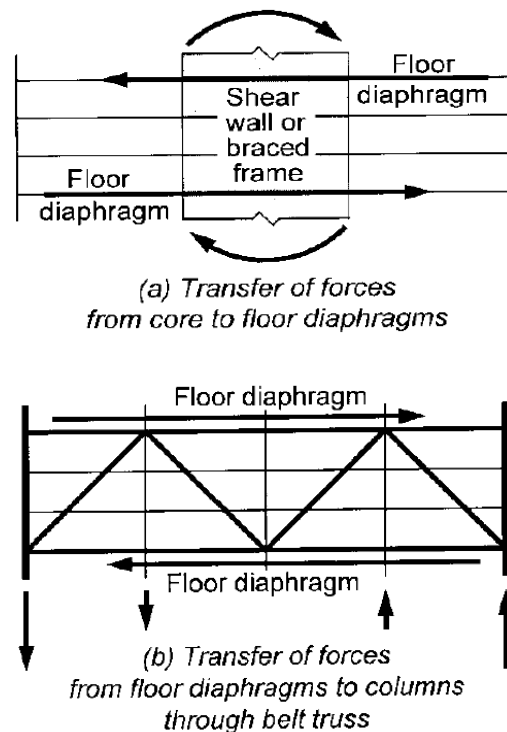


Figure 2.14 Forces transferred by using belt trusses as virtual outriggers (R.S.Nair, 1998)

By using the above modified system, R.S.Nair (1998) stated the following benefits:

- There are no space required to pass trusses between the core and the external columns.
- There are fewer constraints at the location of exterior columns. Since the requirement of having larger exterior columns which are connected to the core by vertical outriggers is not needed in the virtual outrigger system.
- All exterior columns participate in resisting overturning moment.
- There is not special type of connection to join the outrigger trusses to the core.
- Complications caused by differential shortening of the core and the outrigger columns are avoided.

2.3 Studying the use of computer program -----Drain-2DX

DRAIN-2DX is a general purpose computer program for static and dynamic analysis of plane structures. It is capable of performing either nonlinear static or dynamic analyses. For dynamic analysis, it considers ground accelerations, ground displacements, imposed dynamic loads (e.g., wind), and specified initial velocities (e.g., impulse loading). Moreover, both static and dynamic loads can be applied in any sequence.

Drain-2DX uses analytical models to simulate the inelastic behavior of structural members. Depending on the purposes, particular element type is implemented in Drain-2DX, for instance, element type 02 is used to simulate the inelastic behavior of

beam-column members, and element type 05 is used for modeling inelastic behavior of brace members. Therefore, the setup of Drain-2DX model is a straight-forward process due to the aforementioned feature.

Drain-2DX has been widely used in the field of structural analysis since the '80s. The previous studies of zipper frame structure presented by Sabelli (2001), Tirca and Tremblay (2004), as well as Yang and Leon (2003), were all conducted in Drain-2DX.

CHAPTER THREE

Design Methodology of Zipper Braced Frame and Outrigger Trusses

The zipper braced frame (ZBF) structure is designed based on the strong zipper approach proposed by Tremblay and Tirca (2003). The ZBF system is defined as a concentrically braced frame in chevron-bracing configuration to which a vertical member, labeled zipper column, is added with the aim to join the beams of two adjacent floors at the beam-to-brace intersection point. Thus, by adding zipper columns, several braces are triggered to yield and buckle almost simultaneously, while the formation of storey mechanism is prevented. However, previous studies recommended to limit the height of this system at 12-storey. To overcome this drawback, in this study, the author proposes to add an outrigger or belt truss to the existing ZBF system, while the design of the outrigger truss followed the concept of displacement compatibility method proposed by Stafford & Salim (1981) and the graphic method developed by Hoenderkamp & Bakker (2003). In this study, design is conducted in agreement with the NBCC 2005 and S16-2009 provisions.

3.1 Design methodology of Zipper braced frame structure

According to Tremblay and Tirca (2003), the design of zipper braced frame follows the procedure given below:

- In the first step, the CBF members such as: braces, beams, and columns are designed;
- In the second step, all zipper columns are designed as tension-compression members, which must be proportioned to behave elastically while carrying forces transferred from braces and adjacent zippers.

3.1.1 Calculation and distribution of seismic forces

In the preliminary design, the equivalent static force procedure is applied to calculate the seismic forces. According to the NBCC 2005, the base shear, V is a function of design spectral acceleration value, $S(T_a)$, the high mode factor, M_v , the importance factor, I_E , the building weight, W , the ductility-related force modification factor, R_d , and the over-strength-related force modification factor, R_o . By combining all the above parameters, the base shear equation is given below:

$$V = S(T_a)M_vI_EW/(R_dR_o) \quad (3.1)$$

For a seismic force resisting system (SFRS) designed with $R_d \geq 1.5$, the NBCC2005 also requires that V shall not be less than:

$$V_{min} = S(2.0)M_v I_E W / (R_d R_0) \quad (3.2)$$

and not larger than:

$$V_{max} = \frac{2}{3} S(0.2) I_E W / (R_d R_0) \quad (3.3)$$

In addition, for a building with a fundamental period larger than 0.7s, the seismic force shall be distributed in such a way that a portion is concentrated at the roof level, F_t , and the reminding amount ($V-F_t$) is distributed along the building height. Thus, $F_t = 0.07T_a V$ but should not exceed $0.25V$. The distribution of the base shear force is illustrated in Figure 3.1 and is based on the following equation:

$$F_i = (V-F_t) W_i h_i / (\sum_{m=1}^n W_m h_m) \quad (3.4)$$

where h_n is the total height of the structure; F_i and W_i are the storey force and seismic weight of the i^{th} floor, respectively; and h_i is the height of the i^{th} floor measured from the ground floor level.

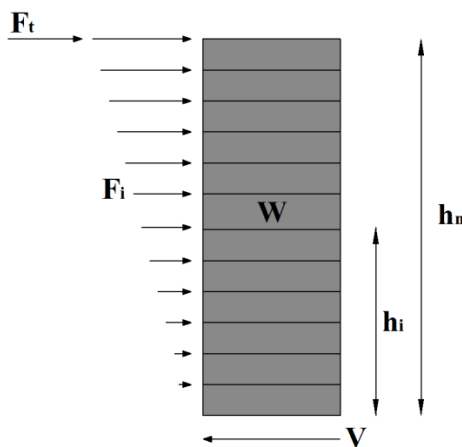


Figure 3.1 The distribution of seismic forces

3.1.2 Design of braces in chevron configuration

Brace members resist the combination of storey shear, F_i and gravity load component transferred from the above storey to the CBF's columns in agreement with the NBCC 2005 loading combination: $1.0E + 1.0DL + 0.5LL + 0.25SL$. Based on this design requirement, the storey shear in the i^{th} floor is equally distributed among the tensile and compressive brace as follows:

$$T_{f(i)} = C_{f(i)} = V_i / (2 \cos \theta_i) \quad (3.5)$$

Following the design regulation, the compressive and tensile resistance of braces should be larger than the factored loads, while the C_r and T_r are given below

$$C_r = 0.9AF_y(1 + \lambda^{2n})^{-1/n} \quad (3.6)$$

$$T_r = 0.9AF_y \quad (3.7)$$

where, A is the cross-sectional area of the brace member; F_y is the strength of steel material, $n= 1.34$ for hot-rolled, fabricated structural sections, and hollow structural sections manufactured according to CSA Standard G40.20, Class C (cold-formed non-stress-relieved) and λ is the slenderness ratio.

3.1.3 Design of beams and columns in concentrically braced frame

The beams and columns in CBF shall be designed by applying the capacity design concept.

- Beam design

The beams in braced frames are not only carrying gravity loads from the floor, but also an extra portion of load transferred from the braces in the same floor. Therefore, depending on braces buckled or not, two scenarios should be considered:

- In the first scenario, braces have buckled and beam has lost its support from the braces. In this case, the beam should carry the entire gravity component $DL+0.5LL$ without considering braces support. In addition, it should carry the axial load developed when the compressive brace reached the probable post-buckling strength $C_u = 0.2AF_yR_y$, and the tensile brace may reach the probable yielding strength $T_u = AR_yF_y$.
- In the second scenario, braces are on the verge of buckling and support beams at their mid-span. The compression braces reach their probable compressive strength $C_u = 1.2(R_y/\phi)C_r$ while $R_y = 1.1$ and $\phi = 0.9$ and the tensile braces have their probable tensile strength as $T_u = AR_yF_y$.
- Column design

In this study, columns of CBF are designed as continuous columns over two adjacent stories and should be proportioned to resist the gravity load in addition to the vertical projection of braces capacity in compression. Herein, the vertical projection of tensile forces acts as uplift forces. In addition, a fraction of bending moment computed as $0.2ZF_y$ must be considered in interaction to the axial force, where Z is the plastic section modulus of the column section.

3.1.4 Design of zipper columns

For zipper columns design, two scenarios are considered. Thus, to design zippers loaded in tension, it is assumed that brace buckling is initiated at the ground floor level and buckling is propagating upward. Similarly, to design zippers acting in compression, it is considered that the first buckling brace is located at the most upper floor and propagates downward. With the aim to simplify the design, two assumptions are made:

- For simplicity, plastic hinges are assumed to form at the mid-span of the beams where the buckled braces are connected;
- It is also assumed that braces maintain their compressive strength constantly as C_u until they buckled. If the brace buckles at ground floor level and buckling is propagating upward, at the level of calculation the brace reaches its buckling strength, braces below have reached their post-buckling strength while braces in the remaining upper floors are still able to develop their compressive capacity while supporting the zipper column.

In this study, the selected structures are a 12-storey and a 16-storey building located in Victoria, BC. Based on the concept presented above, two scenarios of brace buckling are considered to capture the maximum tensile and compressive force developed in zipper columns. In general, for the 12- and 16-storey buildings the higher modes effect will influence the ZBF behaviour. However, it is uncertain which of these two scenarios nor-

mally happens during an earthquake; moreover, for most of the time both cases can be encountered during the same ground motion excitation. Therefore, for plotting the zipper force envelope in tension and compression, both scenarios are required.

For the first scenario, buckling is initiated at the first floor and the unbalanced force is transfer to the zipper column located at the lower floor while all other members remain in the elastic range. Thus, the attached zipper column behaves in tension and it pushes the compressive brace belonging to the floor above to buckle successively. To summarize, after the compression brace of the ground floor has buckled, its compressive strength equates the probable post-buckling compression strength, $C_{u,1}$ while the corresponding tensile brace doesn't reach yet its probable tensile strength, $T_{u,1}$. Therefore, the unbalanced force developed when a brace reaches $T_{b,1}$ and the other $C_{u,1}$ is transferred to the attached beam which hinges in bending while the zipper attached from the above is loaded in tension. This type of load transferring mechanism is propagated above. Thus, the tensile force developed in the zipper column of the second floor is calculated as:

$$T_{z,2} = (T_{b,1} - C'_{u,1}) \sin \theta_1 - 4M_{p,1}/L_b \quad (3.8)$$

where, θ_1 is the angle between brace member and the horizontal line; M_{p1} is the plastic moment of the attached beam and $4M_{p,1}/L_b$ is the applied concentrated force corresponding to the development of M_{p1} . Successively, the computed tensile force triggered in zip-

per $T_{z,2}$ is transferred to the zipper above as $T_{z,3}$, while forcing the corresponding brace to buckle:

$$T_{z,3} = (T_{b,2} - C_{u,2}) \sin \theta_2 - 4Mp, 2/L_b + T_{z,2} \quad (3.9)$$

Following Khatib et al.'s concept (1988), after the first brace of the ground floor level has buckled, the buckling of braces will propagate upward, and all braces in the compression side will reach the verge of buckling almost simultaneously. Therefore, to draw the tensile force envelope, (N-1) cases must be evaluated, where N is the total number of stories.

On the other hand, for the second scenario which evaluates the maximum compression forces in zipper, brace buckling initiates at the top level of the building and propagates downward. In this case, the maximum compressive forces in zipper columns can be calculated by applying the similar procedure as for determining the tension force envelope.

3.2 The influence of pattern load selection on the preliminary design of zipper columns

According to FEMA356 (2000), different lateral load patterns influence the magnitude of forces triggered in zippers. Therefore, in order to estimate the probable compressive and tensile forces developed in zippers of the studied buildings, four different load patterns

(Triangular, Sequential Triangular, Parabolic, Sequential Parabolic) are considered in this study.

To achieve more accurate results concerning the finding of the maximum tension and compression forces developed in zipper columns, the four lateral load patterns mentioned above are used in this study.

According to FEMA356 (2000), the lateral load F_x applied at any floor level x shall be determined in accordance with the following two equations:

$$F_x = C_{vx} \times V \quad (3.10)$$

$$C_{vx} = \frac{w_x h_x^k}{\sum_{i=1}^n w_i h_i^k} \quad (3.11)$$

Herein, C_{vx} is the vertical distribution vector; k is a coefficient which is $k = 2$ for $T > 2.5s$ and $k = 1.0$ for $T \leq 2.5$ s. For intermediate values, k is calculated by linear interpolation. In addition, V is the design base shear, w_i is the building weight at the i^{th} floor, w_x is the weight of the x^{th} floor, while h_i and h_x is the height from the base to the i^{th} floor and x^{th} floor, respectively.

Depending on the value of k , the vertical distribution vectors can be calculated and plotted as in Figure. 3.2.

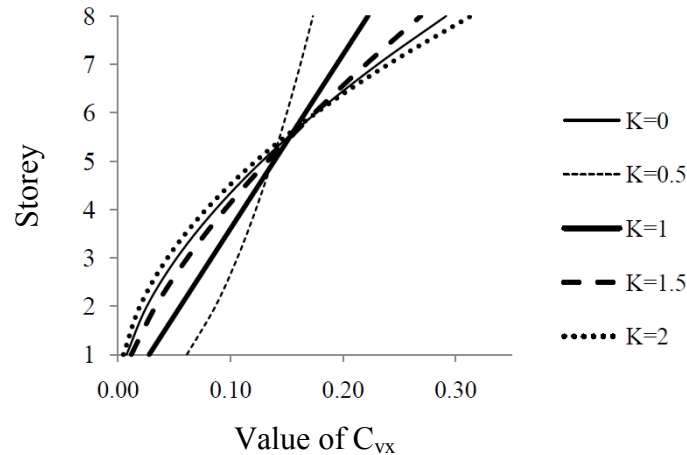


Figure 3.2 Vertical distribution vectors of lateral forces with different k (Chen, 2011)

In this study, two conventional load distribution patterns: as triangular (LP – T) and parabolic (LP – P) are applied and are shown in Figure 3.3. In addition, two sequential loading distribution patterns are added: LP – ST and LP – SP to the full height load distribution pattern: LP – T and LP – P.

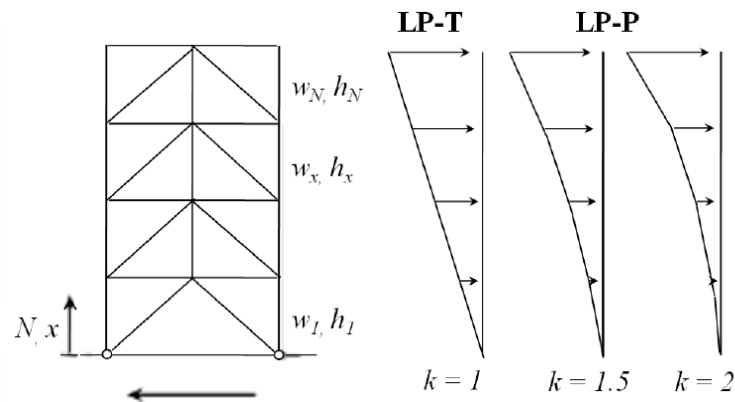


Figure 3.3 Lateral force distribution vectors (Chen, 2011)

- LP-ST: Sequential Triangular load pattern

As mentioned earlier in this chapter, the employment of the LP-ST distributed load pattern is similar to that used by Tremblay and Tirca (2003), as well as Chen (2011). For

both scenarios defined by zippers acting in tension and in compression, the linear distribution of internal forces is proportioned to the ratio F_i/F_1 and F_i/F_n respectively. In addition, these forces are limited to the summation of horizontal projections of the probable buckling strength, C_u and post-buckling strength, C'_u of braces, as well as the afferent tensile force of the corresponding brace. The sequential triangular load pattern of both scenarios is shown in Figure 3.4.

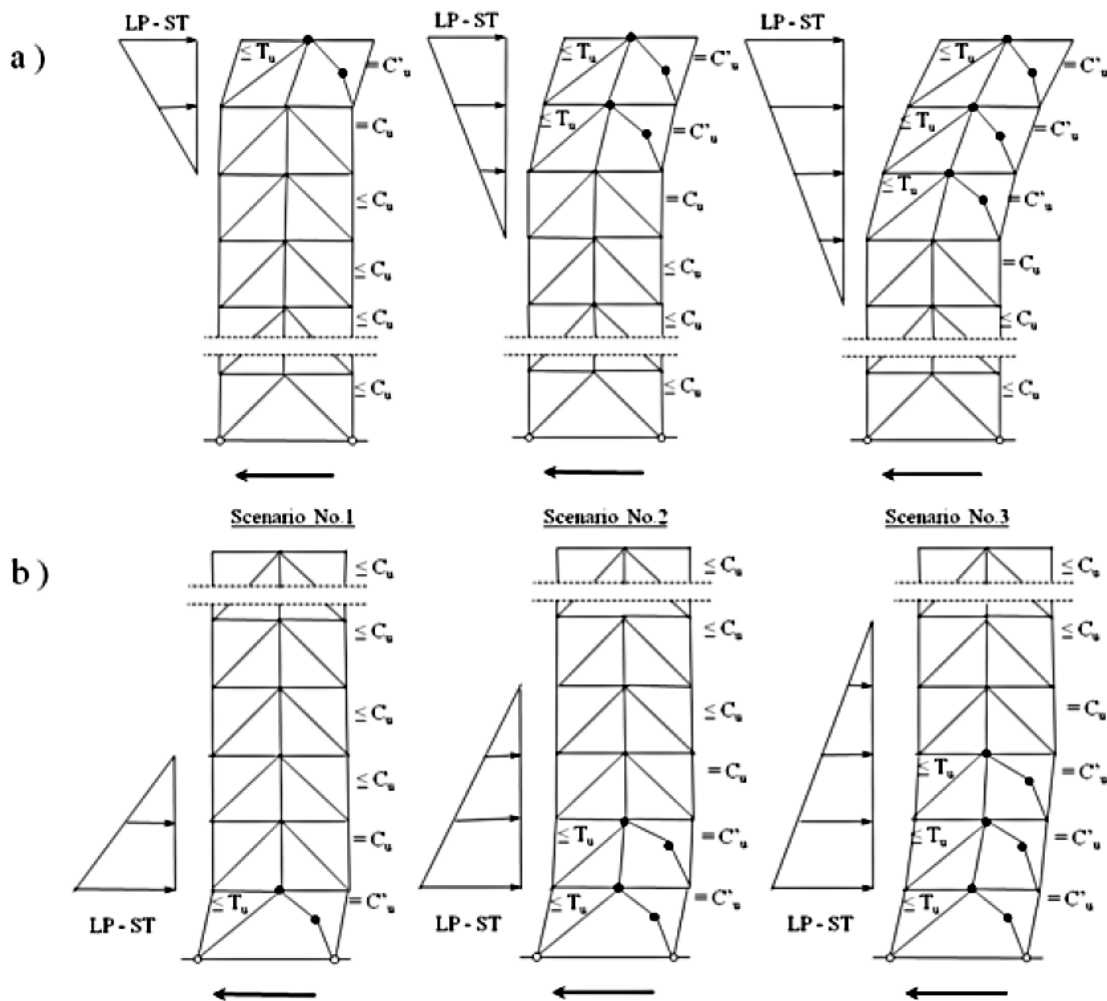


Figure 3.4 Load pattern LP-ST: a) buckling initiates at top; b) buckling initiates at bottom (Chen, 2011)

For example, when the brace buckling initiates at the first floor of the 12-storey ZBF building, the load distribution vectors corresponding to the LP-ST pattern should

Table 3.4 Sequential Triangular distribution vectors for assessing the tensile force in zippers of 16-storey building

| St. of brace buckled Story No. | 1 st | 2 nd | 3 rd | 4 th | 5 th | 6 th | 7 th | 8 th | 9 th | 10 th | 11 th | 12 th | 13 th | 14 th | 15 th |
|-----------------------------------|-----------------|-----------------|-----------------|-----------------|-----------------|-----------------|-----------------|-----------------|-----------------|------------------|------------------|------------------|------------------|------------------|------------------|
| | 16 | 0 | 0 | 0 | 0 | 0 | 0 | 0 | 0 | 0 | 0 | 0 | 0 | 0 | 0 |
| 15 | 0 | 0 | 0 | 0 | 0 | 0 | 0 | 0 | 0 | 0 | 0 | 0 | 0 | 0.07 | 0.13 |
| 14 | 0 | 0 | 0 | 0 | 0 | 0 | 0 | 0 | 0 | 0 | 0 | 0 | 0.07 | 0.13 | 0.19 |
| 13 | 0 | 0 | 0 | 0 | 0 | 0 | 0 | 0 | 0 | 0 | 0 | 0.077 | 0.14 | 0.2 | 0.25 |
| 12 | 0 | 0 | 0 | 0 | 0 | 0 | 0 | 0 | 0 | 0 | 0.083 | 0.154 | 0.21 | 0.27 | 0.31 |
| 11 | 0 | 0 | 0 | 0 | 0 | 0 | 0 | 0 | 0 | 0.091 | 0.167 | 0.231 | 0.29 | 0.33 | 0.38 |
| 10 | 0 | 0 | 0 | 0 | 0 | 0 | 0 | 0 | 0.1 | 0.182 | 0.25 | 0.308 | 0.36 | 0.4 | 0.44 |
| 9 | 0 | 0 | 0 | 0 | 0 | 0 | 0 | 0.111 | 0.2 | 0.273 | 0.333 | 0.385 | 0.43 | 0.47 | 0.5 |
| 8 | 0 | 0 | 0 | 0 | 0 | 0 | 0.13 | 0.222 | 0.3 | 0.364 | 0.417 | 0.462 | 0.5 | 0.53 | 0.56 |
| 7 | 0 | 0 | 0 | 0 | 0 | 0.14 | 0.25 | 0.333 | 0.4 | 0.455 | 0.5 | 0.538 | 0.57 | 0.6 | 0.63 |
| 6 | 0 | 0 | 0 | 0 | 0.17 | 0.29 | 0.38 | 0.444 | 0.5 | 0.545 | 0.583 | 0.615 | 0.64 | 0.67 | 0.69 |
| 5 | 0 | 0 | 0 | 0.2 | 0.33 | 0.43 | 0.5 | 0.556 | 0.6 | 0.64 | 0.667 | 0.692 | 0.71 | 0.73 | 0.75 |
| 4 | 0 | 0 | 0.25 | 0.4 | 0.5 | 0.57 | 0.63 | 0.67 | 0.7 | 0.73 | 0.75 | 0.769 | 0.79 | 0.8 | 0.81 |
| 3 | 0 | 0.33 | 0.5 | 0.6 | 0.67 | 0.71 | 0.75 | 0.78 | 0.8 | 0.81 | 0.833 | 0.846 | 0.86 | 0.87 | 0.88 |
| 2 | 0.5 | 0.67 | 0.75 | 0.8 | 0.83 | 0.86 | 0.88 | 0.89 | 0.9 | 0.91 | 0.917 | 0.923 | 0.93 | 0.93 | 0.94 |
| 1 | 1 | 1 | 1 | 1 | 1 | 1 | 1 | 1 | 1 | 1 | 1 | 1 | 1 | 1 | 1 |

- LP-SP: Sequential Parabolic load pattern

This pattern load depicts a parabolic distribution applied in sequences as described above for the LP-ST pattern. Thus, the values of lateral forces decrease from maximum to zero along a sequential height of the building where stories with buckled braces are assumed to be intercepted. To assess the development of compression forces in zippers it is assumed that the first brace buckles at the top floor and buckling of braces propagates downward, while for the tensile forces estimation it is assumed that buckling of the first brace is initiated at the bottom floor and evolves upward as shown in Figure 3.5. To cal-

calculate the distribution vectors C_{vx} , equation 3.11 is applied and the unknown exponent factor, k is related to the fundamental period of the structure, T_1 . According to NBCC 2005, T_1 can be calculated as given bellow:

$$T_1 = 0.025h_N \quad (3.12)$$

where, h_N is the total height of the structure. According to NBCC 2005, if the fundamental period of the structure calculated from a dynamic analysis is equal to or greater than $2T_1$, it will be taken as $2T_1$. For the 12-storey building studied, h_N is 45.6 meter and

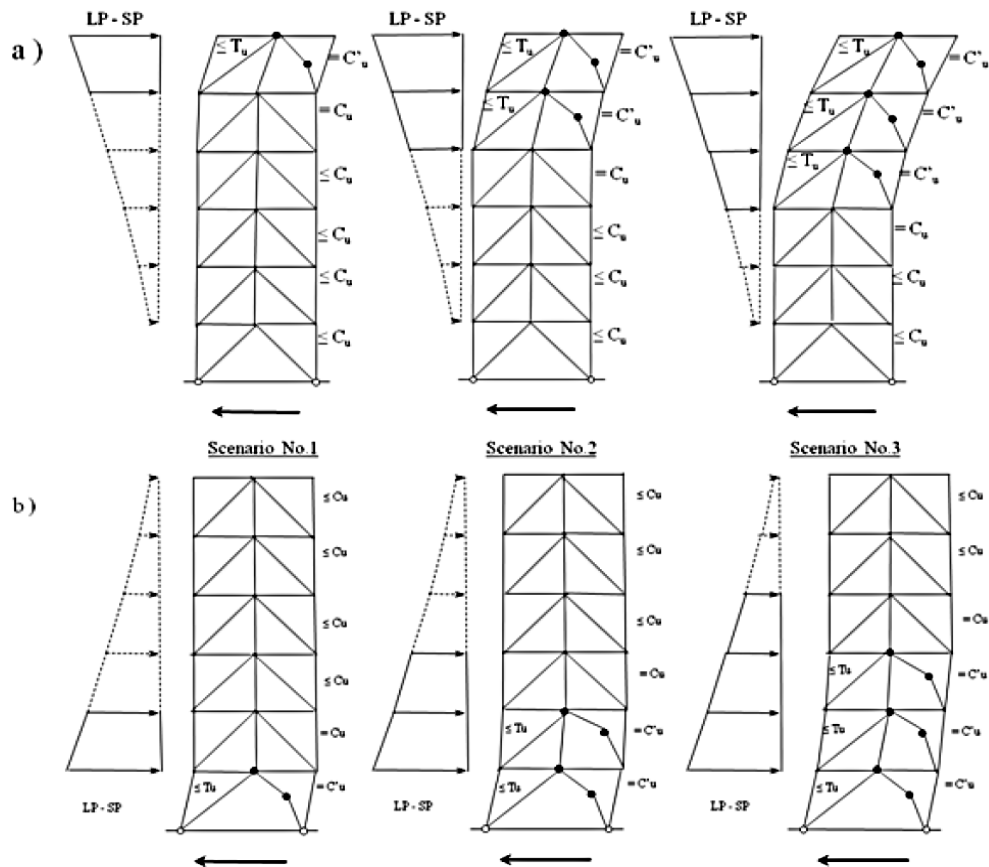


Figure 3.5 Load pattern LP-SP: a) buckling of braces initiates at top; b) buckling of braces initiates at the bottom (Chen, 2011)

Table 3.8 Sequential Parabolic distribution factors for assessing the tensile force in zippers of 16-storey building

| St. of brace buckled St. No. | 1 st | 2 nd | 3 rd | 4 th | 5 th | 6 th | 7 th | 8 th | 9 th | 10 th | 11 th | 12 th | 13 th | 14 th | 15 th |
|---------------------------------|-----------------|-----------------|-----------------|-----------------|-----------------|-----------------|-----------------|-----------------|-----------------|------------------|------------------|------------------|------------------|------------------|------------------|
| 16 | 0 | 0 | 0 | 0 | 0 | 0 | 0 | 0 | 0 | 0 | 0 | 0 | 0 | 0 | 0.06 |
| 15 | 0 | 0 | 0 | 0 | 0 | 0 | 0 | 0 | 0 | 0 | 0 | 0 | 0 | 0.07 | 0.13 |
| 14 | 0 | 0 | 0 | 0 | 0 | 0 | 0 | 0 | 0 | 0 | 0 | 0 | 0.07 | 0.13 | 0.19 |
| 13 | 0 | 0 | 0 | 0 | 0 | 0 | 0 | 0 | 0 | 0 | 0 | 0.08 | 0.14 | 0.20 | 0.25 |
| 12 | 0 | 0 | 0 | 0 | 0 | 0 | 0 | 0 | 0 | 0 | 0.08 | 0.15 | 0.21 | 0.27 | 0.31 |
| 11 | 0 | 0 | 0 | 0 | 0 | 0 | 0 | 0 | 0 | 0.1 | 0.17 | 0.23 | 0.29 | 0.33 | 0.38 |
| 10 | 0 | 0 | 0 | 0 | 0 | 0 | 0 | 0 | 0.1 | 0.2 | 0.25 | 0.31 | 0.36 | 0.40 | 0.44 |
| 9 | 0 | 0 | 0 | 0 | 0 | 0 | 0 | 0.11 | 0.2 | 0.3 | 0.33 | 0.38 | 0.43 | 0.47 | 0.50 |
| 8 | 0 | 0 | 0 | 0 | 0 | 0 | 0.13 | 0.22 | 0.3 | 0.4 | 0.42 | 0.46 | 0.50 | 0.53 | 0.56 |
| 7 | 0 | 0 | 0 | 0 | 0 | 0.14 | 0.25 | 0.33 | 0.4 | 0.5 | 0.50 | 0.54 | 0.57 | 0.60 | 0.63 |
| 6 | 0 | 0 | 0 | 0 | 0.17 | 0.29 | 0.38 | 0.44 | 0.5 | 0.5 | 0.58 | 0.62 | 0.64 | 0.67 | 0.69 |
| 5 | 0 | 0 | 0 | 0.2 | 0.33 | 0.43 | 0.50 | 0.56 | 0.6 | 0.6 | 0.67 | 0.69 | 0.71 | 0.73 | 0.75 |
| 4 | 0 | 0 | 0.25 | 0.4 | 0.5 | 0.57 | 0.63 | 0.67 | 0.7 | 0.7 | 0.75 | 0.77 | 0.79 | 0.80 | 0.81 |
| 3 | 0 | 0.33 | 0.5 | 0.6 | 0.67 | 0.71 | 0.75 | 0.78 | 0.8 | 0.8 | 0.83 | 0.85 | 0.86 | 0.87 | 0.88 |
| 2 | 0.5 | 0.67 | 0.75 | 0.8 | 0.83 | 0.86 | 0.88 | 0.89 | 0.9 | 0.9 | 0.92 | 0.92 | 0.93 | 0.93 | 0.94 |
| 1 | 1 | 1 | 1 | 1 | 1 | 1 | 1 | 1 | 1 | 1 | 1 | 1 | 1 | 1 | 1 |

- LP-T: Triangular load pattern

It is assumed a triangular distribution pattern load along the height of the structure.

- LP-P: Parabolic load pattern

A parabolic load distribution pattern can be considered as the case of braces buckled in all stories, and the same process of LP-SP can be applied to determine the distribution vectors for this particular case. As mentioned in previous section, this lateral force distribution is related to the fundamental period of the structure, respectively to the stiffness and masses distribution over the structure height. This parabolic pattern load distribution

considers the inelastic behavior of the ZBF system which is influenced by the stiffness provided by braces, masses and building height, as well as the contribution of the higher modes effects.

3.3 Design methodology of outrigger trusses

As mentioned in Chapter 2, the design of the outrigger truss elements follows the displacement compatibility method initially proposed by Stafford and Salim (1981) and later developed by Hoenderkamp and Bakker (2003). By matching the overall rotation of braced frame with that of outrigger trusses, the top level displacement expression can be computed and limited to the code requirement. Thus, the outrigger truss elements must bring sufficient lateral stiffness to reduce the lateral building deflection.

Prior to the preliminary design of outrigger trusses, the authors of the proposed design method (Stafford and Salim, 1981 and Hoenderkamp and Bakker, 2003) have considered several assumptions as follow:

- The structure is linearly elastic.
- Only axial forces are induced in the columns.
- The outriggers are rigidly connected to the braced frame and pin connected to exterior columns.
- The section properties of the braced frame and columns are uniform through their height.

About the last assumption, according to Stafford Smith and Coull (1991), the factors of concern for a preliminary analysis are predominantly influenced by the structural properties assigned to the lowest floors region. Although it was mentioned (Smith & Coull, Tall building Structures: Analysis and Design, 1991) that an analysis of a structure with uniform cross-sections having the properties computed for the lowest region of the actual structure, gives sufficient accurate results, in this study, the properties of braces, beams and columns sections resulted from design are considered.

3.3.1 Calculation of rotations in outrigger belted braced frame

The preliminary design method that was early proposed by Stafford & Salim(1981) is employed. Referring to their research, it has been shown that the lateral deflection of an outrigger braced concrete shear wall can be represented by a single bending stiffness parameter, and the deformation due to shear forces can be neglected. Later on Hoenderkamp and Snijder (2000) pointed out that the racking shear deformation should be also included in the analysis. They extended the research and replaced the concrete shear wall with steel braced frame, while the system was labeled outrigger belted braced frame. By adding the outriggers, reverse rotations are generated. The restraining moment will causes reverse bending and racking shear rotation in the braced frame as illustrated in Figure 3.6. Compatible rotations are developed in outriggers due to the restraining moment, M_r , and restraining shear F_r developed in outriggers. Moreover, the exterior columns are ac-

tivated to provide reverse rigid body rotation due to their shortening and lengthening under axial loading F_a . The equations for rotation and deflection calculation of ZBF with outrigger trusses are given below.

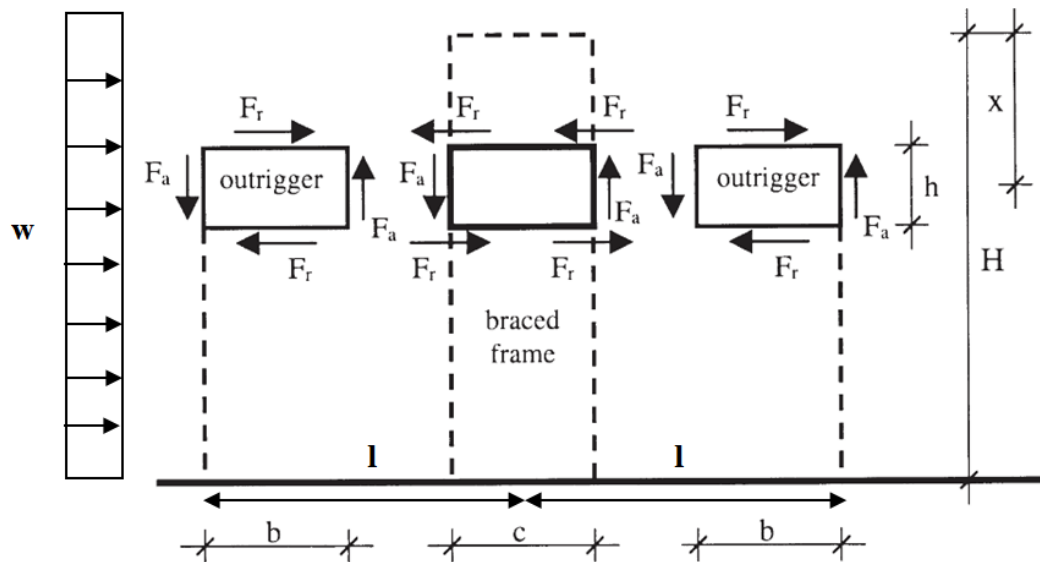


Figure 3.6 Free body diagram of outrigger belted braced frame (Hoenderkamp & Bakker, 2003)

3.3.1.1 Rotations of the braced frame

The main contribution to the lateral deflection of the braced frame is the bending rotation computed directly under the lateral loads which are considered uniformly distributed, w , along the structure height. Accordingly to the method proposed by Hoenderkarp and Bakker (2003), the braced frame is considered as a cantilever beam with a length H and bending stiffness EI_t . The bending rotation is developed due to the axial strain developed in the ZBF's columns and is expressed as:

$$\theta_{t;b;w} = \frac{w(H^3-x^3)}{6EI_t} \quad (3.13)$$

where x is the distance between the top to the central line of the outrigger. The bending stiffness of the brace frame is:

$$EI_t = EA_a c^2 / 2 \quad (3.14)$$

where A_a is the cross-sectional area of the columns in the braced frame at the outrigger level, and c is the span of the braced frame.

The bending rotation is accompanied by the racking shear rotation which is developed due to the axial strain encountered in braces of ZBF. The expression of racking shear rotation is:

$$\theta_{t;s;w} = \frac{wx}{GA_t} \quad (3.15)$$

where GA_t is the racking shear stiffness of the braced frame and is computed as per Figure 3.7 and the equation (3.16), given below.

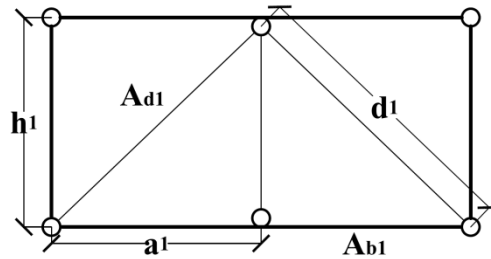


Figure 3.7 Individual segment of the braced frame (after (Hoenderkamp & Bakker, 2003))

$$GA_t = \frac{(2a_1)^2 h_1 E}{\frac{2d_1^3}{A_{d1}} + \frac{(2a_1)^3}{4A_{b1}}} \quad (3.16)$$

Herein, a_l , d_l , and h_l are the relevant dimension of the braced frame, A_{dl} is the cross-sectional area of the brace sections and A_{bl} is the cross-sectional area of the top and bottom beams as shown in Figure 3.7.

As illustrated in Figure 3.6, the outrigger action causes a restraining moment in the brace frame, M_r that can be expressed as:

$$M_r = F_a \times (2b + c) = F_a \times 2l \quad (3.17)$$

where F_a is the restraining force in the exterior columns, l is the distance from exterior columns to the central-line of the braced frame, b is the distance from exterior column to the braced frame interface, and c is the width of the braced frame.

Therefore, the reverse rotation of braced frame caused by restraining moment, M_r can be calculated by analogy with a vertical cantilever beam subjected to M_r at the location of outriggers as given below:

$$\theta_{t;b;Mr} = -\frac{M_r(H-x)}{EI_t} \quad (3.18)$$

In addition, the racking shear rotation in the braced frame due to the restraining moment, M_r , is determined as follow:

$$\theta_{t;s;Fr} = -\frac{M_r}{h_1 \alpha G A_t} \quad (3.19)$$

where the dimensionless parameter is $\alpha = \frac{l}{b}$.

Therefore, by adding the bending and shear rotation of braced frame and subtracted the bending and racking shear rotation due to the restrained moment, M_r , the total rotation of the braced frame at the outrigger level is:

$$\theta_t = \frac{w(H^3-x^3)}{6EI_t} + \frac{wx}{GA_t} - \frac{M_r(H-x)}{EI_t} - \frac{M_r}{h_1\alpha GA_t} \quad (3.20)$$

3.3.1.2 Rotations of outriggers

Two outriggers are employed in line with the ZBF system, such that the ZBF system is located in the middle part as is shown in Figure 3.6. In general the height of the outrigger truss is equal to storey height, h , and each truss panel is formed by a single diagonal as shown in Figure 3.9. Thus, there are two truss panels in the right and left of the braced frame.

Referring to Figure 3.8, for the two outrigger panels added at each side of the braced frame, the bending rotation due to the restraining forces F_r is expressed as:

$$\theta_{r;b;Fr} = \frac{M_r b}{24\alpha EI_o} \quad (3.21)$$

where, EI_o is the bending stiffness of the outrigger. It can be calculated as:

$$EI_o = \frac{EA_{b2}h_2}{2} \quad (3.22)$$

where, A_{b2} is the cross-sectional area of the top and bottom chord of the outrigger truss.

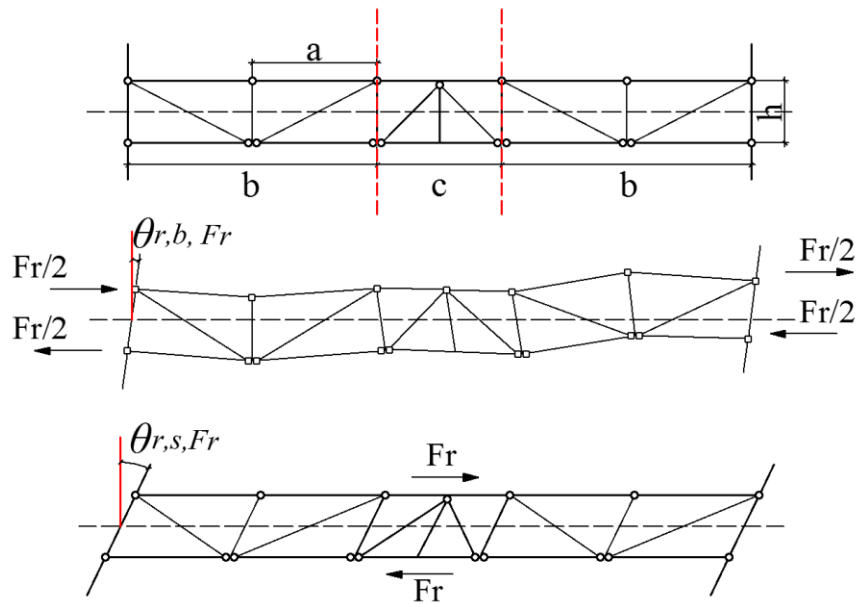


Figure 3.8 Outrigger bending and shear deformations of the ZBF with outrigger truss

The restraining force, F_r causes axial strain in the diagonals of the outrigger trusses, and the generated axial strain in these diagonals implies the shear rotations, expressed below:

$$\theta_{r;s;Fr} = \frac{M_r}{h_2 \alpha G A_0} \quad (3.23)$$

where, $G A_0$ is the total racking shear stiffness of all the segments of two outriggers and can be calculated as per Equations 3.24 and 3.25.

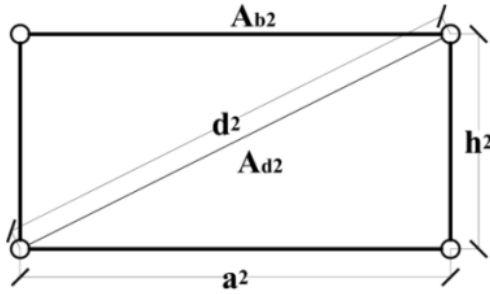


Figure 3.9 Individual panels of the outrigger truss (after (Hoenderkamp & Bakker, 2003))

$$GA_0 = \sum_{i=1}^s GA_i \quad (3.24)$$

$$GA_i = \frac{a_2^2 h_2 E}{\frac{d_2^3}{A_{d2}} + \frac{a_2^3}{A_{b2}}} \quad (3.25)$$

In Eq. 3.24, s represents the total number of panels in the two outriggers and GA_i is the racking shear stiffness of a single panel of length a_2 as shown in Figure 3.9. The expression of GA_i as illustrated in Figure 3.9 is given in Equation 3.25. Besides the rotation caused by the lateral force, restraining moment and restraining shear, three rigid body rotations contribute to the total rotation of the outriggers, while the combined effect is shown in Figure 3.10.

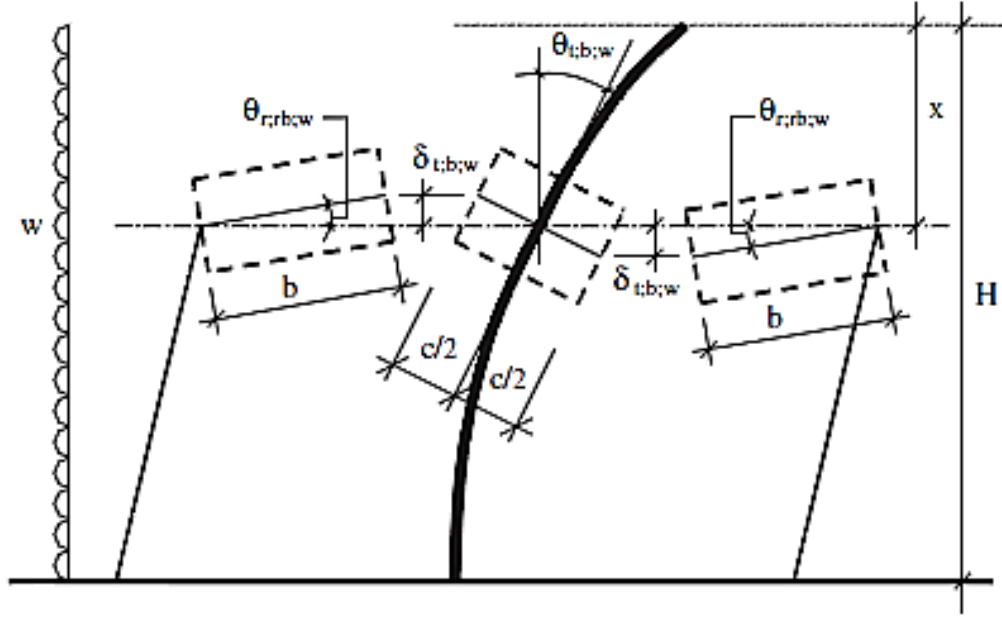


Figure 3.10 Rigid body rotations of outriggers (Hoenderkamp & Bakker, 2003)

The shortening and lengthening of columns in braced frame occurred due to lateral loading, which caused reverse rotation of outrigger trusses which is calculated as:

$$\theta_{r;rb;w} = -\delta_{t;b;w}/b = -\frac{c\theta_{t;b;w}}{2b} = -\left\{\frac{w(H^3-x^3)}{6EI_t}\right\} \frac{c}{2b} \quad (3.26)$$

The second rigid body rotation is caused by axial strain developed in the ZBF's columns due to the restraining moment M_r . In this case the outriggers rotate clockwise and the ZBF counterclockwise as per Figure 3.10, while the rotation is given below:

$$\theta_{r;rb;Mr} = -\left\{\frac{M_r(H-x)}{EI_t}\right\} \frac{c}{2b} \quad (3.27)$$

The third rigid body rotation results due to the shortening and lengthening of the exterior columns when subjected to the restraining force F_a . The expression is given in Eq. (3.28).

$$\theta_{f;c;Fa} = \frac{M_r(H-x)\alpha}{EI_c} \quad (3.28)$$

The stiffness EI_c is the bending stiffness of the exterior columns and can be determined as:

$$EI_c = 2EA_c l^2 \quad (3.29)$$

where A_c is the cross-sectional area of the exterior column.

Therefore, the total rotation of the outriggers can be expressed as:

$$\theta_r = \frac{M_r b}{12\alpha EI_r} + \frac{M_r}{h_2 \alpha GA_r} - \left\{ \frac{w(H^3 - x^3)}{6EI_t} \right\} \left\{ \frac{c}{2b} \right\} + \left\{ \frac{w(H-x)}{EI_t} \right\} \left\{ \frac{c}{2b} \right\} + \frac{M_r(H-x)\alpha}{EI_c} \quad (3.30)$$

3.3.2 Compatibility of rotations

The compatibility of rotations is achieved by matching the rotation of the outrigger, θ_r , with the total rotation of the braced frame θ_t on the center-line of outriggers.

$$\theta_t = \theta_r \quad (3.31)$$

Substitutes the two sides of the above equation by Equations (3.20) and (3.30) yields to:

$$\frac{w(H^3 - x^3)}{6EI_t} + \frac{wx}{\alpha GA_t} = \frac{M_r(H-x)}{EI_t} + \frac{M_r}{h\alpha^2 GA_t} + \frac{M_r b}{24\alpha^2 EI_o} + \frac{M_r}{h\alpha^2 GA_o} + \frac{M_r(H-x)}{EI_o} \quad (3.32)$$

Apparently, the only unknown in Equation (3.32) is the restraining moment M_r . By solving this equation and also inducing two characteristic parameters, S_v and S_h which are given in equations (3.33) and (3.34), the expression of restraining moment M_r is set as per equation (3.35).

$$S_v = \frac{H}{EI_t} + \frac{H}{EI_c} \quad (3.33)$$

$$S_h = \frac{1}{\alpha^2} \left\{ \frac{b}{24EI_o} + \frac{1}{hGA_o} + \frac{1}{hGA_t} \right\} \quad (3.34)$$

$$M_r = \left\{ \frac{w(H^3 - x^3)}{6EI_t} + \frac{wx}{\alpha GA_t} \right\} \left\{ \frac{H}{(H-x)S_v - HS_h} \right\} \quad (3.35)$$

Therefore, the top level deflection can be calculated as:

$$y_{top} = \frac{wH^4}{8EI_t} + \frac{wH^2}{2GA_t} - \frac{M_r(H^2 - x^2)}{2EI_t} - \frac{M_r}{\alpha GA_t} \quad (3.36)$$

In equation (3.36), the first two terms in the right side are the lateral deflection at the top level due to bending and racking shear resulted directly from the lateral forces, the third term is a combination of lateral deflection at outrigger level caused by restraining moment M_r and rotation at outrigger level. The last term represents a horizontal deflection in the ZBF over the storey height at the outrigger level.

The process of selecting outrigger truss sections is based on equation (3.36). By setting the top level displacement as the code limit (2.5% storey height), the restraining moment M_r can be solved. After that, using the compatibility equation (3.32), the only unknown is the cross-sectional area of the outrigger truss elements. These characteristics are necessary to compute the demanded stiffness in order to control the top level drift below the code limit.

3.4 Preliminary design of zipper braced frame structure and outrigger truss

As mentioned in the previous Chapters, a 12- and 16-storey building with and without outrigger trusses, as shown in Figure 3.11 were selected for analysis.

3.4.1 Building description

The plan view of the studied building is shown in Figure 3.11. The structures were assumed to be located on a firm ground site in Victoria, BC, Canada. The occupancy of the building is considered as office building, therefore, the live load is considered as 2.4 kPa according to NBCC 2005 requirement. The live load on the roof level is considered as being the snow load which is calculated as 1.48 kPa . The dead load is considered as 3.4 kPa at the roof level, and 4.5 kPa at the floor level.

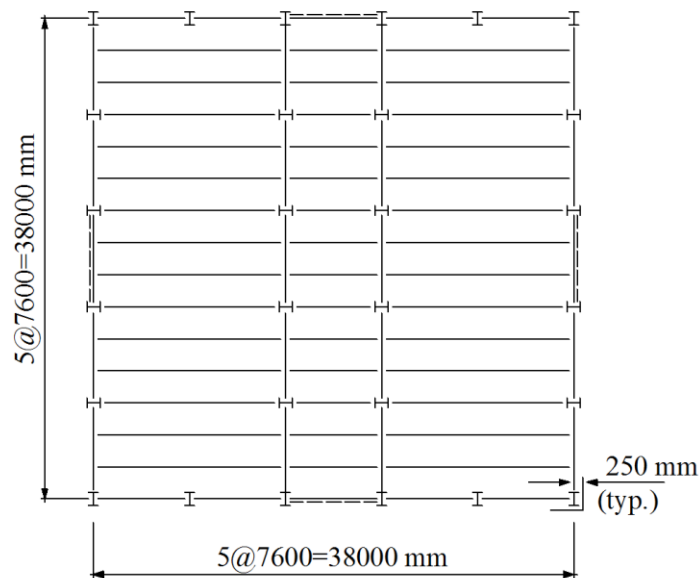


Figure 3.11 Plan view of the studied building

3.4.2 Preliminary design of zipper braced frame

The zipper braced frame is assumed to be at the same performance level as the moderately ductile concentrically braced frames, type MD (Moderately Ductile). Therefore, the ductility related force modification factor, R_d , which reflects the capability of the struc-

ture to dissipated energy through inelastic incursions, is considered as $R_d = 3$ and the over-strength related force modification factor R_o is 1.3. The higher modes effect factor, M_v is calculated based on the building fundamental period. The analytical model of the frame is shown in Figure 3.12. Gravity columns taking into account the P-delta effect were added to the model. The gravity columns are connected to the frame through rigid links which transfer only the lateral force to the frame.

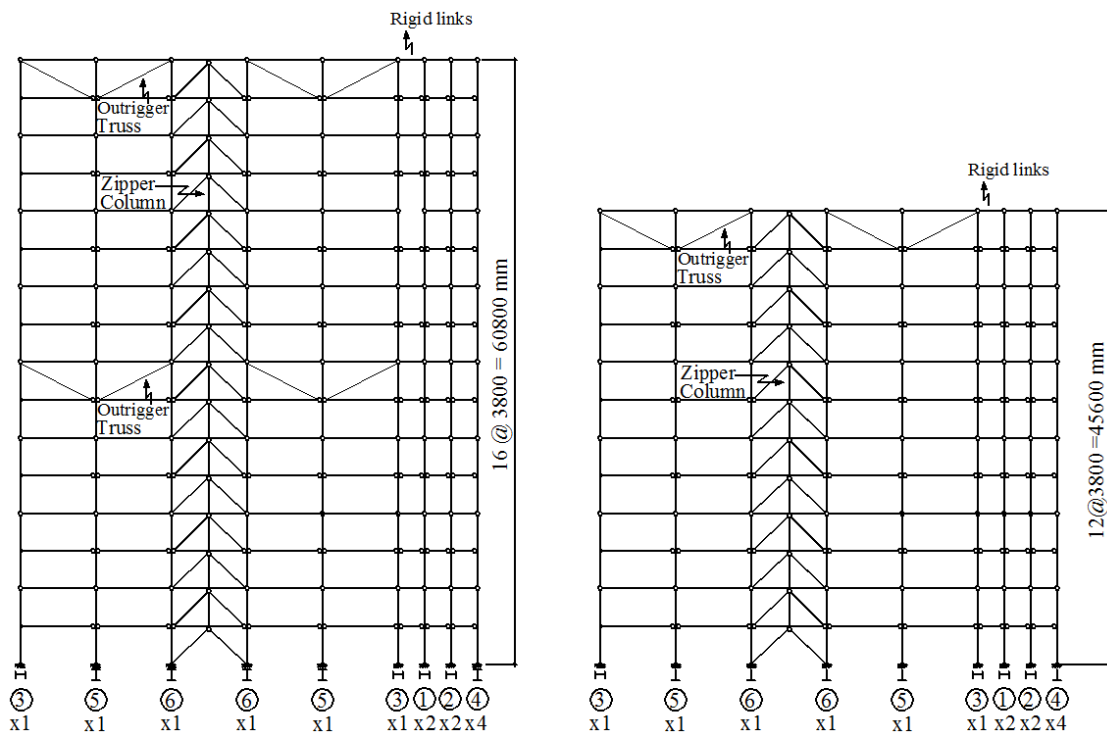


Figure 3.12 Computer model of the 12- and 16-storey ZBF system with outrigger trusses

The braces, beams and columns were designed in Phase I, following the NBCC 2005 requirements. The designed sections are shown in Tables 3.9 and 3.10.

Table 3.9 Phase I: Member sections of the 12-storey building

| Storey | Braces | Beams | Columns |
|--------|-----------------|---------|------------|
| 12 | HSS127x127x8.0 | W360x39 | W200x 52 |
| 11 | HSS152x152x8.0 | W360x51 | W200x 52 |
| 10 | HSS152x152x9.5 | W360x51 | W310x107 |
| 9 | HSS178x178x9.5 | W360x51 | W310x107 |
| 8 | HSS178x178x9.5 | W360x51 | W310x202 |
| 7 | HSS178x178x13 | W360x57 | W310x202 |
| 6 | HSS203x203x 9.5 | W360x57 | WWF350x263 |
| 5 | HSS203x203x 9.5 | W360x57 | WWF350x263 |
| 4 | HSS203x203x 13 | W360x64 | WWF450x409 |
| 3 | HSS203x203x 13 | W360x64 | WWF450x409 |
| 2 | HSS203x203x 13 | W360x64 | WWF550x503 |
| 1 | HSS203x203x 13 | W360x64 | WWF550x503 |

As for preliminary design, a comparison between the zipper forces envelopes as calculated from each one of the four considered load distribution patterns applied on the 12- and 16-storey building without outrigger trusses is shown in Figure 3.13.

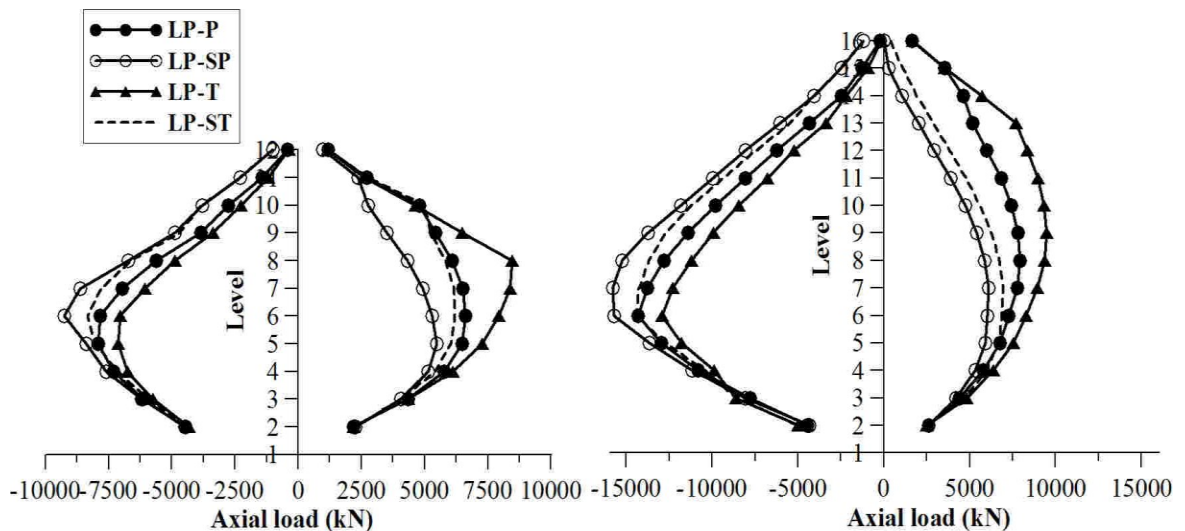


Figure 3.13 Axial force envelopes developed in zippers of the 12- and 16-storey building without outriggers under load patterns: LP-ST; LP-SP; LP-T and LP-P

Table 3.10 Phase I: Member sections of the 16-storey building

| Storey | Braces | Beams | Columns |
|--------|----------------|---------|------------|
| 16 | HSS152x152x9.5 | W360x33 | W310x74 |
| 15 | HSS178x178x8.0 | W360x51 | W310x74 |
| 14 | HSS178x178x9.5 | W360x51 | W310x158 |
| 13 | HSS178x178x13 | W360x57 | W310x158 |
| 12 | HSS178x178x13 | W360x57 | W360x262 |
| 11 | HSS203x203x13 | W360x64 | W360x262 |
| 10 | HSS203x203x13 | W360x64 | WWF450x409 |
| 9 | HSS203x203x13 | W360x64 | WWF450x409 |
| 8 | HSS203x203x13 | W360x64 | WWF500x561 |
| 7 | HSS203x203x13 | W360x72 | WWF500x561 |
| 6 | HSS203x203x13 | W360x72 | WWF550x721 |
| 5 | HSS254x254x13 | W360x91 | WWF550x721 |
| 4 | HSS254x254x13 | W360x91 | WWF650x864 |
| 3 | HSS254x254x13 | W360x91 | WWF650x864 |
| 2 | HSS254x254x13 | W360x91 | WWF650x864 |
| 1 | HSS254x254x13 | W360x91 | WWF650x864 |

When the load distribution pattern LP-SP for the 12-storey is considered, the envelope of the axial compressive force is too large and the axial tension force is relatively too small. This trend is similar for the 16-storey as well. On the other hand, a similar envelope was obtained under the consideration of the LP-T pattern. In light of this, these load distribution patterns LP-SP and LP-T were not selected for design. The remaining load distribution patterns, potentially to be used in the zipper column design, are LP-ST (sequential triangular) and LP-P (parabolic). In the compression side for both 12- and 16-storey buildings, the larger force is generated under the LP-ST pattern than under the

LP-P pattern. It is noted that these two envelopes overlapped at the lower half of the structure and slowly diverged in the upper part. In the tension side, for the 12-storey building, the LP-ST pattern and the LP-P pattern are very close, but still LP-P pattern is slightly larger in the middle floors and is proposed for design. Regarding the 16-storey building, the axial tensile force envelope of zipper columns is larger under the LP-P pattern than that under the LP-ST pattern. Thus, it is concluded that the LP-ST pattern is recommended to be considered for designing the zipper columns under the axial compressive envelope and the LP-P for the tensile envelope. Preliminary designs of zippers are carried out following the methodology discussed in this chapter, and the sections chosen are as shown in Table 3.11.

3.4.3 Preliminary design of outrigger truss

As mentioned early in this chapter, the preliminary analysis method of outrigger truss is based on a compatibility concept. According to this method, by matching the rotations of the braced frame and outriggers, the top level deflection of the building can be calculated by using equation (3.36). Inspired by this, having all other parameters unchanged but setting a limit of the top level deflection, it is possible to conduct a reverse derivation to determine the cross-sectional area of the outrigger truss such that it provides sufficient stiffness to reduce the deflection at the top floor level.

Table 3.11 Zipper column sections for 12- and 16-storey buildings

| Storey | Zipper columns– 16storey bldg. | Zipper columns – 12storey bldg. |
|--------|--------------------------------|---------------------------------|
| 16 | W310x60 | |
| 15 | W310x86 | |
| 14 | W310x129 | |
| 13 | W310x143 | |
| 12 | W360x179 | HSS152x152x8.0 |
| 11 | W360x216 | HSS178x178x13 |
| 10 | W360x262 | HSS254x254x13 |
| 9 | W360x314 | HSS305x305x13 |
| 8 | W360x314 | (2) HSS254x254x 13* |
| 7 | W360x347 | (2) HSS254x254x 13* |
| 6 | W360x347 | (2) HSS254x254x 13* |
| 5 | W360x314 | (2) HSS254x254x 13* |
| 4 | W360x262 | (2) HSS254x254x 13* |
| 3 | W360x216 | (2) HSS254x254x9.5* |
| 2 | W310x143 | HSS305x305x 13 |
| 1 | - | - |

* Built-up sections

Referring to equation (3.36), the only parameters associated to the properties of outrigger truss members is the structural characteristic parameter, S_h (Eq. 3.34). If S_h is known, by using Equations (3.24) and (3.25), the cross-sectional area of outrigger truss members, A_{d2} can be calculated. Therefore, the top level deflection is set as the code limit, which is $2.5\%hs$ and the M_r is calculated from equation (3.36).

Rewrite equation 3.36 as below:

$$M_r = \left(\frac{wH^4}{8EI_t} + \frac{wH^2}{2GA_t} - y_{top} \right) / \left(\frac{(H^2-x^2)}{2EI_t} - \frac{1}{\alpha GA_t} \right) \quad (3.37)$$

where “ $\frac{wH^4}{8EI_t} + \frac{wH^2}{2GA_t} - y_{top}$ ” is the required reduction of the top level deflection, Δ_{top} .

According to Hoenderkamp and Bakker (2003), the first two terms of the right side of equation 3.37 represents the free deflection at the top level of the building. In this study, the aforementioned two terms: $\frac{wH^4}{8EI_t} + \frac{wH^2}{2GA_t}$ are replaced by the values of top level deflection outputed from Drain-2Dx models. Taking the maximum values for consideration, the free displacement at the top level of subjected buildings, y_{free} is equal to 1.150m for 12-storey building without outriggers; and is equal to 1.543m for 16-storey building without outriggers. Therefore, the required reduction of top deflection, Δ_{top} can be calculated.

Meanwhile, rewrite Equation (3.35) as below,

$$\left\{ \frac{H}{(H-x)S_v - HS_h} \right\} = M_r / \left\{ \frac{w(H^3-x^3)}{6EI_t} + \frac{wx}{\alpha GA_t} \right\} \quad (3.38)$$

Since M_r is calculated in equation 3.37, by using equation 3.14 for EI_t , equation 3.16 for GA_t , and equation 3.33 for S_v , the only unknown is S_h in equation 3.34. Therefore, S_h can be solved.

Therefore, rewrite equation 3.34 as below,

$$GA_0 = \frac{1}{h(S_h \alpha^2 - \frac{b}{24EI_0} - \frac{1}{hGA_t})} \quad (3.39)$$

After S_h is found from equation (3.38), the total racking shear stiffness of two outriggers, GA_0 can be calculated by using equations(3.39) and (3.24). Thus, the racking shear stiffness of individual outrigger segment, GA_i can be found.

Eventually, rewrite equation 3.25 as below,

$$A_{d2} = \frac{d_2^3}{\frac{a_2^2 h_2 E}{GA_i} - \frac{a_2^3}{A_{b2}}} \quad (3.40)$$

Because GA_i is calculated in equation 3.39, by using equation 3.40, the cross-sectional area of outriggers, A_{d2} can be determined from equation (3.40).

The aforementioned design parameters of outrigger truss members are summarized in Table 3.12 given below.

Table 3.12 Design parameters of outrigger truss

| storey | cases | y_{top} | Free | Required | Restraining | S_h | GA_0 | A_d |
|--------|-----------|-----------|-------------------|----------------|-------------|----------|----------|---------|
| | | | delfection | deflection | | | | |
| | | | at the top | reduction, | M_r | | | |
| | | | level, y_{free} | Δ_{top} | | | | |
| | | [m] | [m] | [m] | [kN*m] | | | |
| 12 | Top-truss | 1.14 | 1.15 | 0.01 | 2.67E+03 | 5.44E-07 | 1.06E+06 | 4556.33 |
| 16 | Top truss | 1.52 | 1.543 | 0.023 | 5.15E+03 | 4.78E-07 | 1.31E+06 | 5954.27 |
| | Mid-truss | 1.52 | 1.543 | 0.023 | 7.21E+03 | 5.30E-07 | 5.32E+05 | 2055.32 |
| | Two truss | 1.52 | 1.543 | 0.0115 | 2.57E+03 | 1.14E-06 | 2.14E+05 | 775.72 |
| | | | | 0.0115 | 3.61E+03 | 1.13E-06 | 1.84E+05 | 663.29 |

Moreover, the preliminary design sections of outrigger trusses are given in Table 3.13.

Table 3.13 Outrigger truss sections for 12- and 16-storey buildings

| Storey | Cases | Outrigger truss sections | |
|--------|-------------|--------------------------|-----------------------|
| | | External truss pannel | Internal truss pannel |
| 12 | Top truss | HSS152x152x9.5 | HSS152x152x9.5 |
| 16 | Top truss | HSS203x203x8.0 | HSS203x203x8.0 |
| | Two trusses | HSS152x152x9.5 | HSS152x152x9.5 |
| | | HSS152x152x9.5 | HSS152x152x9.5 |

3.5 Design summary

The seismic design and buildings characteristics are presented in Table 3.16. The periods of vibration in the first three modes T_1 , T_2 and T_3 , computed from the elastic dynamic analysis by using the modal response spectrum method as implemented in ETABS are given in Table 3.16. Also, the periods of vibration in the first three modes T_1 , T_2 , and T_3 resulted from a nonlinear time-history analysis conducted by using finite element program: Drain-2DX are given in the same table. A good correlation between the structure periods computed in Drain-2DX, ETABS, and the equivalent static procedure was observed. As is shown in Table 3.16, for the 12-storey building, the difference between the design fundamental period T_a and that computed in Drain-2DX, T_1 , is around 15%, but decreases to 7.5% after adding one outrigger truss at the roof level. For the 16-storey building, the difference between T_a and T_1 is 19%, and decreases to 11% after adding one outrigger truss at the roof level. Then, by adding one more outrigger truss at the mid-height of the building, the difference decreases to 1.2%.

To summarize, the member sections of the 12- and 16-storey buildings with and without outrigger trusses are shown below in Tables 3.14 and 3.15.

Table 3.14 Member sections of the 12-storey building

| Storey | Braces | Beams | Columns | Zippers | Outriggers |
|--------|----------------|---------|------------|---------------------|----------------|
| 12 | HSS127x127x8.0 | W360x39 | W200x52 | HSS152x152x8.0 | HSS152x152x9.5 |
| 11 | HSS152x152x8.0 | W360x51 | W200x52 | HSS178x178x 13 | |
| 10 | HSS152x152x9.5 | W360x51 | W310x107 | HSS254x254x 13 | |
| 9 | HSS178x178x9.5 | W360x51 | W310x107 | HSS305x305x 13 | |
| 8 | HSS178x178x9.5 | W360x51 | W310x202 | (2) HSS254x254x13** | |
| 7 | HSS178x178x 13 | W360x57 | W310x202 | (2) HSS254x254x13** | |
| 6 | HSS203x203 9.5 | W360x57 | WWF350x263 | (2) HSS254x254x13** | |
| 5 | HSS203x203x9.5 | W360x57 | WWF350x263 | (2) HSS254x254x13** | |
| 4 | HSS203x203x 13 | W360x64 | WWF450x409 | (2) HSS254x254x13** | |
| 3 | HSS203x203x 13 | W360x64 | WWF450x409 | (2)HSS254x254x9.5** | |
| 2 | HSS203x203x 13 | W360x64 | WWF550x503 | HSS305x305x 13 | |
| 1 | HSS203x203x 13 | W360x64 | WWF550x503 | - | |

** Built-up section

Table 3.15 Member sections of the 16-storey building

| Storey | Braces* | Beams | Columns | Zippers | Outriggers* | |
|--------|------------|---------|------------|----------|-------------|------------|
| | | | | | Top | Two |
| 16 | HSS152x9.5 | W360x33 | W310x74 | W310x60 | HSS203x8.0 | HSS152x9.5 |
| 15 | HSS178x8.0 | W360x51 | W310x74 | W310x86 | | |
| 14 | HSS178x9.5 | W360x51 | W310x158 | W310x129 | | |
| 13 | HSS178x 13 | W360x57 | W310x158 | W310x143 | | |
| 12 | HSS178x 13 | W360x57 | W360x262 | W360x179 | | |
| 11 | HSS203x 13 | W360x64 | W360x262 | W360x216 | | |
| 10 | HSS203x 13 | W360x64 | WWF450x409 | W360x262 | | |
| 9 | HSS203x 13 | W360x64 | WWF450x409 | W360x314 | | |
| 8 | HSS203x 13 | W360x64 | WWF500x561 | W360x314 | | HSS152x9.5 |
| 7 | HSS203x 13 | W360x72 | WWF500x561 | W360x347 | | |
| 6 | HSS203x 13 | W360x72 | WWF550x721 | W360x347 | | |
| 5 | HSS254x 13 | W360x91 | WWF550x721 | W360x314 | | |
| 4 | HSS254x 13 | W360x91 | WWF650x864 | W360x262 | | |
| 3 | HSS254x 13 | W360x91 | WWF650x864 | W360x216 | | |
| 2 | HSS254x 13 | W360x91 | WWF650x864 | W310x143 | | |
| 1 | HSS254x 13 | W360x91 | WWF650x864 | - | | |

*Square tubular sections: width x thickness

Table 3.16 Seismic design and buildings characteristics

| Storey | Equivalent static force procedure | | | | | | Dynamic analysis | | | | | | |
|------------------------|-----------------------------------|--------|------|-------|---------|----------|------------------|-------|-------|-----------|-------|-------|-------|
| | Height | W | Ta | S(Ta) | V/frame | Ft/frame | ETABS | | | Drain-2DX | | | |
| | [m] | [kN] | [s] | [g] | [kN] | [kN] | T1 | T2 | T3 | T1 | T2 | T3 | T1/Ta |
| 12-ZBF | 45.6 | 87035 | 2.28 | 0.17 | 2490 | 397 | 2.508 | 0.797 | 0.418 | 2.61 | 0.802 | 0.427 | 1.145 |
| 12 ZBF-RT | 45.6 | 87105 | 2.28 | 0.17 | 2491 | 398 | 2.399 | 0.725 | 0.391 | 2.45 | 0.745 | 0.4 | 1.074 |
| 16 ZBF | 60.8 | 116525 | 3.04 | 0.13 | 3334 | 709 | 3.471 | 1.047 | 0.531 | 3.615 | 1.053 | 0.551 | 1.189 |
| 16 ZBF-RT | 60.8 | 116595 | 3.04 | 0.13 | 3336 | 710 | 3.369 | 0.971 | 0.515 | 3.38 | 0.981 | 0.524 | 1.112 |
| 16 ZBF-RT&M | 60.8 | 116719 | 3.04 | 0.13 | 3339 | 710 | 2.916 | 0.964 | 0.474 | 3.077 | 0.981 | 0.5 | 1.012 |

CHAPTER FOUR

Nonlinear Time-History Analysis of ZBF Building Structures with and without Outrigger Trusses

The studied 12- and 16-storey zipper braced frame (ZBF) structures are designed and illustrated in Chapter 3. According to Tremblay and Tirca (2003), when the higher modes effect influences the ZBF behaviour, large axial force is triggered in zipper columns at upper floors and dynamic instability may occur after the full-height zipper mechanism is formed. Therefore, to improve the seismic performance of ZBF structures, it is proposed to add an outrigger truss at the roof level. However, the location of outrigger truss could be optimized such that a uniform distribution of interstorey drift over the structure height is obtained. In this light, researchers have proposed (Hoenderkamp et al., 2003) to select the optimum location for outrigger trusses among the upper one third floors. In this study, the design of the outrigger truss is conducted by applying the compatibility concept proposed by Taranath (1974) and by using the graphical method developed by Hoenderkamp (2003). The purpose of this study is not extended to find the optimal location of outrigger trusses added to the 12- and 16-storey ZBF systems, but to analyze the response of the ZBF system when outrigger trusses are added to the external zipper braced frame as shown in Figure 3.11. Regarding this, the 12-storey ZBF system equipped with outriggers at the roof

level is labeled ZBF–RT; the 16-storey ZBF equipped with roof trusses is labeled ZBF–RT and the 16-storey ZBF system equipped with outriggers at the roof floor level and at building mid-height is labeled ZBF–M&RT. To study the seismic response of the designed ZBFs with and without outrigger trusses located in Victoria, BC, three ensembles of seismic ground motions such as: crustal, subduction and near-field with forward directivity are considered, while the total number of selected records is 21. Thus, each one of the three ensembles contains seven ground motions. A detailed description of the analytical models is provided and the results of nonlinear time-history dynamic analysis are presented in this chapter. All nonlinear time-history analyses were conducted using the Drain 2DX software (Sabelli 2001, Tirca & Tremblay 2003, Leon & Yang 2003, Chen, 2011, and Tirca & Chen 2012), although Chen (2011) has considered Drain 2DX and OpenSees software.

4.1 Zipper braced frame & Outrigger truss modeling

The Zipper braced frame system was proposed by Khatib and Mahin (1988) with the aim to improve the behavior of CBFs that are usually prone to soft-storey mechanism formation. As noted in Chapter 2, there are differences between the design method initially proposed by Tremblay and Tirca (2003) and Leon and Yang (2003). In the first case, the zipper column was designed to behave in elastic range, while in the second case a truss was added at the top of the structures, the top floor braces were designed to respond in elastic range and zipper columns were allowed to yield in tension. In this study, the design method

proposed by Tremblay and Tirca (2003) and later on refined by Chen (2011) and Tirca and Chen (2012) is employed.

Prior to numerical modeling of ZBF with and without outrigger trusses, the following assumptions have been made:

- For simplicity, the building sample has a symmetrical layout as given in Figure 3.11 and the accidental in plan torsion was omitted.
- In Drain 2DX, the zipper braced frame is modeled as a 2D frame. Therefore, the out-of-plane buckling of brace elements was neglected.
- To take into account the effect of the overall stiffness, all gravity columns belonging to half of the building (there are two ZBF systems in the N-S direction and two in the E-W direction) were also considered in the 2D layout of the braced frame. These gravity columns were connected to the braced frame through rigid links.
- All the connections within the structures are assumed to be pin connections, which include the brace end connections, beam to column connections, column ends connections. However, columns were considered continue over two stories.
- The outrigger truss members are pin-connected to the external gravity columns and columns of ZBF system.

Thus, the mathematical model of the ZBF system is illustrated in Figure 4.1 and the model of ZBF system equipped with outrigger trusses is shown in Figure 4.2.

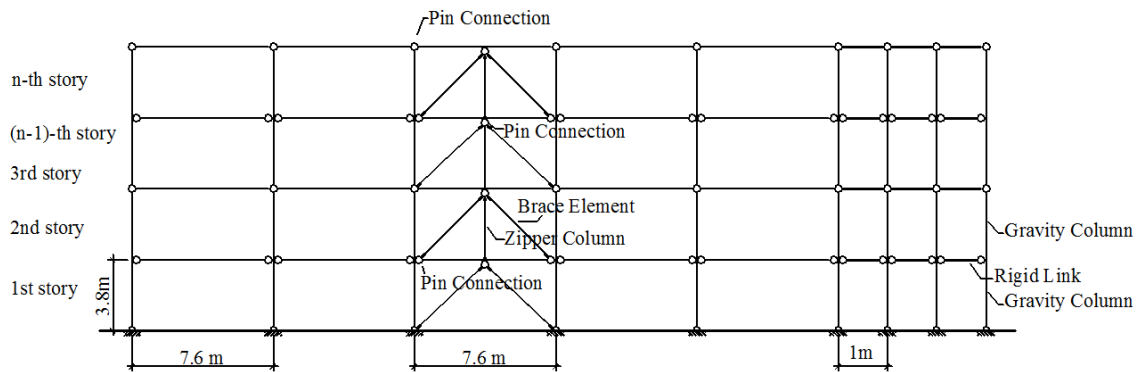


Figure 4.1 Model of the ZBF system in Drain 2DX

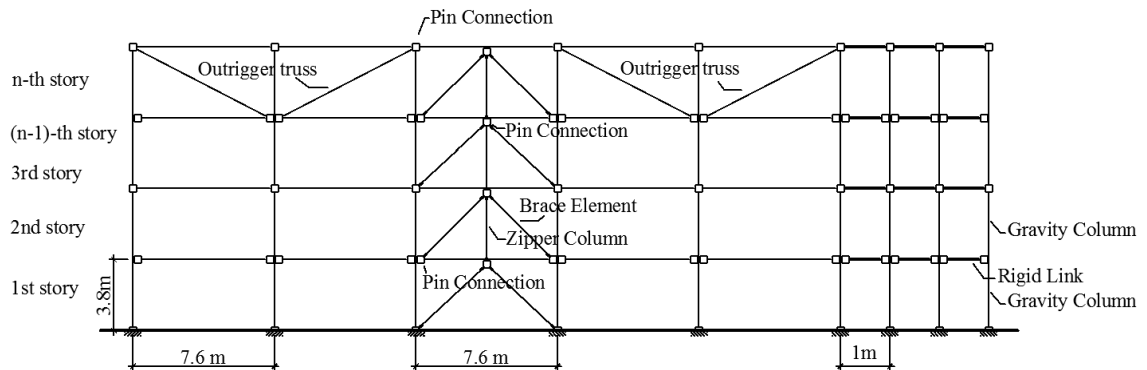


Figure 4.2 Model of the ZBF system equipped with outrigger trusses in Drain 2DX

4.2 Selection and scaling procedure of ground motions

4.2.1 Ground motion selection

As stated above, seven ground motions were selected for each ensemble. This number of records is in agreement with ASCE/SEI –7 procedure and it allows users to consider the mean response of the studied structures. It is mentioned that the crustal and subduction ensemble characterize the seismic hazard of Victoria region. Herein, the near-field ensemble is added for the comparison purpose. Moreover, it is also suggested that selecting records by their acceleration spectral shape close to the design spectral acceleration de-

mand may further increase the accuracy and efficiency of the procedure (Reyes & Kalkan, 2011).

In this light, the crustal ensemble contains records selected from moderate to large crustal earthquakes with magnitude ranged from M6.5 to M7.5 and source-to-site distances ranged from low to intermediate. All records were selected from the PEER database (http://peer.berkeley.edu/peer_ground_motion_database). The subduction ensemble is composed of 6 records selected from the mega-thrust Tohoku earthquake (March 11, 2011) and one simulated record (Atkinson and Maccis, 2010). As noted by Atkinson (2009), a potential mega-thrust earthquake with magnitude ranged from M8 to M9 and longer duration (around 300 s) may happen in the Cascadia subduction zone. The Near-field group consists of 7 ground motions characterized by pulse effect and forward directivity. In this study, the 7 crustal records were selected from a group of 21 randomly chosen Californian records, the 6 subduction records were selected from a group of 18 Tohoku records and the simulated record from 6 artificial ground motions as proposed by Atkinson and Macias (2009). The artificial subduction record was adjusted against the strong Japan's subduction ground motions recorded during the M8.3 Tokachi Oki earthquake, occurred on September 23th, 2003 (Atkinson and Macias, 2009). Although the simulations made for distances larger than 84 km from the fault and firm soil conditions (site class C) are characterized by low ($\sim 0.1g$) peak ground acceleration (PGA), these selected ground motions contains larger energy content and have long durations. Records selected from Tohoku earthquake

show $PGA \approx 0.15g$ at epicentral distances around 350 km and higher $PGA \approx 0.6g$ at distances larger than 100 km. The near-field ensemble is composed of 7 near-field records that were selected among a group of 12 records.

According to Reyes and Kalkan (2011), the selection of ground motions was made such that to minimize the discrepancy between the scaled spectrum of each record and the uniform hazard spectrum over the period of interest ($0.2T_1 \sim 1.5T_1$). The relevant characteristics such as magnitude – M_w , the hypocentral distance – R , the peak ground acceleration – PGA , the peak ground velocity – PGV , the PGV/PGA ratio as a measure of the frequency content, the Trifunac duration – t_d , and the total duration of the selected records – t , are summarized in Table 4.1.

Table 4.1 Ground motion characteristics

| No. | Event | M _w | R (km) | Station | Comp. (degree) | PGA (g) | PGV (m/s) | PGV PGA | t _d (s) | t (s) |
|----------------------------------|---------------------------------|----------------|-----------|-------------------------------|-------------------|------------|--------------|------------|-----------------------|----------|
| Crustal ground motions | | | | | | | | | | |
| C1 | Oct.18, 1989 Loma Prieta | 6.93 | 19.9 | Anderson Dam Down- str. | 250 | 0.244 | 0.203 | 0.83 | 10.51 | 40.00 |
| C2 | Oct.18, 1989 Loma Prieta | 6.93 | 19.3 | Presidio | 90 | 0.200 | 0.320 | 1.60 | 5.70 | 30.00 |
| C3 | Oct.15, 1979 Imperial Valley | 6.53 | 15.2 | Cerro Prieto | 147 | 0.170 | 0.120 | 0.71 | 19.70 | 63.74 |
| C4 | Jan.17, 1994 Northridge | 6.70 | 17.3 | St. Monica City Hall | 360 | 0.369 | 0.253 | 0.68 | 10.72 | 40.00 |
| C5 | Jan.17, 1994 Northridge | 6.70 | 20.1 | Castaic, Old Ridge Route | 90 | 0.568 | 0.520 | 0.92 | 9.10 | 40.00 |
| C6 | Apr.25, 1992 Cape Mendacino | 7.00 | 40.2 | Eureka | 90 | 0.178 | 0.280 | 1.57 | 18.80 | 89.00 |
| C7 | Apr.13 1949 Western Wash. | 7.10 | 76.0 | Olympia Test Lab | 86 | 0.280 | 0.170 | 0.61 | 18.80 | 89.06 |
| Near-field ground motions | | | | | | | | | | |
| N1 | Jan.17, 1995 Kobe | 6.9 | 0.6 | JMA | 90 | 0.83 | 0.92 | 1.08 | 8.38 | 48.00 |
| N2 | Jan.17, 1995 Kobe | 6.9 | 1.5 | Takatori | 90 | 0.61 | 1.27 | 2.08 | 9.94 | 40.96 |
| N3 | Jan.17, 1994 Northridge | 6.7 | 7.1 | Rinaldi | 228 | 0.84 | 1.75 | 2.02 | 7.05 | 14.95 |
| N4 | Jan.17, 1994 Northridge | 6.7 | 7.2 | Newhall | 90 | 0.58 | 1.18 | 2.03 | 5.92 | 60.00 |
| N5 | Jan.17, 1994 Northridge | 6.7 | 9.9 | Sylmar County Hosp. | 90 | 0.65 | 1.08 | 1.62 | 7.08 | 60.00 |
| N6 | Jan.17, 1994 Northridge | 6.7 | 6.4 | Sylmar Converter Sta- tion | 52 | 0.60 | 1.22 | 2.03 | 11.99 | 44.00 |
| N7 | Dec.23, 1985 Nahanni, | 6.8 | 2.5 | Site 1 | 10 | 0.98 | 0.46 | 0.50 | 7.90 | 20.56 |
| Subduction ground motions | | | | | | | | | | |
| S1 | March 11, 2011 Tohoku | 9.0 | 156.0 | IWT007E | E-W | 0.66 | 0.29 | 0.44 | 80.96 | 300.0 |
| S2 | March 11, 2011 Tohoku | 9.0 | 201.0 | FKSH19N | N-S | 0.61 | 1.27 | 2.08 | 89.07 | 300.0 |
| S3 | March 11, 2011 Tohoku | 9.0 | 272.0 | IBRH16E | E-W | 0.57 | 0.31 | 0.55 | 66.91 | 300.0 |
| S4 | March 11, 2011 Tohoku | 9.0 | 357.0 | CHB001N | N-S | 0.14 | 0.28 | 2.00 | 83.78 | 300.0 |
| S5 | March 11, 2011 Tohoku | 9.0 | 376.0 | TKY027E | E-W | 0.16 | 0.28 | 1.90 | 93.75 | 300.0 |
| S6 | March 11, 2011 Tohoku | 9.0 | 380.0 | TKY026E | E-W | 0.16 | 0.28 | 1.90 | 99.06 | 300.0 |
| S7 | Simulated Cascadia | 9.0 | 84.0 | VIC084E | E-W | 0.10 | 0.28 | 2.80 | 38.06 | 262.0 |

4.2.2 *Scaling ground motions*

The selected ground motions are required to be scaled to match the design spectrum in a period range between $0.2T_1$ and $1.5T_1$, where T_1 is the fundamental period of the structure.

Several scaling procedures could be found in literature: (Kalkan & Chopra 2010; Kalkan & Chopra 2011, Baker 2010). In addition to the mentioned procedures, the NBCC 2005 requires that the scale ground motions to fit the ordinate of the uniform hazard spectrum, UHS which corresponds to the fundamental period $S(T_1)$, as well as the UHS should match or be above of all points corresponding to higher modes. In this study the ASCE/SEI -7 procedure is adopted. Accordingly, the mean obtained from at least 7 acceleration spectra must fit the UHS over the period of interest $0.2T_1 - 1.5T_1$. The boundary of the shorter period means higher modes, while the boundary of the longer period means the degradation of stiffness due to the building's incursions in the plastic range. In addition, Beyer and Bommer (2007) have suggested selecting only one record's component for analyzing a 2-D building's model. As mentioned earlier in this chapter, 21 crustal Californian records were ranked based on the fundamental period of the studied buildings and in accordance to Reyes and Kalkan methodology (2010). Thus, the fundamental periods of the 12-storey ZBF and 12-storey ZBF-RT is $T_1 = 2.61s$ and $T_1 = 2.45s$ respectively. For the 16-storey ZBF building, the fundamental period is $T_1 = 3.615s$, and for the 16-storey ZBF-RT and ZBF-M&RT the fundamental period is $T_1 = 3.378s$ and $T_1 = 3.1s$, respectively. By using Reyes and Kalkan methodology, the record with the lowest scaling factor

is ranked the highest. The fundamental periods of each configuration in 12- and 16-storey ZBF are shown in Table 4.2. The scaled spectrums of the selected ground motions are plotted together with the UHS for Victoria region and are illustrated in Figure 4.3 and 4.4 for the 12-storey building and in Figures 4.5 to 4.7 for the 16-storey building. Meanwhile, for each ground motion ensemble, the mean of the scaled response spectrums is also illustrated in the plots. In addition, the scaling factors (SF) for the selected ground motions of 12-storey and 16-storey are given in Table 4.3 and Table 4.4.

Table 4.2 The fundamental periods of 12- and 16-storey ZBF with different configurations of outrigger trusses

| Type of Building | Type of configuration | Fundamental period, T_1 (s) |
|------------------|-----------------------|-------------------------------|
| 12-storey | ZBF | 2.61 |
| | ZBF-RT | 2.45 |
| 16-storey | ZBF | 3.61 |
| | ZBF-RT | 3.38 |
| | ZBF-M&RT | 3.08 |

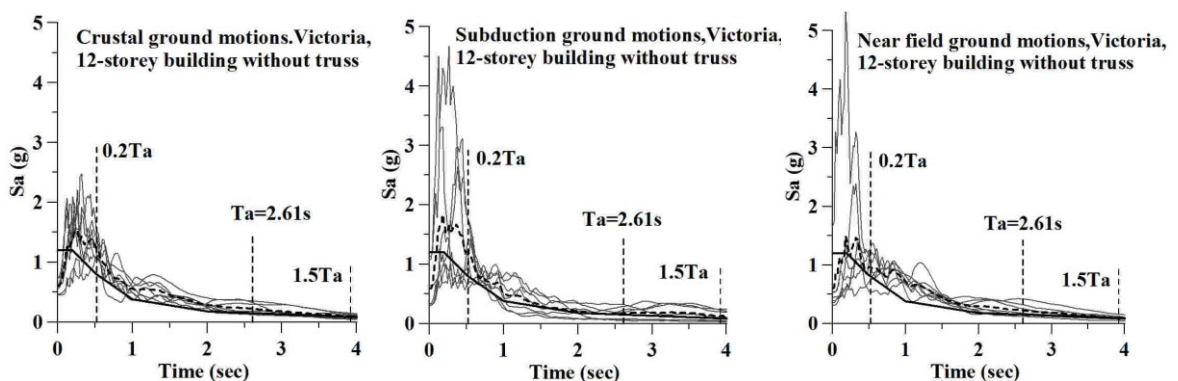


Figure 4.3 Design and scaled acceleration response spectrum for the 12-storey ZBF building

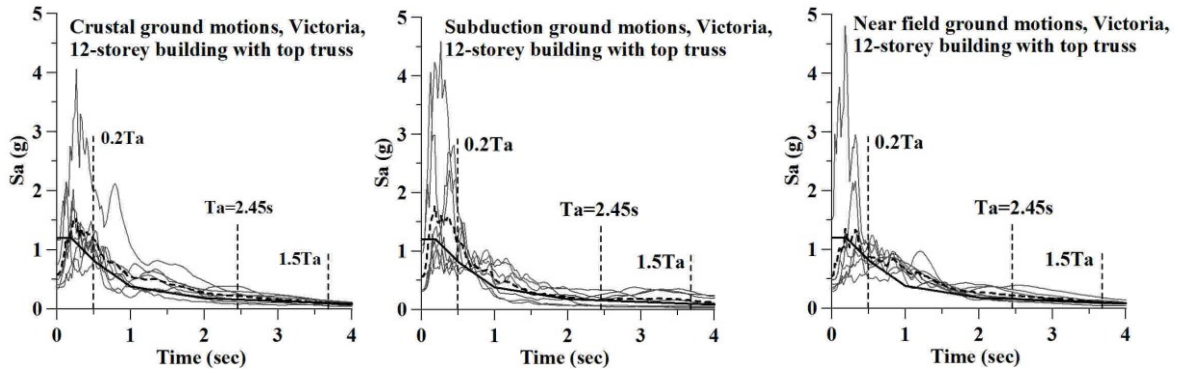


Figure 4.4 Design and scaled response spectrum of the selected accelerograms for 12storey ZBF-RT building

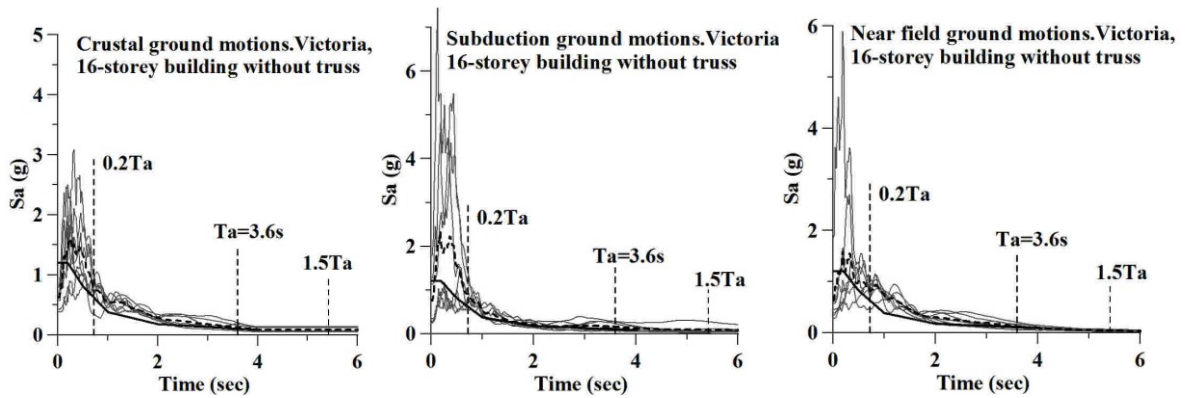


Figure 4.5 Design and scaled response spectrum of the selected accelerograms for the 16-storey ZBF building

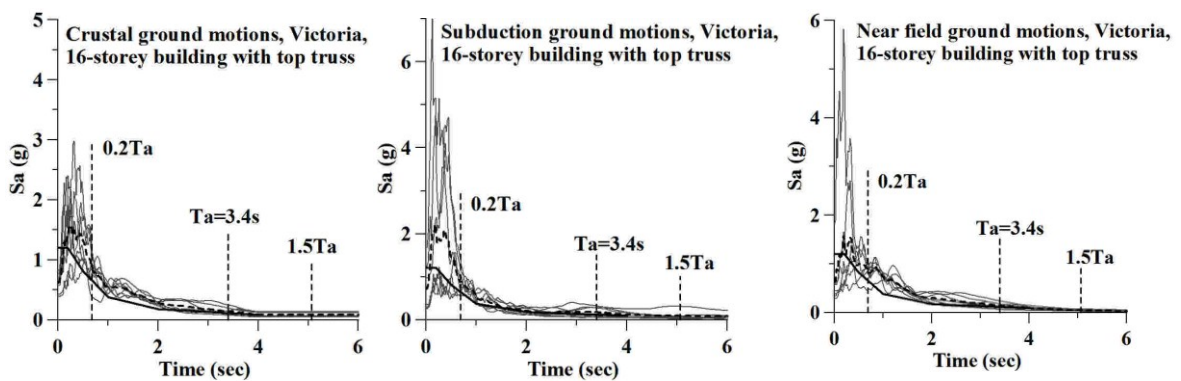


Figure 4.6 Design and scaled response spectrum of the selected accelerograms for 16-storey ZBF-RT building

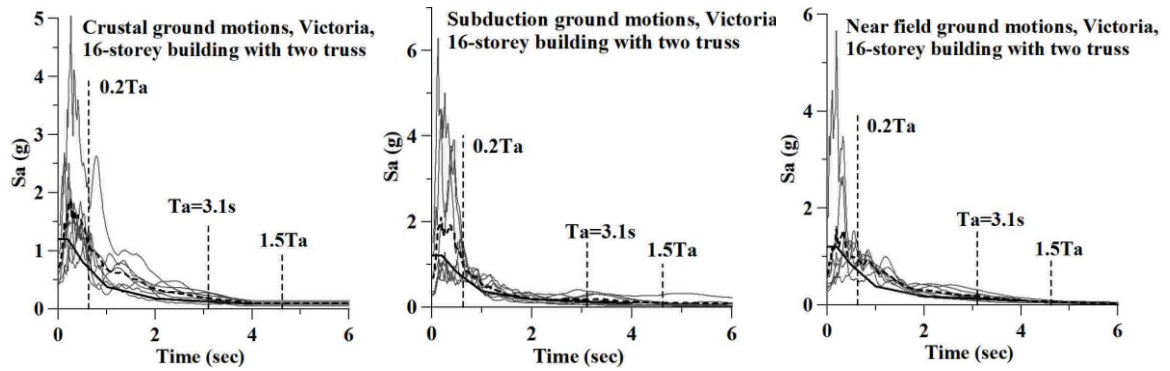


Figure 4.7 Design and scaled response spectrum of the selected accelerograms for 16-storey ZBF-M&RT building

Table 4.3 Scaling factors of selected ground motions for analyzing the 12-storey buildings

| No. | Event | 12-storey ZBF bldg. | | 12-storey ZBF-RT bldg. | |
|-----|----------------------------------|---|--------|---|--------|
| | | $T_{\text{range}}: 0.52 - 3.92\text{s}$ | | $T_{\text{range}}: 0.49 - 3.68\text{s}$ | |
| | | SF | PGA(g) | SF | PGA(g) |
| C1 | Anderson Dam, Loma Prieta | 2.325 | 0.567 | 1.886 | 0.494 |
| C2 | Presidio, Loma Prieta | 2.355 | 0.472 | 2.073 | 0.422 |
| C3 | Cerro Prieto, Imperial Valley | 3.698 | 0.639 | 3.073 | 0.541 |
| C4 | St. Monica City Hall Northridge | 1.989 | 0.734 | 1.760 | 0.666 |
| C5 | Castaic Old Ridge R., Northridge | 0.981 | 0.627 | 0.986 | 0.569 |
| C6 | Eureka, Cape Mendacino | 2.482 | 0.447 | 2.299 | 0.408 |
| C7 | Olympia Test Lab, West. Wash | 2.618(2.346)* | 0.742 | 2.324 | 0.661 |
| S1 | IWT007E, Tohoku | 1.685 | 1.112 | 1.519 | 1.002 |
| S2 | FKSH19N, Tohoku | 1.031 | 0.629 | 0.934 | 0.570 |
| S3 | IBRH16E, Tohoku | 1.957(1.607)* | 1.115 | 1.923(1.753)* | 1.096 |
| S4 | CHB001N, Tohoku | 2.173(1.373)* | 0.304 | 2.229(1.489)* | 0.312 |
| S5 | TKY027E, Tohoku | 1.895(0.955)* | 0.303 | 1.952(1.052)* | 0.312 |
| S6 | TKY026E, Tohoku | 2.012(0.907)* | 0.322 | 2.009(1.209)* | 0.321 |
| S7 | VIC084E, simulated | 3.753(1.753)* | 0.375 | 3.808(1.733)* | 0.381 |
| N1 | JMA, Kobe | 0.516 | 0.442 | 0.476 | 0.403 |
| N2 | Takatori, Kobe | 0.494 | 0.305 | 0.466(0.422)* | 0.284 |
| N3 | Rinaldi, Northridge | 0.461 | 0.387 | 0.423 | 0.358 |
| N4 | New Hall, Northridge | 0.891 | 0.526 | 0.823 | 0.478 |
| N5 | Sylmar C. Hosp., Northridge | 0.857 | 0.577 | 0.796 | 0.522 |
| N6 | Sylmar Conv.St., Northridge | 0.545 | 0.349 | 0.539 | 0.324 |
| N7 | Site 1, Nahanni | 1.670 | 1.656 | 1.508 | 1.498 |

(*)* rescaled ground motions

Table 4.4 Scaling factors of selected ground motions for analyzing the 16-storey building

| No. | Event | 16-storey ZBF bldg. | | 16-storey ZBF-RT bldg. | | 16-storey ZBF-M&RT bldg. | |
|-----|----------------------------------|--------------------------------------|--------|--------------------------------------|--------|--------------------------------------|--------|
| | | T _{range} : 0.72 – 5.42s | | T _{range} : 0.68 – 5.07s | | T _{range} : 0.62 – 4.62s | |
| | | SF | PGA(g) | SF | PGA(g) | SF | PGA(g) |
| C1 | Anderson Dam, Loma Prieta | 2.773 | 0.677 | 2.666 | 0.677 | 2.520 | 0.615 |
| C2 | Presidio, Loma Prieta | 2.124 | 0.425 | 2.140 | 0.425 | 2.269 | 0.454 |
| C3 | Cerro Prieto, Imperial Valley | 4.687 (3.834*) | 0.797 | 4.521 (3.738)* | 0.797 | 4.127 (3.973)* | 0.702 |
| C4 | St. Monica City Hall Northridge | 1.845 | 0.681 | 1.845 | 0.681 | 1.919 | 0.708 |
| C5 | Castaic Old Ridge R., Northridge | 1.003 | 0.570 | 1.010 | 0.570 | 1.067 | 0.606 |
| C6 | Eureka, Cape Mendacino | 2.126 (1.526)* | 0.378 | 2.202 (1.607)* | 0.378 | 2.386 (1.616)* | 0.425 |
| C7 | Olympia Test Lab, West. Wash | 2.910 (2.66)* | 0.815 | 2.947 (2.75)* | 0.815 | 2.824 (2.304)* | 0.791 |
| S1 | IWT007E, Tohoku | 2.789 (1.789)* | 1.841 | 2.620 (1.739)* | 1.729 | 2.354 (1.629)* | 1.553 |
| S2 | FKSH19N, Tohoku | 1.818 (1.100)* | 1.109 | 1.561 (1.051)* | 0.952 | 1.301 (1.055)* | 0.794 |
| S3 | IBRH16E, Tohoku | 2.193 | 1.250 | 2.157 | 1.230 | 2.101 | 1.197 |
| S4 | CHB001N, Tohoku | 1.836 (1.176)* | 0.257 | 1.875 (1.443)* | 0.263 | 1.957 (1.691)* | 0.274 |
| S5 | TKY027E, Tohoku | 1.553 (1.093)* | 0.248 | 1.606 (1.133)* | 0.257 | 1.692 (1.170)* | 0.271 |
| S6 | TKY026E, Tohoku | 1.668 (1.198)* | 0.267 | 1.736 (1.183)* | 0.278 | 1.831 (1.274)* | 0.293 |
| S7 | VIC084E, simulated | 3.886 (1.936)* | 0.389 | 4.012 (2.032)* | 0.401 | 4.080 (2.056)* | 0.408 |
| N1 | JMA, Kobe | 0.540 | 0.448 | 0.531 | 0.441 | 0.531 | 0.441 |
| N2 | Takatori, Kobe | 0.456 | 0.278 | 0.465 | 0.283 | 0.480 | 0.293 |
| N3 | Rinaldi, Northridge | 0.456 | 0.383 | 0.455 | 0.382 | 0.458 | 0.385 |
| N4 | New Hall, Northridge | 1.028 | 0.596 | 1.030 | 0.598 | 1.012 | 0.587 |
| N5 | Sylmar C. Hosp., Northridge | 0.938 | 0.610 | 0.945 | 0.614 | 0.942 | 0.613 |
| N6 | Sylmar Conv.St., Northridge | 0.563 (0.493)* | 0.338 | 0.563 (0.443)* | 0.338 | 0.573 (0.470)* | 0.344 |
| N7 | Site 1, Nahanni | 1.872 | 1.835 | 1.847 | 1.810 | 1.798 | 1.762 |

(*)* rescaled ground motions

4.3 Numerical analyses using Drain-2DX

4.3.1 Modeling in Drain-2DX

In this study, the Drain-2DX models are built up by using three types of finite elements: Element 01, Element 02, and Element 05.

Element 01 is a simple elastic truss element which is used for modeling of truss members. In this study, it is used to model the diagonals of the outrigger trusses added to the ZBF structures. This element has two alternative modes of inelastic behavior which are 1) yielding in both tension and compression, and 2) yielding in tension but elastic buckling in compression. The latter mode is considered in the models of this study.

Element 02 is a simple inelastic beam-column element which is used to simulate the behavior of steel beams and beam-column members. The element is made up of an elastic beam segment and two rigid-plastic hinges at its ends. All plastic deformations are concentrated within the plastic hinges. This element is assigned for modeling beams and columns.

Element 05 is a refined physical theory brace model developed by Ikeda and Mahin (1986), which achieved efficiency by combining analytical formulations describing plastic hinge behaviour with empirical formula developed based on a study of experimental data. Element 05 was calibrated by Ikeda and Mahin based on experimental test results. However, these parameters were recalibrated to match the hysteresis behaviour of braces with

hollow sections based on previous experimental tests results (Chen, 2011). This element was used to model both braces and zipper columns.

In this study, a 3% Rayleigh damping was assigned to the model. All the zipper columns and braces are pin connected to the gusset plate. The P-delta effect has been considered for both ZBF columns and gravity columns. The elevation of the computer model is illustrated in Figures 4.1 and 4.2.

4.3.2 Drain 2DX results

The seismic performance of the studied buildings is sensitive to the ground motions characteristics such as: the frequency content, the ratio of PGV/PGA, and the duration. For instance, under crustal ground motions, the maximum tensile forces in zipper columns were triggered in the lower part of the building (e.g. the 4th and the 5th floor), while the maximum compressive forces in zipper columns was developed at the upper floors of the buildings (e.g. 8th ~ 9th floors for the 12-storey and the 13th ~ 15th floor for the 16-storey). Regarding the behavior of building structures under the subduction ground motion ensemble, it was observed a large seismic demand at the lower part of the building, where zipper columns are acting in tension and transfer the tensile force upwards. Whereas, for near-field ground motions, the largest demand applied at the upper part of the buildings; therefore, the zipper columns act in compression while triggering forces downwards. Moreover, as mentioned in Chapter 3, in order to capture the axial force envelope used for preliminary design of zipper columns, several lateral load distribution patterns were considered. By analyzing the tension and compression envelopes from

each load pattern, sequential triangular distribution (LP-ST) is chosen as the compression envelope and parabolic distribution (LP-P) is chosen as the tension envelope for design. This selection is also in agreement with the refined design envelopes proposed by Chen (2011) and Tirca and Chen (2012). The maximum and the mean axial force envelopes developed in zipper columns of the 12- and 16-storey buildings computed in the N-S direction is shown in Figures 4.8 and 4.9. The maximum and the mean interstorey drift of the 12- and 16-storey ZBF under the selected ground motions is plotted in Figures 4.10 and 4.11.

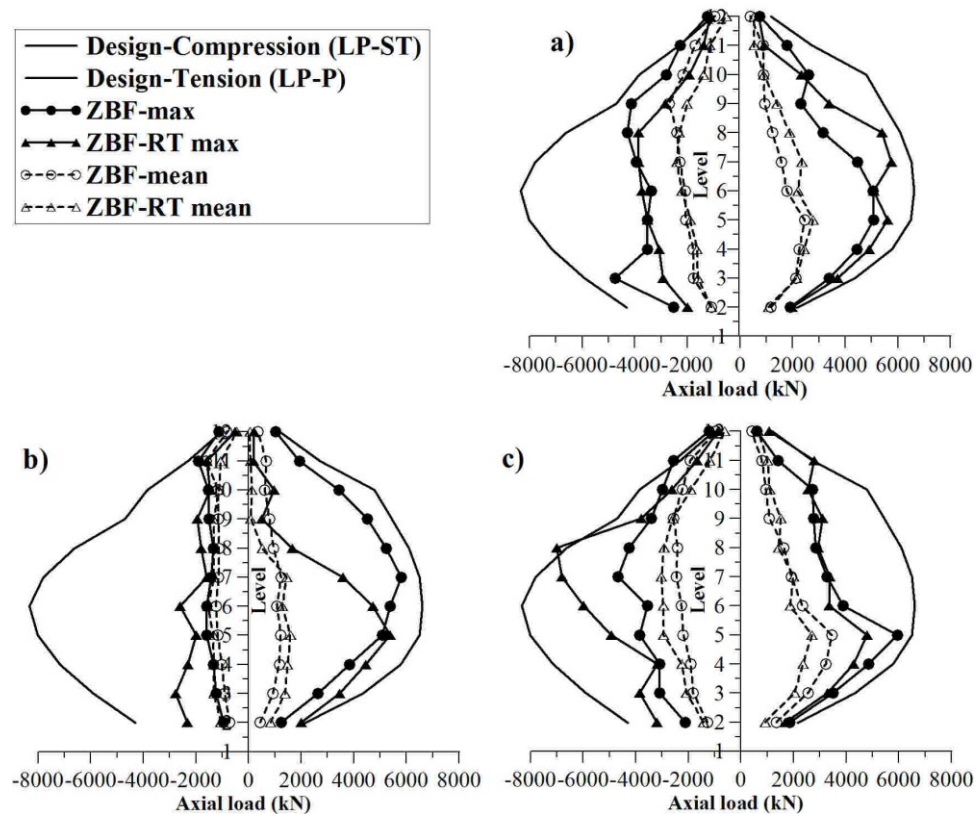


Figure 4.8 Axial force in zipper columns obtained from nonlinear time-history analyses of 12-storey building with and without outrigger trusses: a) Crustal, b) Subduction, c) Near-field

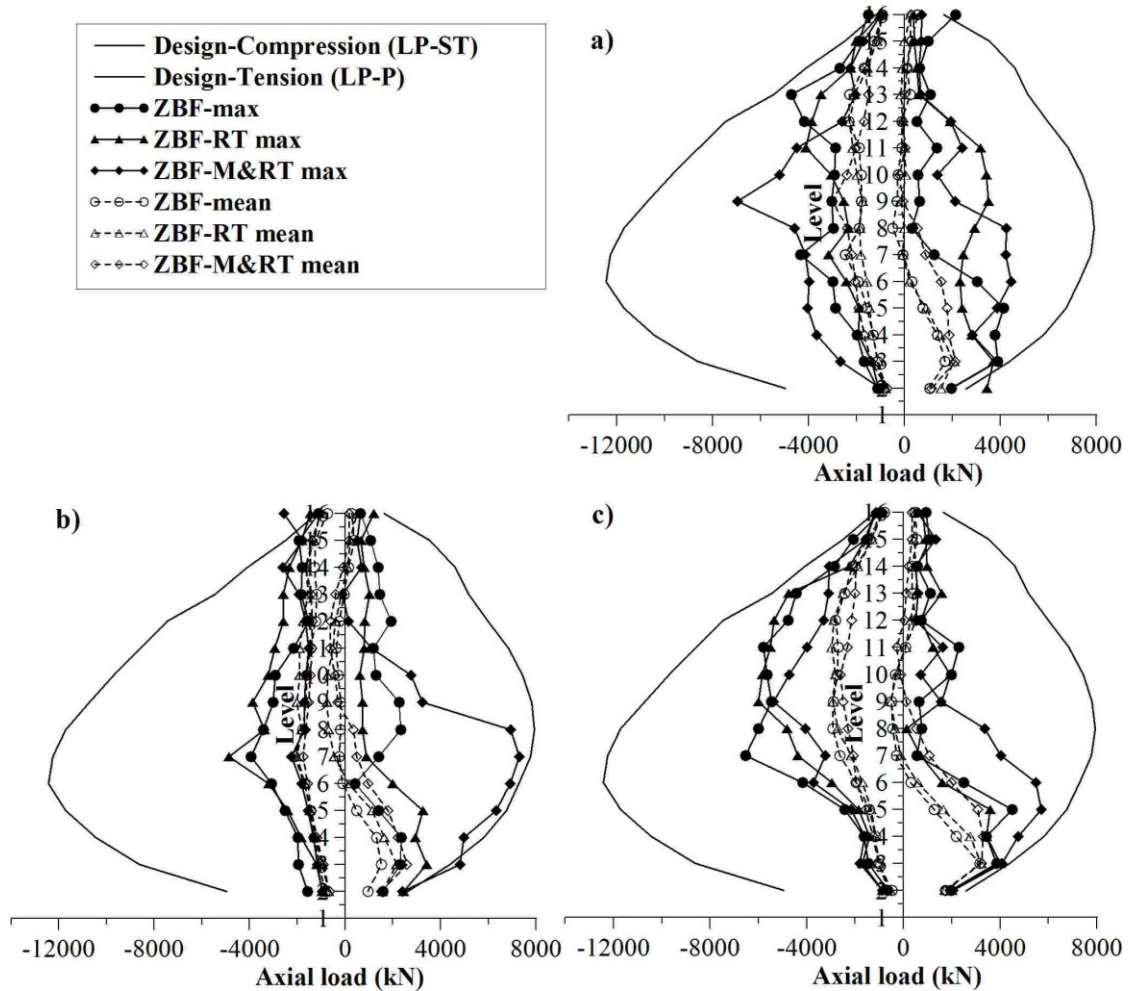


Figure 4.9 Axial force in zipper columns obtained from nonlinear time-history analyses of 16-storey buildings with and without outrigger truss: a) Crustal, b) Subduction, c) Near-field

Referring to Figures 4.8 and 4.9, the mean values of axial forces developed in zipper columns are within the design envelope in both tension and compression side. Furthermore, by observing the difference of the mean values of zipper forces before and after adding outrigger trusses, as expected, the amount of axial load transferred to the zipper column increases which indicate that adding outrigger trusses the lateral resistance of the ZBF system increases as well. To address the concern raised by Tremblay and Tirca (2003)

about the higher modes effect activation, the mean envelopes of zipper forces developed in the ZBF-RT system has diminished the probability of full-height zipper mechanism formation. In addition, the lateral deformations are substantially reduced especially for the 16-storey building as shown in Figures 4.10 and 4.11 for the N-S direction. Thus, by adding outrigger trusses, it provides extra lateral stiffness and activates exterior gravity columns to participate in resisting the applied lateral loads.

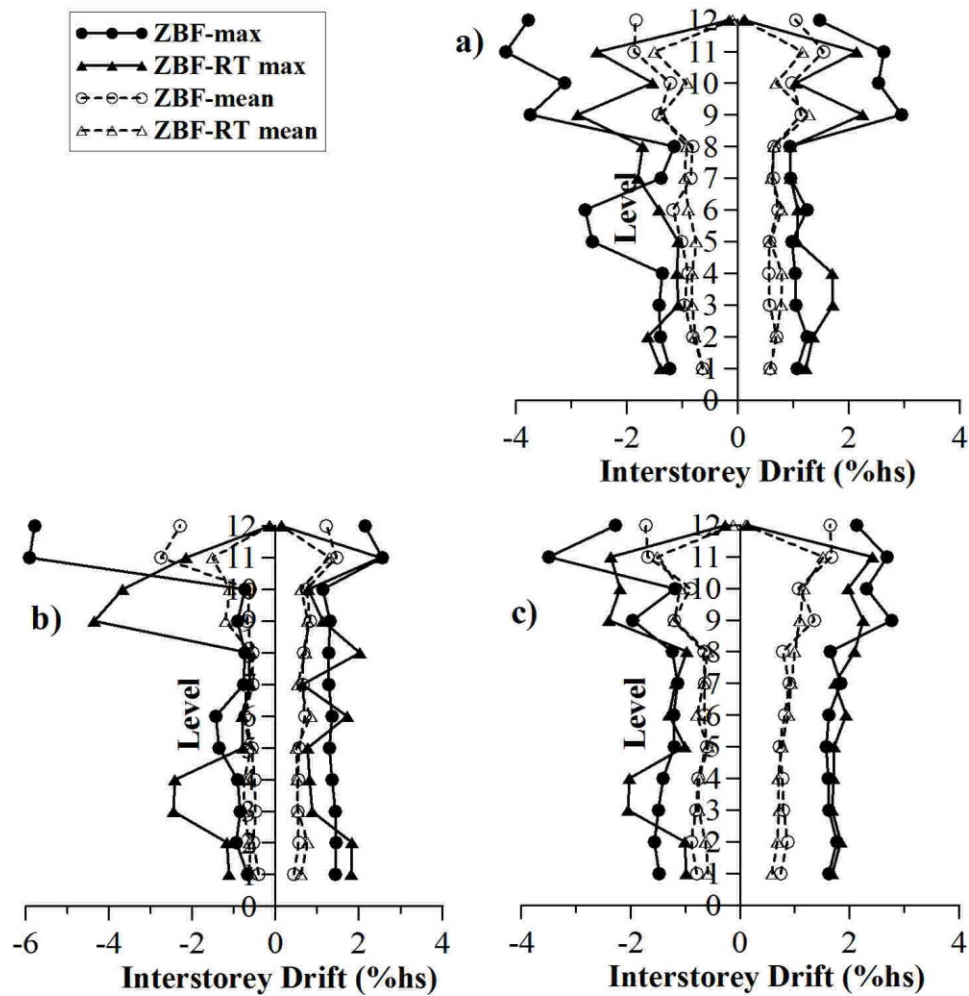


Figure 4.10 Computed interstorey drift for 12-storey building with and without outrigger truss, a) Crustal; b) Subduction; c) Near-field

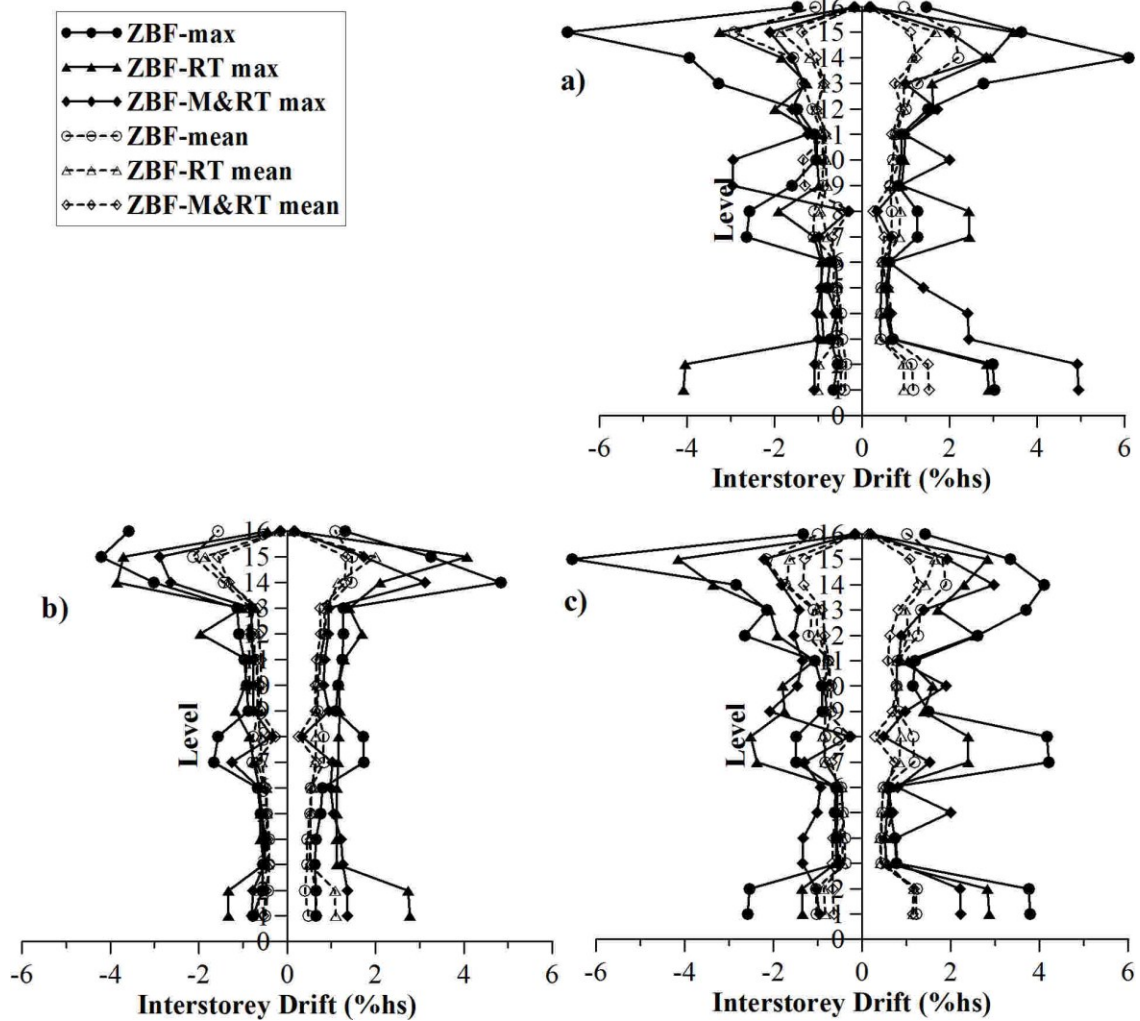


Figure 4.11 Computed interstorey drift for 16-storey building with and without outrigger truss, a) Crustal; b) Subduction; c) Near-field

As illustrated in Figures 4.10 and 4.11, by adding outrigger trusses to the ZBF system, a more uniform distribution of the interstorey drift along the building height is observed. Under all selected ground motions, the mean values of the interstorey drifts for the 12- and 16-storey buildings without outrigger trusses are larger than $2.5\%h_s$ at upper floors (e.g. $4\%h_s$ for the 12-storey and $\sim 5\%h_s$ for the 16-storey, where h_s is the storey height). In addition, the 16-storey building experienced larger interstorey drift values at the 1st and 2nd

floor level, which are in the range of $2.5\%h_s$ to $4\%h_s$. Thus, by adding top outrigger trusses to the 12-storey building in both N-S and E-W direction, the interstorey drift is within the code acceptance ($< 2.5\%h_s$). Regarding the 16-storey building with top outrigger trusses (ZBF-RT), under the crustal ground motions ensemble, the interstorey drift is within the code limit along the building height. However, this is not the case under the subduction and near-field ground motions. In this case, is required either to find an optimum floor location for the outrigger trusses (between the 12- and 15- floor) or to add outrigger trusses at two floor levels as the top and the 8th floor (mid-height).

Details concerning the behavior of the aforementioned structures are given in Chapter 5.

CHAPTER FIVE

Comparative Study of Time-History Response of ZBF Building Structures with and without Outrigger Trusses under various Ground Motions

To investigate the behaviour of low-, middle-, and high-rise seismic resistant ZBF buildings, record-to-record examination of inelastic response is required. In this study, as a measure of ground motion intensity, the PGV/PGA ratio (shown in Table 4.1) is used for identifying different intensity levels of the selected ground motions and studying the influence of ground motions on the inelastic response of the buildings. From high to low PGV/PGA ratio, three records are selected from each of the ground motion ensembles. Therefore, C2, C6, and C4 were selected from the crustal ensemble; S7, S4, and S2 were selected from subduction ensemble; and N6, N1, and N7 were selected from near-field ensemble. In this study, the importance of PGV/PGA ratio and the period cycles was also observed. For example, the N6 and N1 record have the same PGA; however, the PGV/PGA ratio and the period cycles of N6 are twice larger than that of N1. Also, for cases like C2 and C6 which has the same PGA and PGV/PGA ratios but have different period cycles, the applied lateral demand can also be different. Thus, ground motions characterized by similar PGA but large PGV/PGA ratio and large-period cycles may input high demand into the

structure. To emphasize the influence of ground motions and building height on the seismic response of ZBF buildings, 3 x 3 case studies are carried out for each building subjected to crustal, subduction and near-field records selected to cover a large, intermediate and low PGV/PGA ratio. The time-history diagram of the selected ground motions are shown in Figure 5.1. The same explanatory approach was considered by Tirca and Chen (2012).

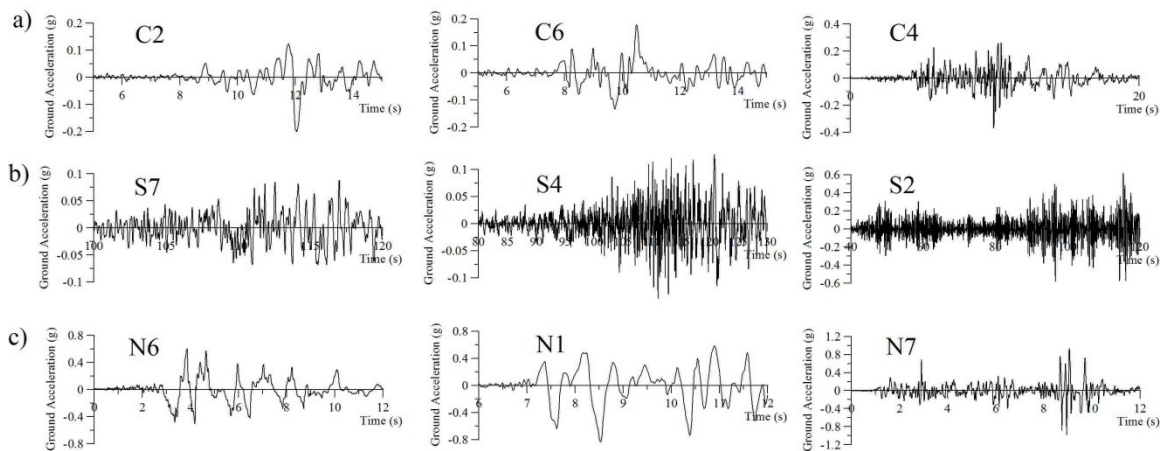


Figure 5.1 Selected records ranked on descended PGV/PGA ratio: a) crustal; b) subduction; c) near-field

In this study the full-height zipper mechanism is defined when the first brace buckling starts either at the bottom floor or the roof level and propagates either upwards or downwards. Thus, when all compression braces reached the post-buckling strength, all tensile braces with few exceptions reached yielding and all ZBF beams have hinged, the full-height zipper mechanism is formed.

The failure status is reached when the lateral loads keep increasing after the full-height zipper mechanism is formed. Shortly, braces reached failure, as well as the attached beams. Theoretically, the dynamic instability is reached when under constant lateral loading the deflected shape continuously increases under the effect of gravity loads.

5.1 Seismic response of the 12-storey ZBF building

As shown in Figure 4.10, under crustal ground motions, the mean interstorey drift values of the 12-storey ZBF are equally distributed over the building height except for the 11th storey where the interstorey drift is 1.86%. Due to the higher modes effect, a larger demand is found at the upper floors. Under the near-field ground motions, the mean envelope of the interstorey drifts is completely within the code limit, and the peak value is captured at the top floor where the value is 1.73%hs. Under subduction ground motions, the mean interstorey drift value reaches 2.74%hs at the 11th floor that exceed the code limit.

Regarding the development of axial force in the zipper columns, as shown in Figure 4.8, the tensile forces in zipper columns are larger than the compressive forces under the crustal and subduction ground motions. However, under near-field ground motions, the axial demand in zipper columns is larger in compression than in tension. The maximum tensile and compressive axial force design envelopes are validated against the time-history ZBF response under the selected 21 ground motions. Thus, the chosen lateral pattern load distribution used to build the axial force design envelopes provided an accu-

rate prediction of axial forces demanded in zipper columns of the 12-storey ZBF building.

As shown for exemplification in Figure 5.2, the deformed shapes of the 12-storey building are subjected to ground motions C2, C6, and C4 that have different PGV/PGA ratios. In this respect, the largest ratio (1.6) occurred for C2 and C6, while C4 is characterized by a smaller ratio (0.68). As demonstrated by Tirca and Chen (2012), the seismic demand increases for larger PGV/PGA ratios. Thus, under the C2, the brace buckling and yielding was propagated in less than 0.35s from the 12th to the 1st floor. Braces that reached buckling are located at the right half-span of the ZBF and the location of the 7 yielding braces was in the left half-span. When the 12-storey building was subjected to the scaled ground motion C6, the studied building almost reaches the failure status. The first brace buckling happens at the bottom floor, but not develops in a strict order. After all the braces buckled or yielded, beam hinges form simultaneously in all the floors, and the building eventually deflected in the 3rd vibration mode. The higher modes were also captured under the ground motion C4. The brace buckling is initiated at the top level; however, buckling of braces is not propagated in a strict order, but the structure deflected in the 2nd vibration mode.

Similarly, under the near-field ground motions, the first brace buckling is captured either at the bottom or the top floor where larger interstorey drift demand is developed.

The time-history response of braces buckling and beams hinging under the N6, N1 and N7 records is illustrated in Figure 5.3.

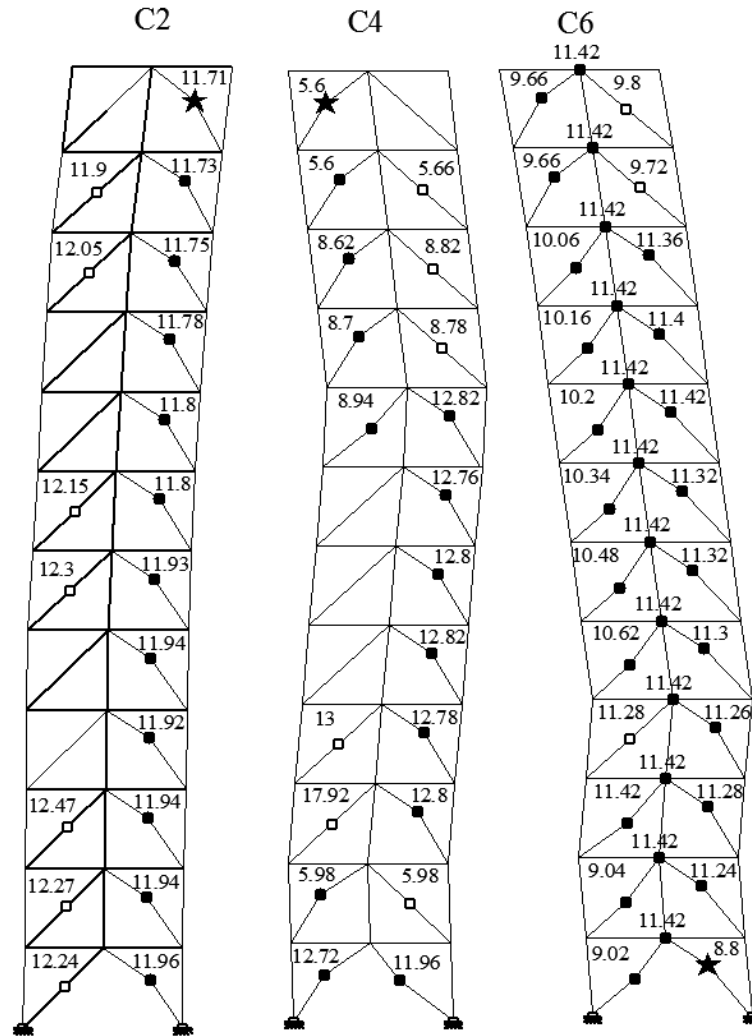


Figure 5.2 Time-history response of brace buckling and beam hinging for 12-storey building without outrigger truss under motions C2, C4, and C6 (* the first buckled brace; ● subsequently buckled brace and beam hinging; ○ yielding of brace)

Under motion N6, buckling of braces initiated at the top level and progressed downward until the bottom floor in only 0.31 s. When ground motion reversed, braces belonging to the other half-span reached buckling starting from the bottom and progressing toward the

top. After almost all braces have buckled and a few reached yielding, beams started hinging in all the floors from top to bottom. Thus, the 12-storey building has reached the collapse status while subjected to 88% of the scaled ground motion N6. Also, under the ground motion N7, the collapse status is reached when the building was subjected to 96% of the scaled ground motion. The first brace buckling occurs at the ground floor and

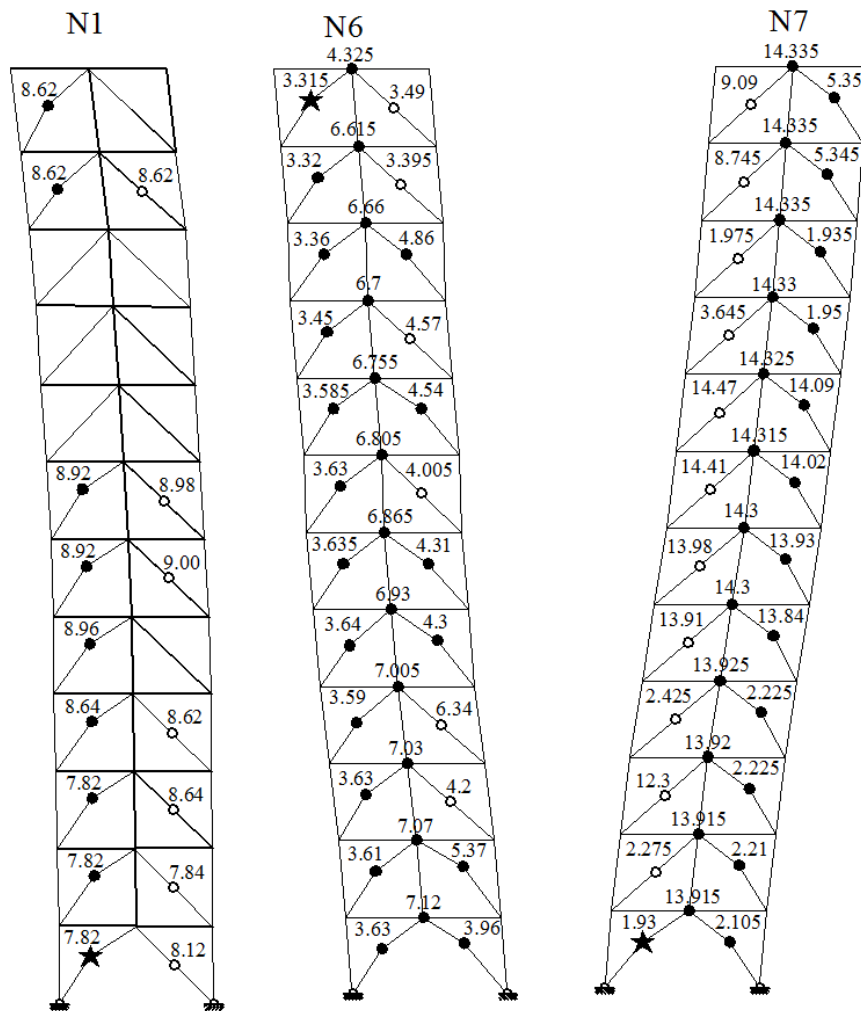


Figure 5.3 Time-history response of brace buckling and beam hinging for 12-storey building without outrigger truss under motions N1, N6, and N7 (★ the first buckled brace; ● subsequently buckled brace and beam hinging; ○ yielding of brace)

propagates upward. Similarly, all beams of the 12-storey building are hinged during the N7 ground motion excitation. The building response under the ground motion N1 shows larger lateral force demand imposed at lower floors. Thus, 9 braces in the left half-span buckled, and 7 braces in the right half-span have reached yielding. Most of the buckling and yielding happened in the lower 7 floors of the building.

Under subduction ground motions, the higher modes of the 12-storey building are also activated. The time history of braces buckling and beams hinging resulted under motions S2, S4, and S7 is showed in Figure 5.4. Within this ensemble, four ground motions characterized by large PGV/PGA ratio (S4 to S7) drove the 12-storey building to collapse. Regarding with this, the studied building is able to carry about 70% of S4, S5, S6 and 53% of the S7 demand. Under motion S7, the 12-storey building reaches the failure status when subjected to 47% of the scaled ground motion. The first brace buckling occurs at the top floor at 109.8 s and progresses downward almost simultaneously. Within 1.1s, all braces on the right half-span buckled from the 12th to 2nd floor. After ground motion reversed, the buckling of braces starts from the bottom floor level and propagates upward but not in sequence. After all braces buckled or yielded, beam hinges start to form at all floors. Under ground motion S4, the 12-storey building also reaches the failure status while subjected to 63% of the scaled ground motion. The first buckled brace was intercepted at the ground floor and in both half-spans buckling of braces propagated upward. After that, the beam hinging starts from the bottom to the top floor level. Under the S2

ground motion, half of braces have either buckled or yielded. However, braces belonging to the 5th floor remained to behave in elastic range. The first brace buckling has initiated at the ground floor and buckling of braces progresses upward.

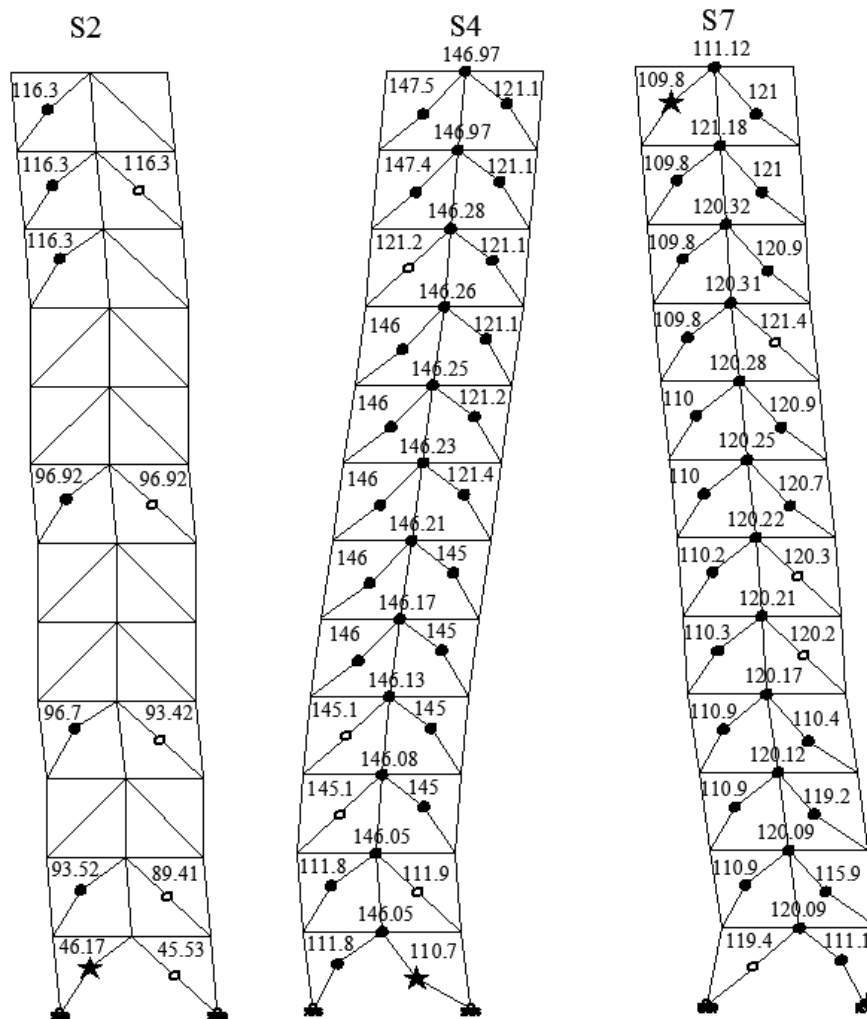


Figure 5.4 Time-history response of brace buckling and beam hinging for 12-storey building without outrigger truss under motions S2, S4, and S7 (★ the first buckled brace; ● subsequently buckled brace and beam hinging; ○ yielding of brace)

5.2 Seismic response of the 12-storey ZBF-RT building

Referring to Figure 4.10 which illustrates the interstorey drift envelope of the 12-storey building with roof outrigger trusses, the mean interstorey values under crustal ground motions are below the code limit at all floor and are uniformly distributed along the building height. After adding one outrigger truss at the top floor level to each ZBF frame, the roof displacements is substantially reduced and the upper stories experience larger lateral demand in term of interstorey drifts than the lower stories. The peak mean value of interstorey drift is captured at the 11th floor and is $1.49\%h_s$. Under the near-field ground motions, the mean envelope of interstorey drift is still within the code limit, $2.5\%h_s$. The interstorey drift values are uniformly distributed except that is concentrated at the 11th floor which is $(1.52\%h_s)$. Under Subduction ground motions, the seismic response of the 12-storey ZBF with roof truss is more stable than that resulted for the structure without outrigger trusses. Thus, we can summarize that roof outrigger trusses control the interstorey drift and make the upper part of the structure stiffer. Thus, larger axial forces in zippers are triggered at the upper tier of the building. In this regard, the peak mean interstorey drift value decreases from $2.74\%h_s$ to $1.47\%h_s$, while this peak has migrated from the 11th floor to the 9th floor.

Moreover, in Figure 4.8, under Near-field ground motions, the axial demand of zipper columns is larger in compression than in tension. Whereas, the tensile forces in zipper columns are larger than compressive forces under the Crustal and Subduction

ground motions. In addition, a summary of all mean values of axial forces developed in zipper columns of the 12-storey ZBF with outrigger trusses under all the selected ground motions indicates that the compressive demand is generally higher than the tensile demand in zipper columns. It also shows that the axial force in zipper columns are generally increased after adding one outrigger truss. The above two findings tells us that by adding roof outrigger trusses in the structural system of the 12-storey ZBF, the system is able to carry a larger axial load in zipper column, and the lateral resistance of the studied building is increased.

Figure 5.5, illustrates the deformed shape of the 12-storey building with roof outrigger trusses subjected to ground motions C2, C6, and C4. Under ground motion C2, the induced forces drive the building in the nonlinear range while deflecting the braced frame in the 3rd vibration mode. Comparing the response to that resulted for ZBF without outrigger trusses, the brace buckling is still initiated at the top level, and 10 brace members reached buckling successively in less than 1.14 s, while buckling is propagating downward. In addition, in the 1st and 3rd floors, braces remain to behave elastically in comparison with the ZBF system without outriggers. A more stable response is captured under ground motions C4 and C6. Thus, under ground motion C4, the first brace buckling occurs at the top level and propagates downward until the 7th floor. Also, buckling of braces occurs at the 1st and 2nd floors as well. However, with the participation of the outrigger truss, the number of brace buckling and yielding is substantially decreased. The percent-

age of the buckled braces drops from 58% to 42%, and the total percentage of buckled and yielded braces drops from 83% to 64.5%. Under the ground motion C6, the brace buckling starts at the top floor level and propagates to the 5th floor within 1.5s (from 9.76s to 11.22s). Moreover, the percentage of buckled braces drops from 90.6% to 58%, and the total percentage of buckled and yielded braces drops from 100% to 62.5%.

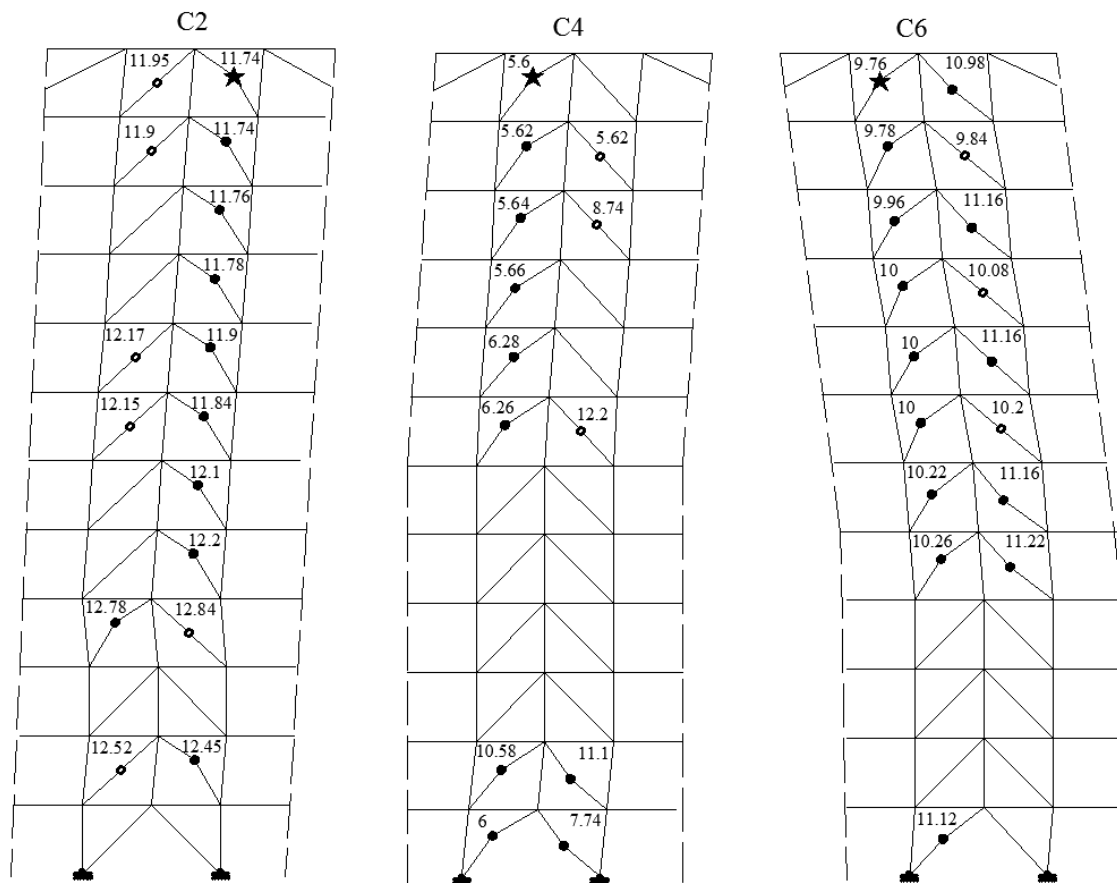


Figure 5.5 Time-history response of brace buckling and beam hinging for 12-storey building with roof outrigger trusses under motions C2, C4, and C6 (★ the first buckled brace; ● subsequently buckled brace and beam hinging; ○ yielding of brace)

The time-history response of braces buckling and beams hinging under ground motions N6, N1 and N7 is illustrated in Figure 5.6. As mentioned before, without adding the

outrigger truss, the studied building reaches the full-height zipper mechanism under ground motions N6 and N7. However, after adding one roof outrigger truss, the building is able to carry forces developed under the scaled ground motions N6. The buckling of braces initiated at the top floor level and progressed downward until the bottom floor.

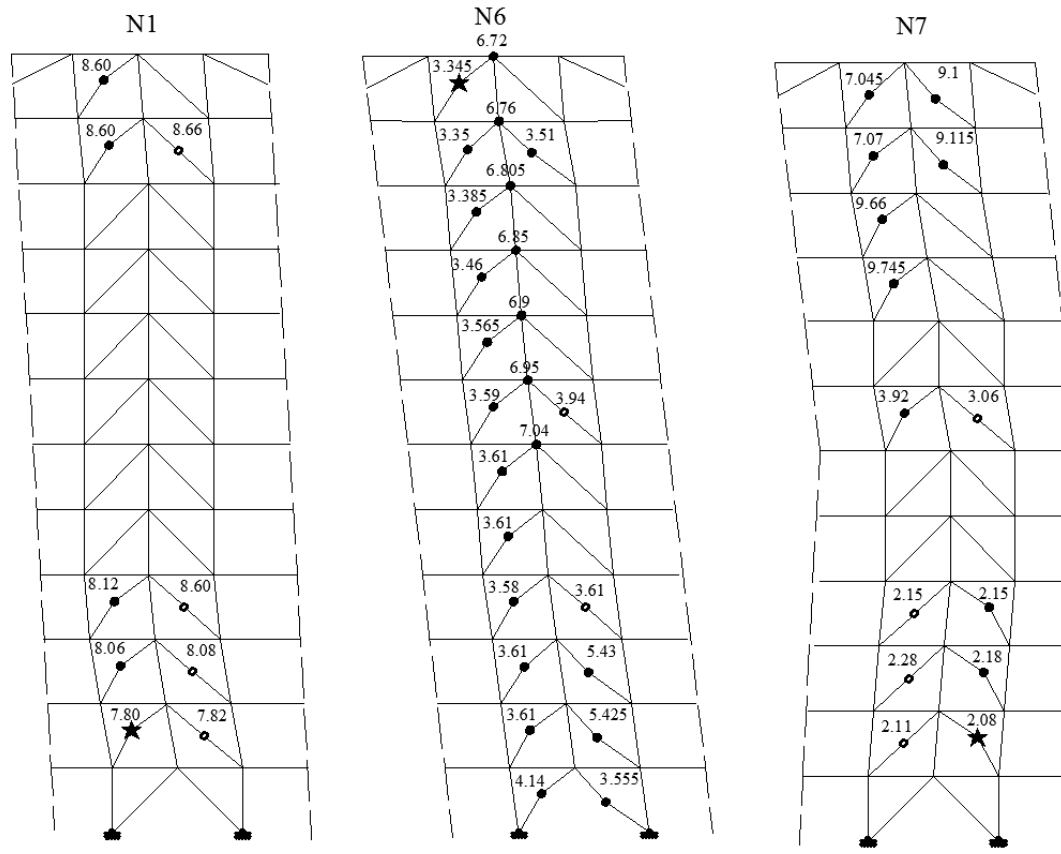


Figure 5.6 Time-history response of brace buckling and beam hinging for 12-storey building with one outrigger truss under motions N1, N6, and N7 (★ the first buckled brace; ● subsequently buckled brace and beam hinging; ○ yielding of brace)

The percentage of the buckled braces decreases from 75% to 67% and the number of beam hinges decreases from 12 to 7%. Under ground motion N7, the first brace buckling occurred at the 2nd floor and then it propagates upward. Comparing to the case without

outrigger trusses, the percentage of brace buckling decreases from 50% to 46%, and the total number of buckled and yielded braces decreases from 100% to 62.5%. In addition, there is no beam hinging observed. The building response under ground motion N1 shows larger lateral demand at lower floors. Thus, five brace members in the left half-span have buckled, and five of the braces in the right half-span yielded. Also, the buckling and yielding mostly occurred from the 2nd to the 4th floor of the building and the number of floors remaining in elastic increases from 3 to 6.

Under ground motions S2, S4 and S7, the history of braces buckling and beams hinging is showed in Figure 5.7. Under ground motion S7, the studied building reaches the failure status when subjected to 45.5% of the scaled ground motion. The first brace still buckles at the top floor level and brace buckling propagates downward until the ground floor within 1.4s. Under the S4 ground motion, the studied building reaches the failure status when subjected to 66.8% of the scaled ground motion. The first brace buckling occurs at the second floor, and after all the braces buckled or yields, beam hinges form in all the stories. Under ground motion S2, the brace buckling starts at the bottom floor, and 28.13% of braces have either buckled or yielded. Comparing to the case without outrigger truss, the seismic performances are similar between them.

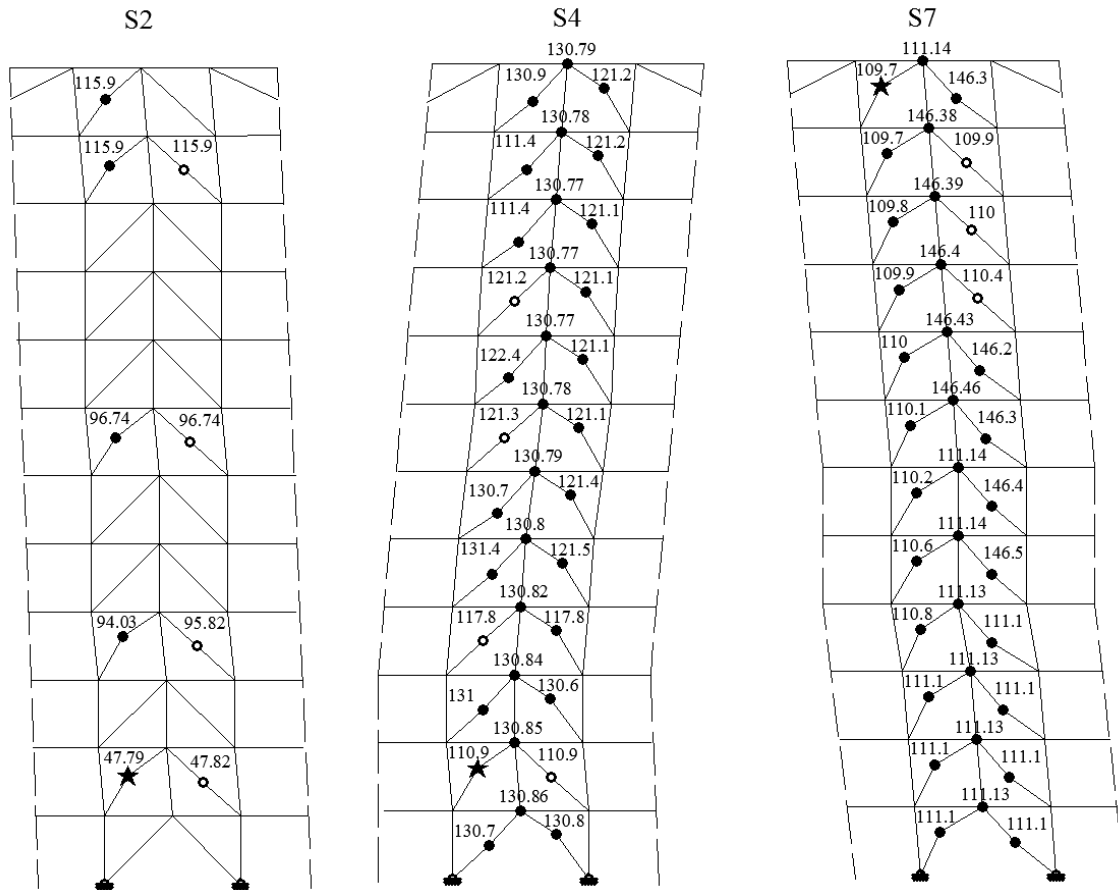


Figure 5.7 Time-history response of brace buckling and beam hinging for 12-storey building with one outrigger truss under motions S2, S4, and S7 (★ the first buckled brace; ● subsequently buckled brace and beam hinging; ○ yielding of brace)

5.3 The behavior of roof outrigger trusses added to the 12-storey building

The geometrical configuration of diagonals in outrigger trusses has an important impact in design if the analyzed elevation supports secondary beams. Regarding this, under the gravity load component, diagonals of outriggers could be subjected to tension or to compression. If the geometry chosen for outrigger diagonals is prone to development of tensile forces, as is shown in Figure 5.8a, the system is cost-efficient. The axial forces developed in diagonals from the gravity load component (DL+0.5LL) are shown in Figure 5.8b. For

comparison purpose, a geometrical configuration of diagonals loaded in compression from the gravity load component (DL +0.5LL) is shown in Figure 5.9. As is expected, the axial force in the internal outrigger panels is almost twice that that in the external outrigger panel. If the time-history loading is applied to the structures in addition to the gravity component, as is shown in Figure 5.8, the forces developed are larger in tension than in

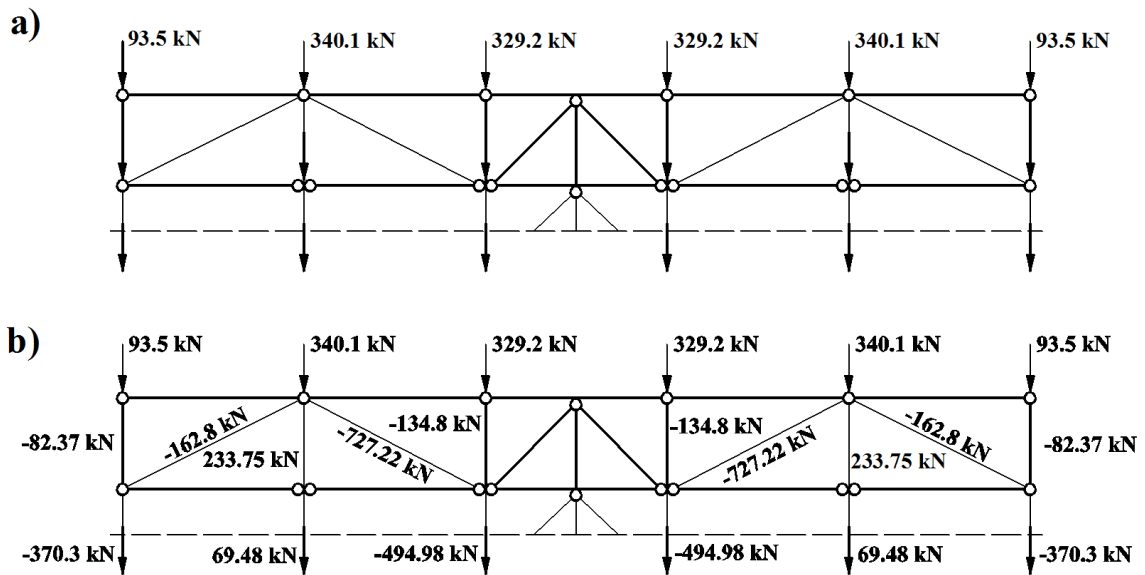


Figure 5.8 Outrigger truss configuration 1 and axial loads developed in the outrigger diagonals under the gravity component

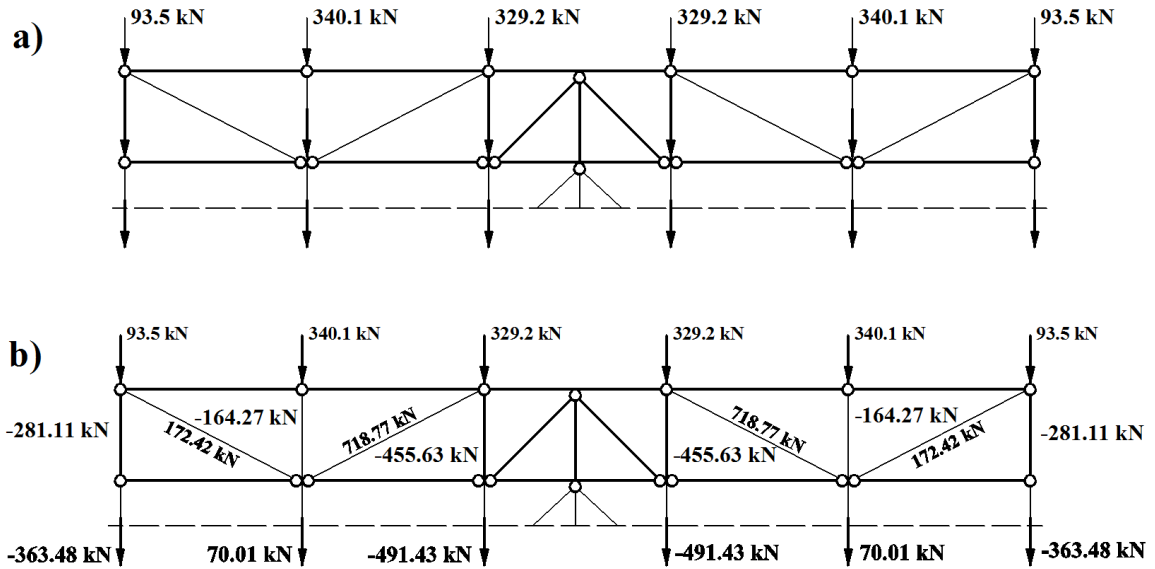
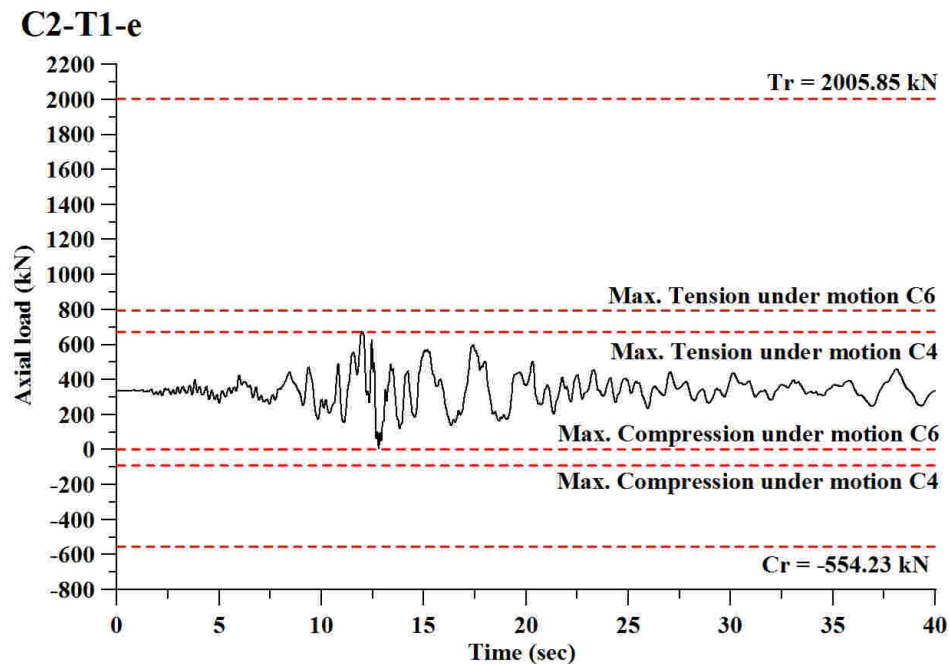


Figure 5.9 Outrigger truss configuration 2 and the axial loads developed in the outrigger diagonals under the gravity component

compression. Time-series of axial force developed in diagonal of roof outriggers under the crustal ground motion C2 are shown in Figure 5.10a for the external panel and in Figure 5.10b for the internal panel. In addition, the maximum value reached under the C4 and C6 ground motions is also indicated in the graph.



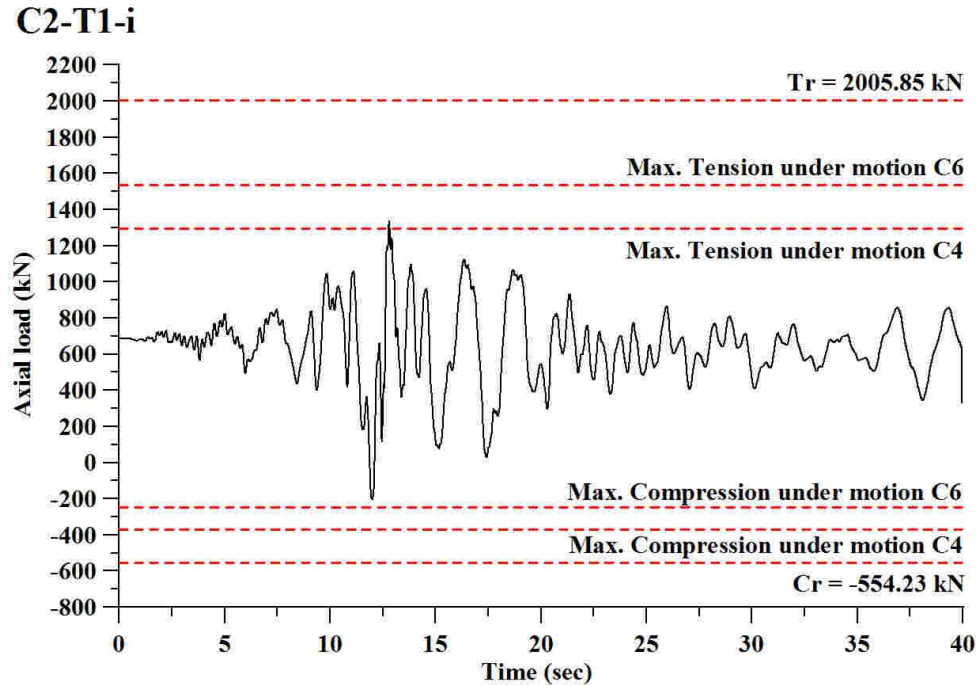
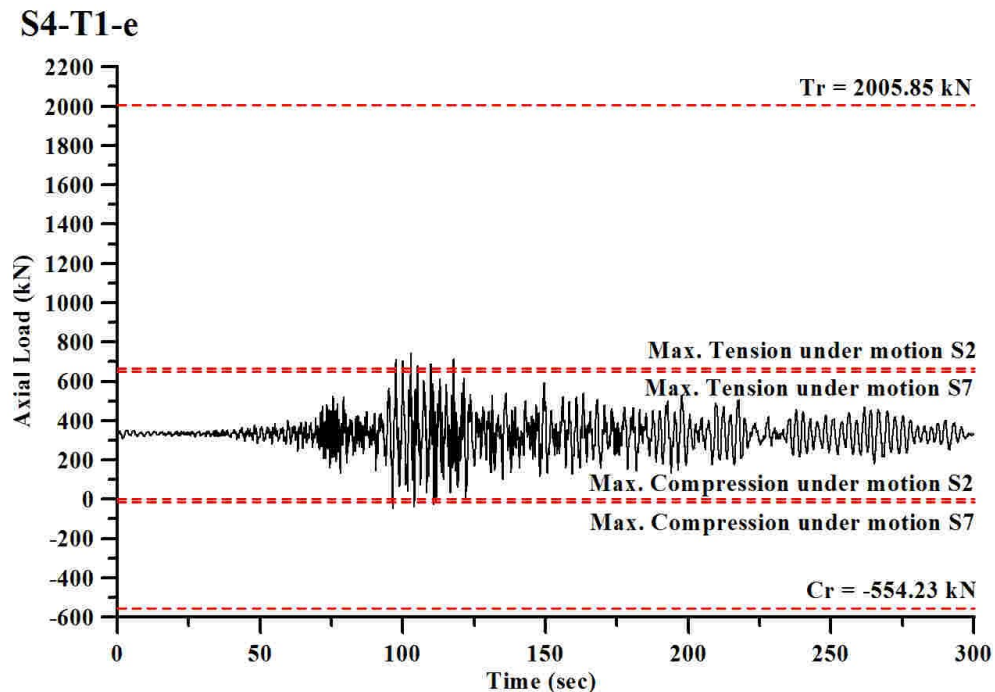


Figure 5.10 Time-history axial load in outrigger truss elements: a) exterior panel T1-e and b) interior panel T1-i under ground motion C2

The time-history series of axial force developed in diagonal of outriggers under the subduction ground motion S4 and near-field ground motion N6 is shown in Figures 5.11 and 5.12



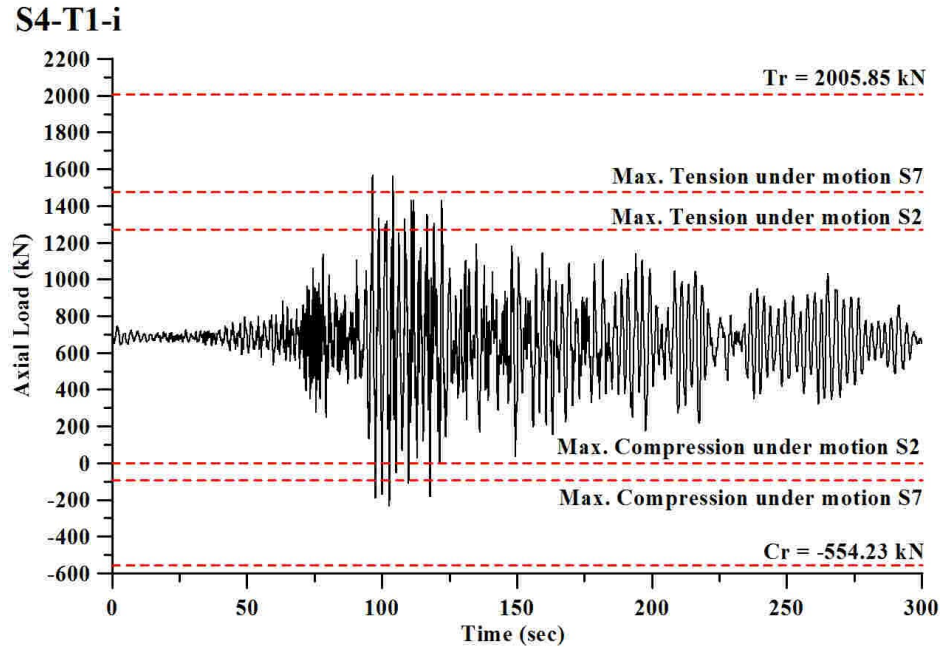
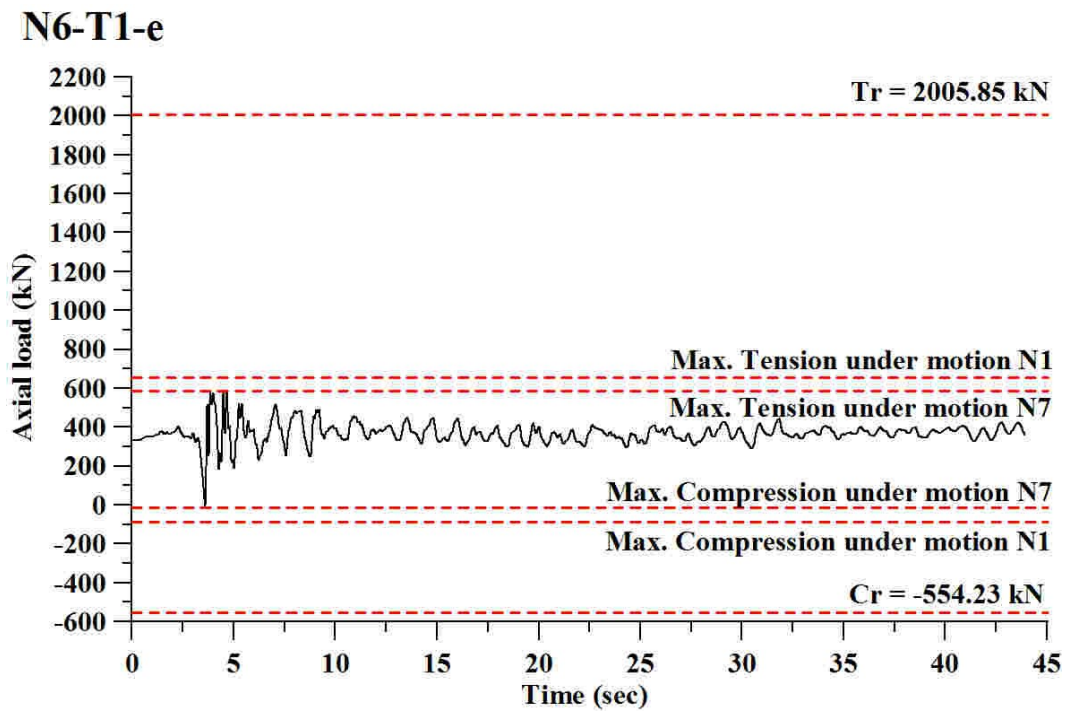


Figure 5.11 Time-history axial load in outrigger truss elements: a) exterior panel, T1-e and b) interior panel T1-i under ground motion S4.

The deflected shape of the entire elevation under the crustal ground motion C2 is shown in Figure 5.13.



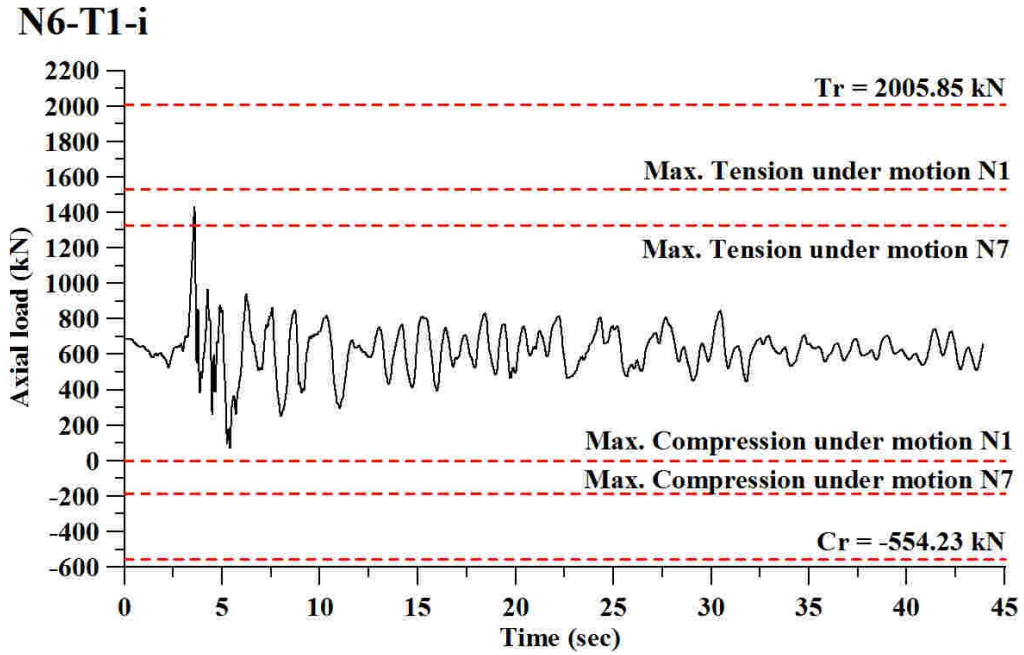


Figure 5.12 Time-history axial load in outrigger truss elements: a) exterior pane T1-e and b) interior pane T1-i under ground motion N6

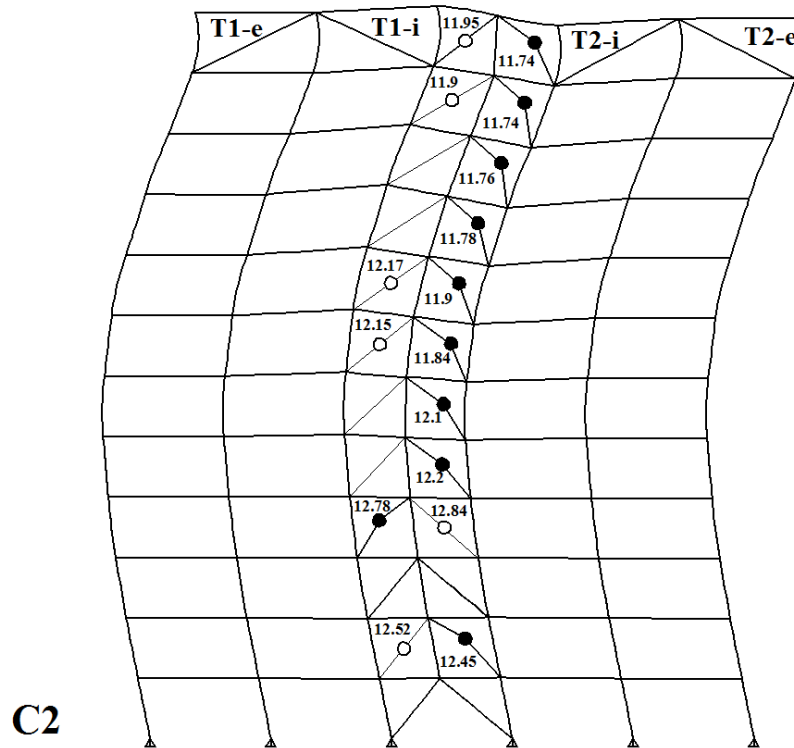


Figure 5.13 Deformed shape of the 12-storey ZBF-RT under ground motion C2

5.4 Seismic response of the 16-storey ZBF building

The interstorey drift envelope of the 16-storey ZBF without outrigger truss is presented in Figure 4.11. Under crustal ground motions, large lateral drift demand is intercepted at the upper stories, and the peak mean value of interstorey drift is obtained at the 15th floor as 2.92%hs which is higher than the code limit. Also, under Near-field ground motions, the peak mean value of interstorey drift is 2.16%hs at the 15th floor. Under Subduction ground motions, the peak mean value of interstorey drift value is 3.13%hs at the 15th storey which also exceed the code limit.

As is shown in Figure 4.9, under Crustal and Near-field ground motions, the axial demand of the zipper columns is larger in compression than in tension. However, under Subduction ground motions, the tensile forces in zipper columns are larger than the compressive forces. By considering all ground motions, the peak mean values of tensile forces are observed at the upper floors, and that of compressive forces are captured in the lower stories. In general, under Subduction ground motions the axial demand is larger in compression than in tension.

In Figure 5.14, the deformed shape of the 16-storey building under ground motions C2, C6, and C4 are shown. Ground motion C2 induced forces that drive the building in the nonlinear range while deflecting in the 3rd vibration mode. The first brace buckling is captured at the top level and buckling progresses downward in less than 2.57 s from the 16th to the 1st floor. When the 16-storey building was subjected to 84% of the scaled mo-

tion C6, the failure status is reached. The first brace buckling occurs at the top level at 9.72s, and propagates from top to bottom in less than 0.84 s (from $t = 9.72\text{s}$ to 10.56s). The beam hinges start to form at 10.66s and then has develop in all the floors. The higher modes were also captured under the C4 ground motion when building deflected in the 3rd vibration mode and buckling of braces has occurred at all floors with 4 exceptions. Moreover, in 8 out of the 16 floors, both brace members belonging to the same floor have reached either buckling and yielding or only buckling after the ground motion reversed. The first brace buckling occurs at the top floor level. However, brace buckling is not developed in a consecutive sequence.

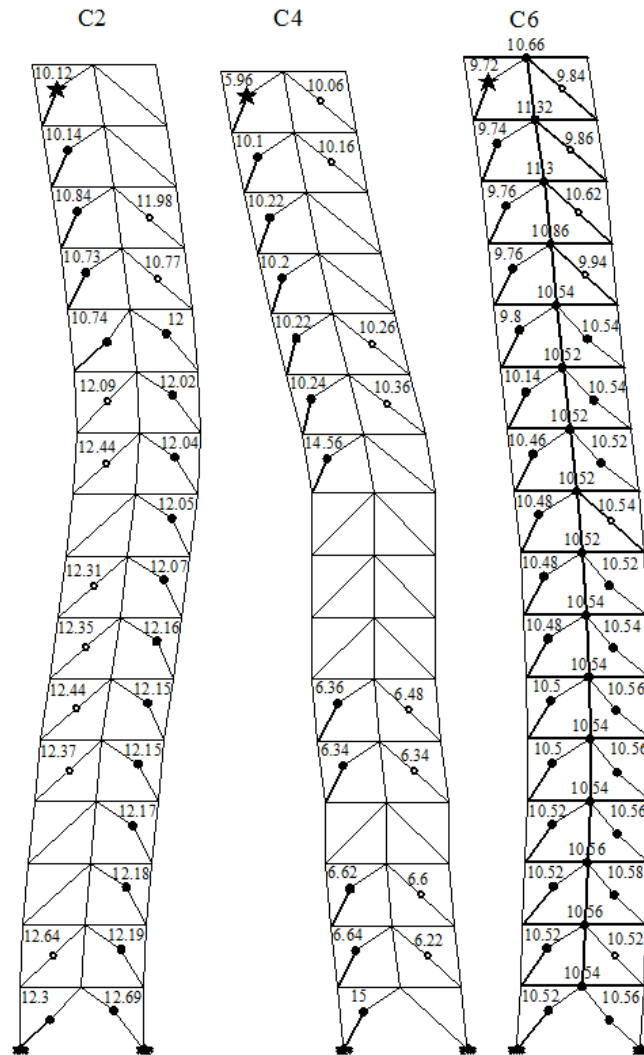


Figure 5.14 Time-history response of brace buckling and beam hinging for 16-storey building without outrigger truss under motions C2, C4, and C6 (★ the first buckled brace; ● subsequently buckled brace and beam hinging; ○ yielding of brace)

The time-history response of braces buckling and beams hinging under ground motions N6, N1 and N7 is illustrated in Figure 5.15. Under ground motion N6, the studied building reaches the failure status when subjected to 87.6% of the scaled ground motion. The brace buckling is initiated at the top level, and propagates to the ground level in 1.64s. All beams hinged after the brace buckling and yielding occurred. Under ground

motion N7, the 16-storey building reached the failure status while subjected to 100% of the scaled ground motion.

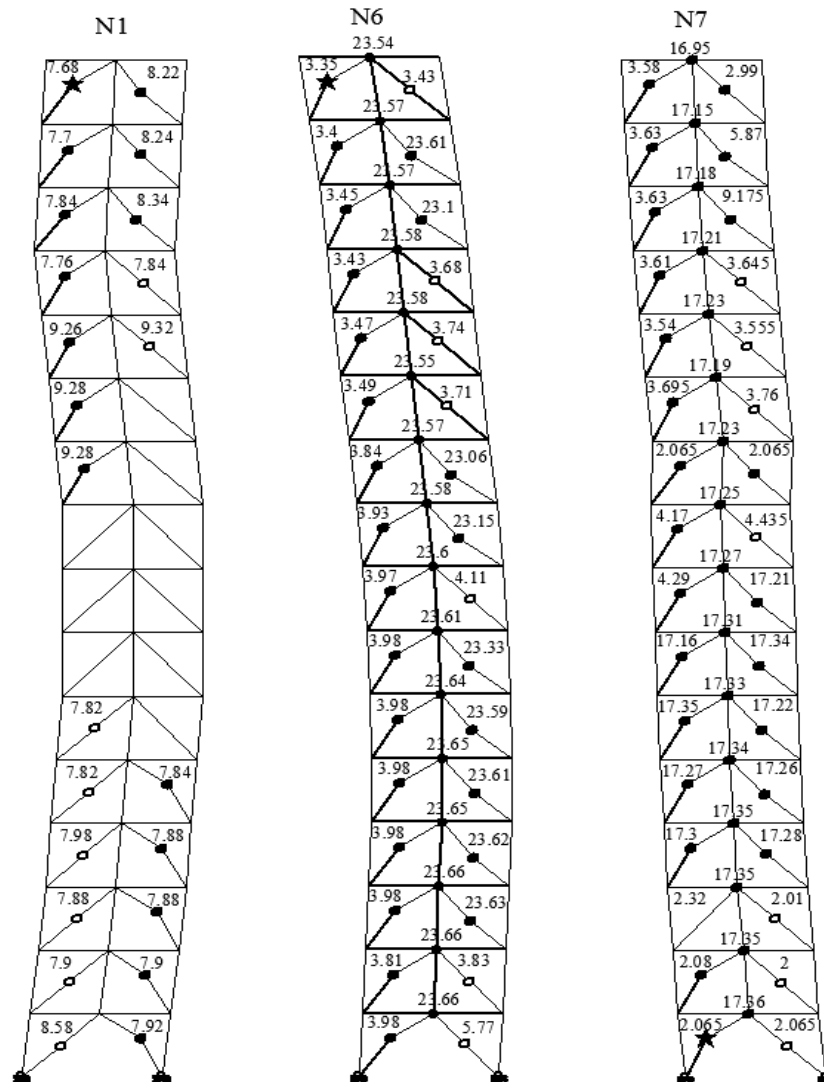


Figure 5.15 Time-history response of brace buckling and beam hinging for 16-storey building without outrigger truss under motions N1, N6, and N7 (★ the first buckled brace; ● subsequently buckled brace and beam hinging; ○ yielding of brace)

The brace buckling starts at the ground floor and then propagates upward. All braces reached either buckling or yielding and beams formed hinges in all the floors. The

building response under the N1 ground motion shows large demand in the upper floors. The brace buckling is initiated at the top floor level, and then propagates from the 16th to the 10th floor. Almost simultaneously, the buckling also starts developing from the 5th to the 1st floor. After the ground motion excitation, there are 3 floors that are still performing in elastic range.

The higher modes of the 16-storey building are also activated under Subduction ground motions. Thus, under ground motions S2, S4 and S7, the history of braces buckling and beams hinging is showed in Figure 5.16. The building reaches the failure status when subjected to 50% of the scaled motion S7. The first brace buckles at the top floor level at 110.7 s and progresses downward almost simultaneously. Within 0.4s, all brace members of the left half span have buckled from the top to the bottom level. After all braces have buckled or yielded, the beam hinging develops at all floors. Under the S4 ground motion, the 16-storey building reached the failure status. The first brace buckling was intercepted at the 3rd floor, and propagates upward. In the studied building, 87.5% of braces have buckled, and plastic hinges formed in all the beams of the ZBF. Under the S2 ground motion, the failure status is also reached. The first brace buckling is captured at the bottom level. Similar to the situation under motion S4, all brace members buckled and all beams formed plastic hinges.

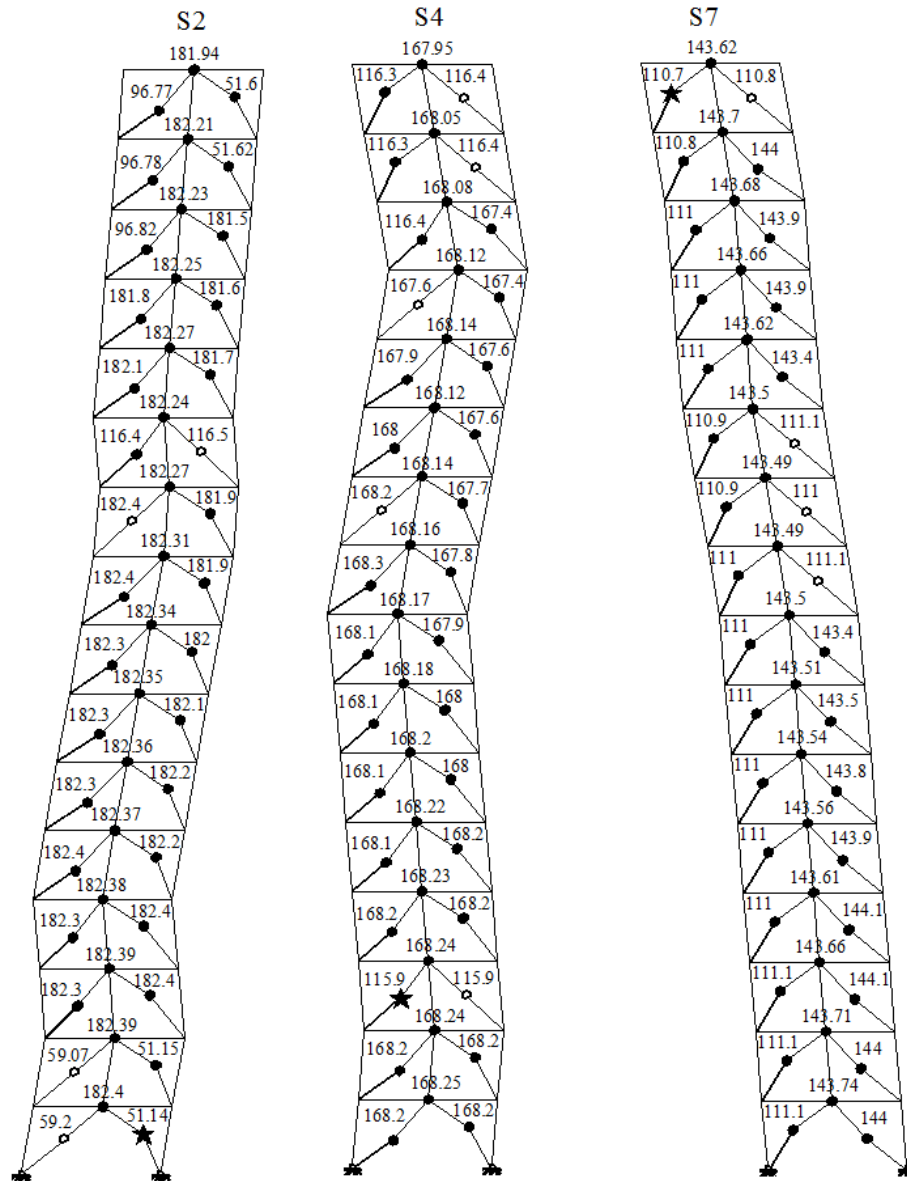


Figure 5.16 Time-history response of brace buckling and beam hinging for 16-storey building without outrigger truss under motions S2, S4, and S7 (★ the first buckled brace; ● subsequently buckled brace and beam hinging; ○ yielding of brace)

5.5 Seismic response of the 16-storey ZBF-RT building

The seismic performance of the 16-storey building with one outrigger truss added at the roof is also studied. Thus, under crustal ground motions, the mean interstorey drift values

were below to the code limit. Since the top floor is belted by the outrigger truss and due to the higher modes effect, the maximum seismic demand is shifted to the 15th floor, and the peak mean value of the drift on that floor decreases from 2.92%hs to 1.85%hs. Under Near-field ground motions, the mean values of interstorey drift are distributed in a similar pattern as under the Crustal ground motions. The peak mean value of interstorey drift is 1.63% at the 15th floor which is less than 2.16%hs resulted from the case of no truss. Under Subduction ground motions, the peak mean value of interstoreydrift decreases from 2.13%hs to 1.32%hs, and it is captured at the 14th floor instead of the 15th floor previously.

Referring to Figure 4.9 and comparing to the case without outrigger truss, the mean values of axial forces in zipper columns are increased in all the floors. Under Crustal and Near-field ground motions, the axial force demand in zipper columns is larger in compression than in tension. However, under Subduction ground motions, the tensile forces in zipper columns are larger than the compressive forces. Among all selected ground motions, the larger mean values of tensile forces are observed in the upper floors, and the larger values of compressive forces are captured in the lower floors. In general, there is larger axial demand in compression than in tension.

In Figure 5.17, the deformed shape of the 16-storey building with roof outrigger trusses is depicted when subjected to ground motions C2, C4, and C6. Under ground motion C2, the induced forces drive the building in the nonlinear range while deflecting also

in the 1st vibration mode. Comparing to the case without outrigger trusses, brace buckling is also initiated at the top floor level. In addition, 11 brace members reached buckling successively from the 16th to the 8th floor within 1.44s. From the 1st to the 7th floor, braces remain to perform elastically. This behavior didn't occur in the case without outriggers.

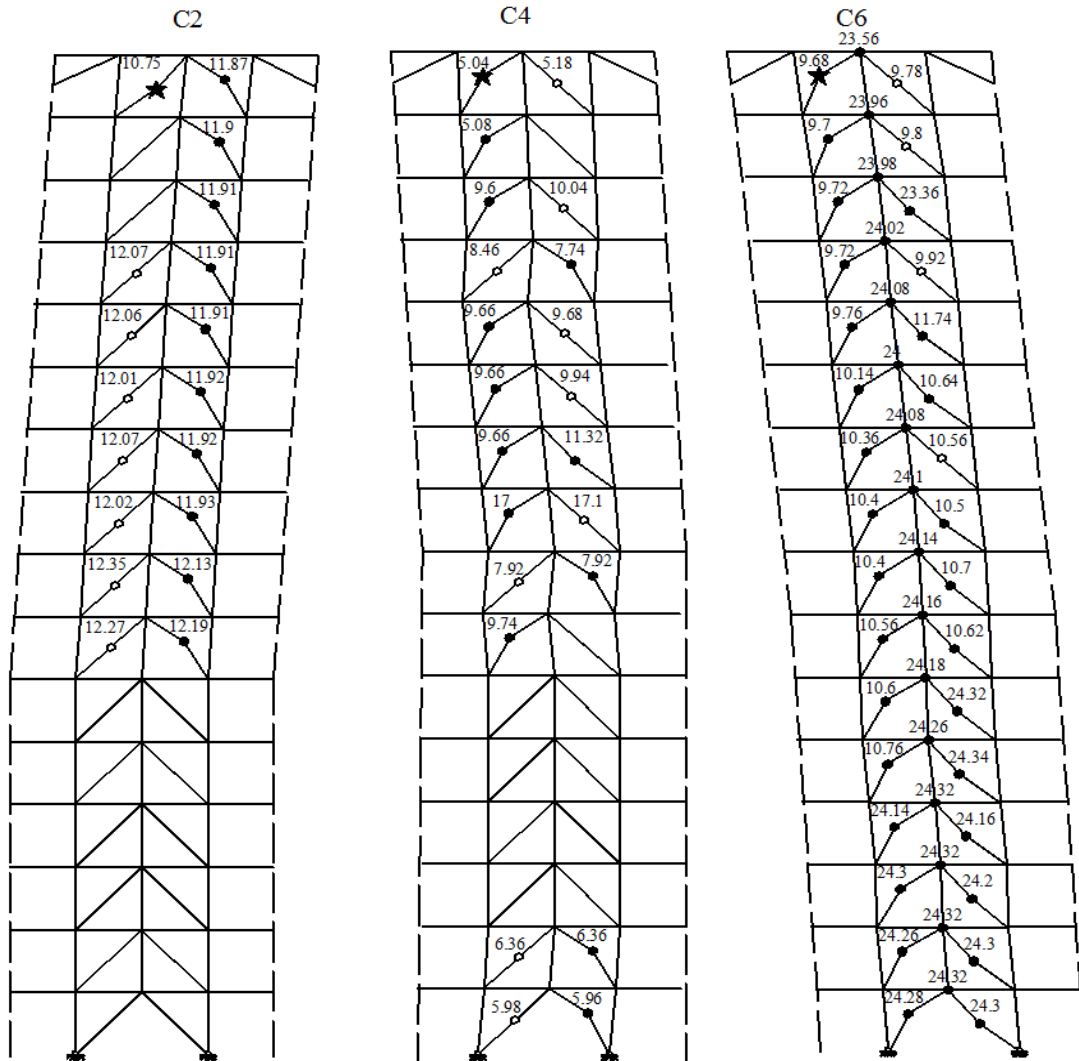


Figure 5.17 Time-history response of brace buckling and beam hinging for 16-storey building with roof outrigger trusses under C2, C4, and C6 (★ the first buckled brace; ● subsequently buckled brace and beam hinging; ○ yielding of brace)

Under ground motion C4, the large lateral demand is mostly carried up to the upper floors. The first brace buckling is captured at the top floor level, but doesn't propagate in a consecutive sequence. Thus, comparing to the case without outrigger trusses, the seismic performance is similar. Under C6 ground motion, the studied building reaches the failure status. The first brace buckling occurs at the top level, and propagates to the 5th floor in 1.08s. Beam hinges form in all the stories.

The time-history response of braces buckling and beams hinging under the N6, N1 and N7 records is illustrated in Figure 5.18. Under ground motions N6 and N7, the seismic performance is more stable when roof outrigger trusses are added to the structural system of the 16-storey building. Under ground motion N6, the 16-storey building with roof outriggers reaches the failure status. The first brace buckling occurs at the top level, and propagates to the 5th floor in 1.6s. Beam hinges form in all the stories. Under motion N7, the 16-storey with roof outriggers was able to respond to 100% of the scaled ground motion. The first brace buckling occurred at the 2nd floor, but did not propagate subsequently. Comparing to the case without outrigger trusses, under the N7 ground motion, the percentage of brace buckling decreases from 75% to 37.5%, and the total number of buckled and yielded braces decreases from 100% to 59.4%. Furthermore, there is no beam hinge formed, and the studied building didn't reach the failed status. The building response under N1 ground motion shows large demand at upper floors.

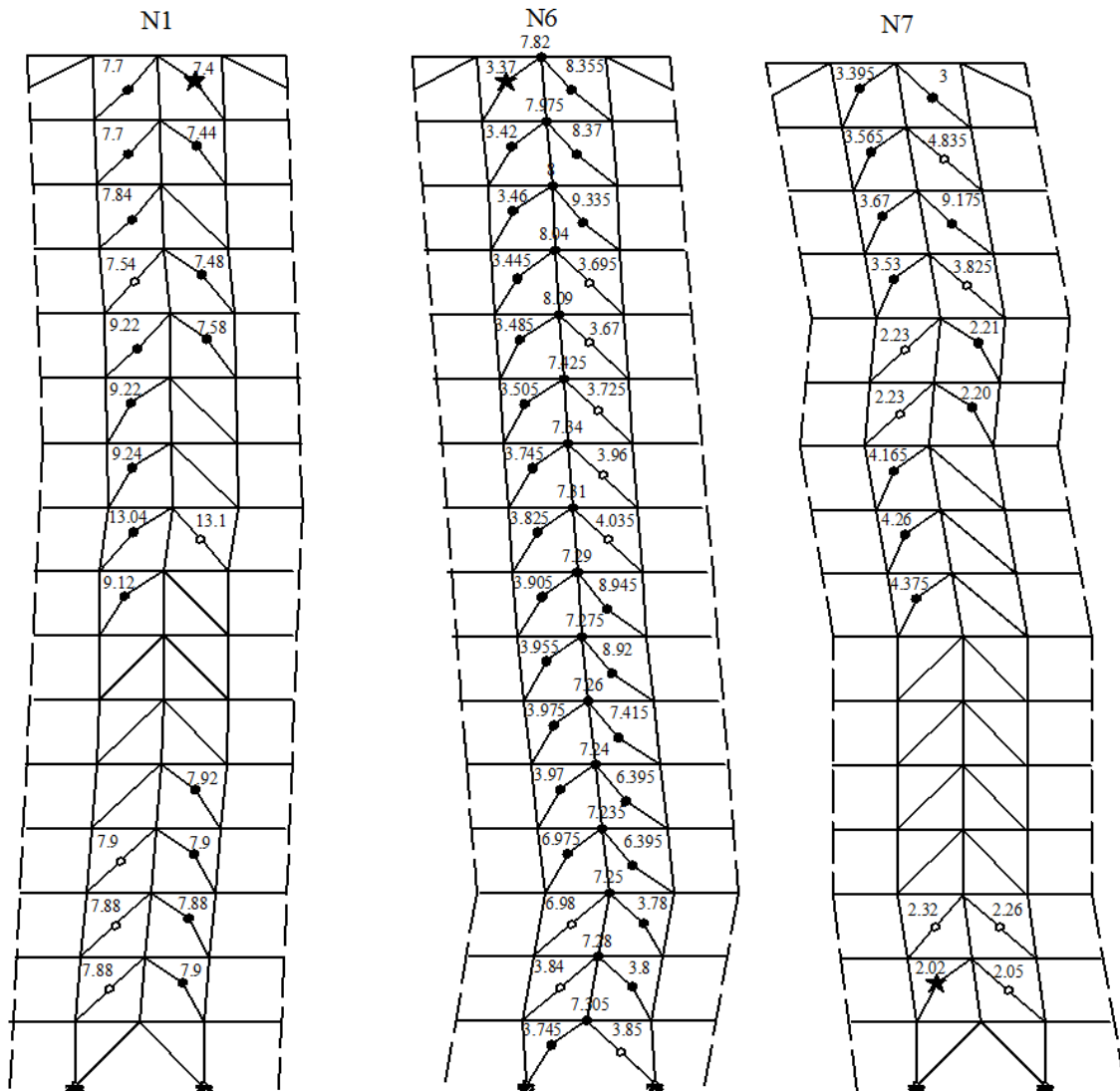


Figure 5.18 Time-history response of brace buckling and beam hinging for 16-storey building with outrigger truss under motions N1, N6, and N7 (★ the first buckled brace; ● subsequently buckled brace and beam hinging; ○ yielding of brace)

Most of the brace buckling and yielding happens in the 8th to 16th floors. Generally, the 16-storey building shows similar seismic response to that without outriggers. Under ground motions S2, S4 and S7, the history of braces buckling and beams hinging is showed in Figure 5.19. Under ground motion S2 the studied building reaches the failure

status when subjected to 67.32% of the scaled ground motion. The first brace buckling occurs at the 2nd floor and beam hinges form in all the stories. Under ground motion S4, the studied building reaches the failure status when subjected to 76.96% of the scaled

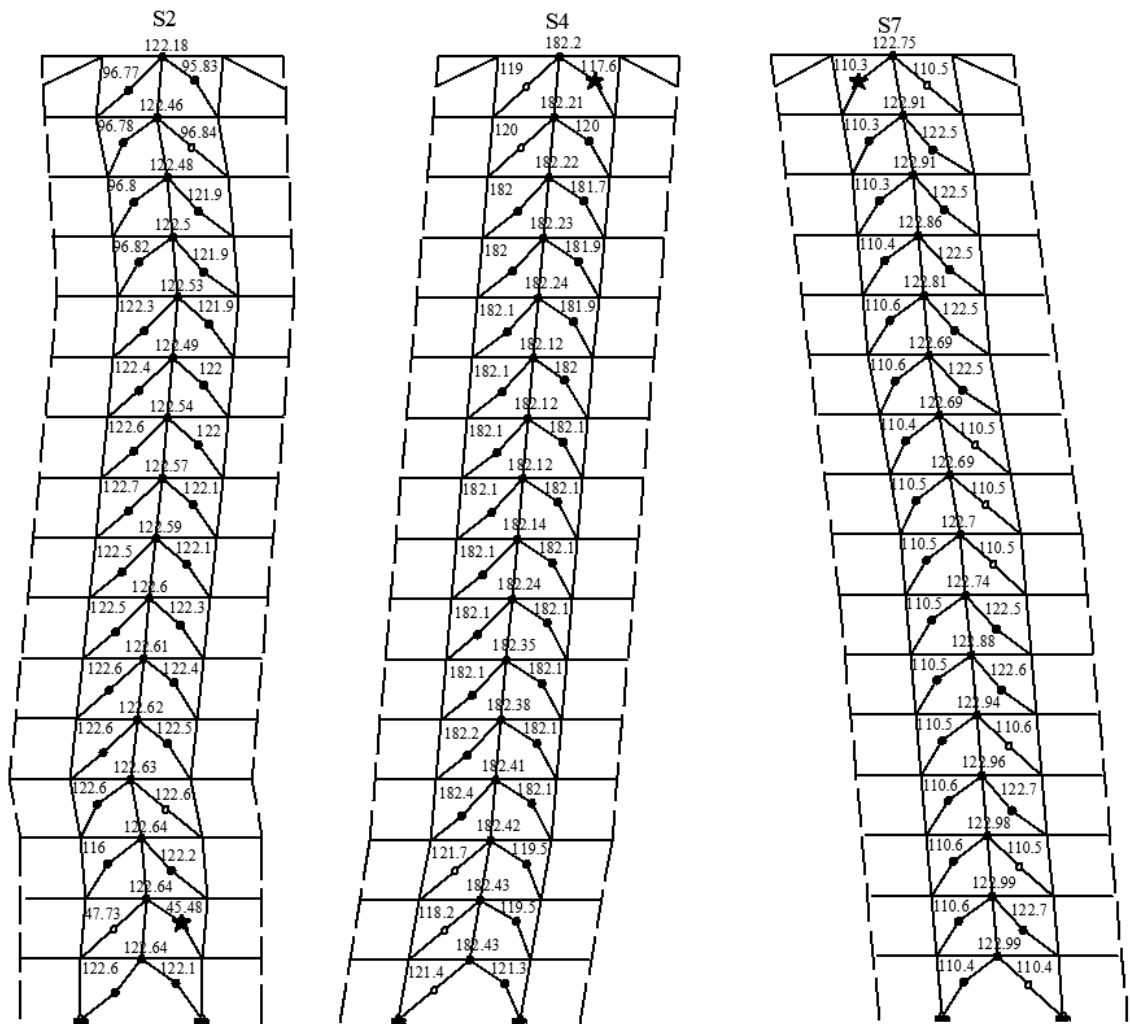


Figure 5.19 Time-history response of brace buckling and beam hinging for 16-storey building with outrigger truss under motions S2, S4, and S7 (★ the first buckled brace; ● subsequently buckled brace and beam hinging; ○ yielding of brace)

ground motion. The first brace buckling occurs at the top level, and propagated until the 2nd floor in 1.9s, while beam hinges form in all the stories. Under ground motion S7, the

studied building reaches the failure status when subjected to 50.65% of the scaled ground motion. The first brace buckling occurs at the top level, and developed to the 2nd floor in 0.3s. After all the braces are buckled and yielded, beam hinges are observed in all the stories.

5.6 The behavior of outrigger trusses added to the roof floor level of the 16-storey building

The time history time series of axial forces developed in the internal and external panel of the outrigger trusses diagonals is shown in Figure 5.20 under the C2 ground motion.

5.7 Seismic response of the 16-storey ZBF-M&RT building

With the participation of two outrigger trusses at the top floor and mid-height of the building, the studied building may achieve the expected seismic performance. Under crustal ground motions, the mean values of interstorey drifts in all stories is less than $2.5\%h_s$, and the peak interstorey drift value captured at the 15th floor is $1.36\%h_s$. A similar response is obtained under the Near-field ground motions. Among all stories, there is no exceeding of the interstorey drift code limit. The peak mean value of the interstorey drift is observed at the 14th floor and is $1.32\%h_s$. Under Subduction ground motions, the maximum drift value is $1.56\%h_s$ and occurred at the 15th floor.

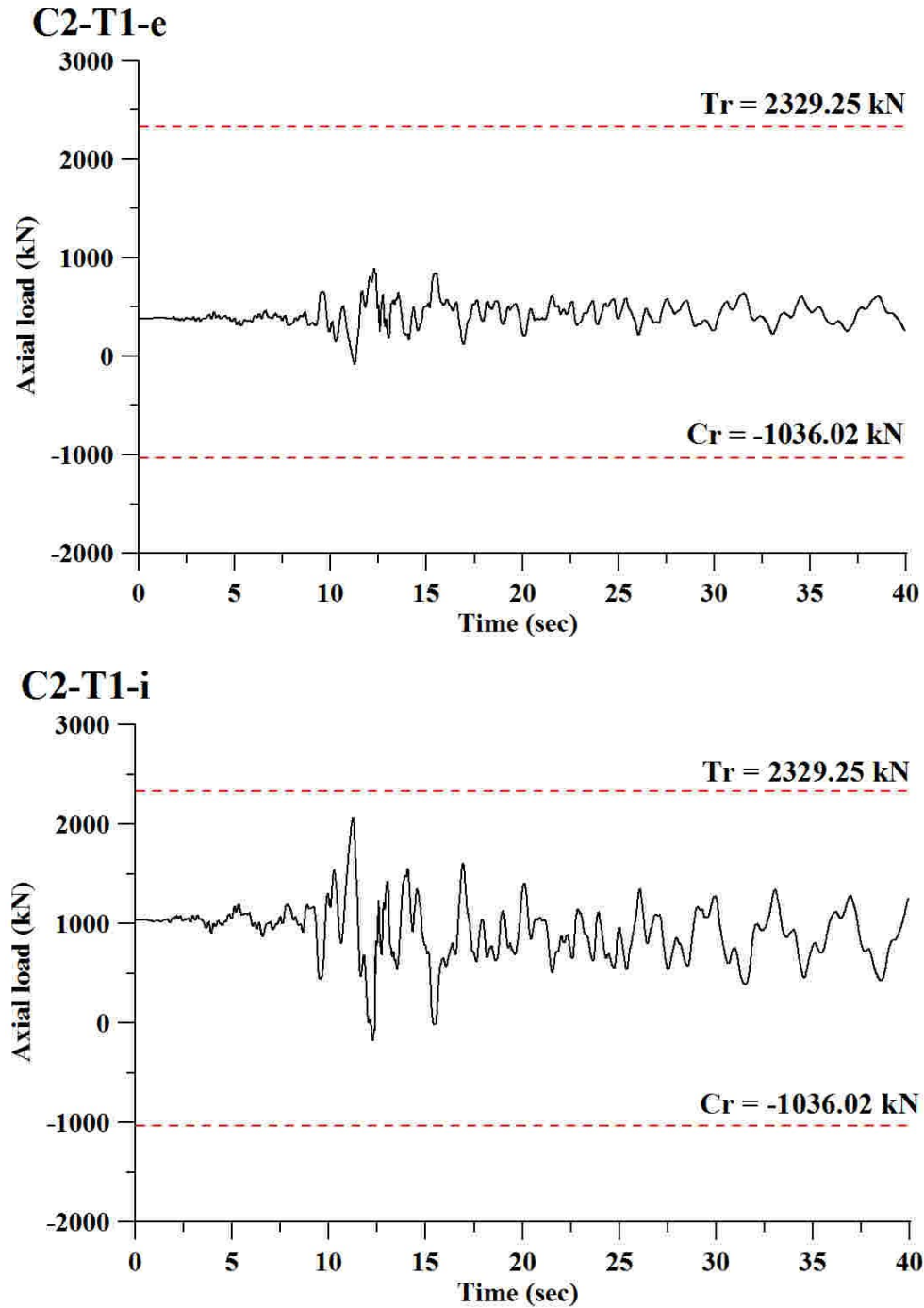


Figure 5.20 Time-history axial load in outrigger truss elements: exterior pane T1-e and interior pane T1-i under motion C2

In Figure 4.9 is shown the envelopes of the maximum and mean axial load developed in zipper columns of the 16-storey building with two outrigger trusses under the se-

lected ground motions. Under Crustal and Near-field ground motions, the axial demand in zipper columns is larger in compression than in tension.

During Subduction ground motions, the tensile forces triggered in zipper columns are larger than the compressive forces. By considering all ground motions, the peak mean values of tensile forces are observed at the lower floors and the peak values of compressive forces are captured in the upper stories. In addition, the overall axial compression demand is higher than the axial tension demand and the axial force envelopes are inside the design envelopes.

Figure 5.21 illustrates the deformed shape of the 16-storey building with two outrigger trusses when subjected to ground motions C2, C4, and C6. Under ground motion C2, the 16-storey building deflected in the 1st vibration mode. Comparing to the case with one outrigger truss, the brace buckling is also initiated at the top floor level and 11 braces have buckled successively from the 16th to the 8th floor within 1.25s. Besides, brace buckling is also observed in the 2nd and the 8th floor. Comparing the response to the case with one outrigger truss, it is observed a stable response especially in the lower part of the building. Under ground motion C4, the larger lateral demand is still carried by the upper floors. The first brace buckling is captured at the top floor level, while the brace buckling does not progress subsequently. Comparing to the case with one outrigger truss, the seismic base shear is slightly increased, while more braces behave elastically. Thus, the percentage of buckled and yielded brace member decreases from 68.75% to 63% and braces

belonging to six floors perform elastically versus braces belonging to four floors in the case with one outrigger truss. Under ground motion C6, the building reaches the failure status. The first brace buckling occurs at the top floor level and all beams are hinged. The time-history response of braces buckling and beams hinging under ground motions N6, N1 and N7 is illustrated in Figure 5.22. Under ground motions N6, the studied building reaches the failure status when subjected to 100% of the scaled ground motion. The buckling of braces initiates at the top floor level and progressed downward until the 7th floor in 1.58s. Under ground motion N7, the response is similar with that resulted in the case with one outrigger truss. Under ground motions S2, S4 and S7, the history of braces buckling and beams hinging is showed in Figure 5.23. Under ground motion S2, the studied building reaches the failure status when subjected to 81.09% of the scaled ground motion. The first brace buckling occurs at the ground floor and beam hinges were formed in all the stories. Under ground motion S4, the studied building reaches the failure status when subjected to 86.4% of the scaled ground motion. The first brace buckling occurs at the top floor level and propagated until the 2nd floor, while beam hinges are formed in all the stories at the brace to beam intersection points. Under ground motion S7, the studied building reaches the failure status when subjected to 50.4% of the scaled ground motion. The first brace buckling occurs at the top floor level, and progressed downward until the 2nd floor in 7.9s. After all braces have buckled and yielded, beam hinges are observed to form in all floors.

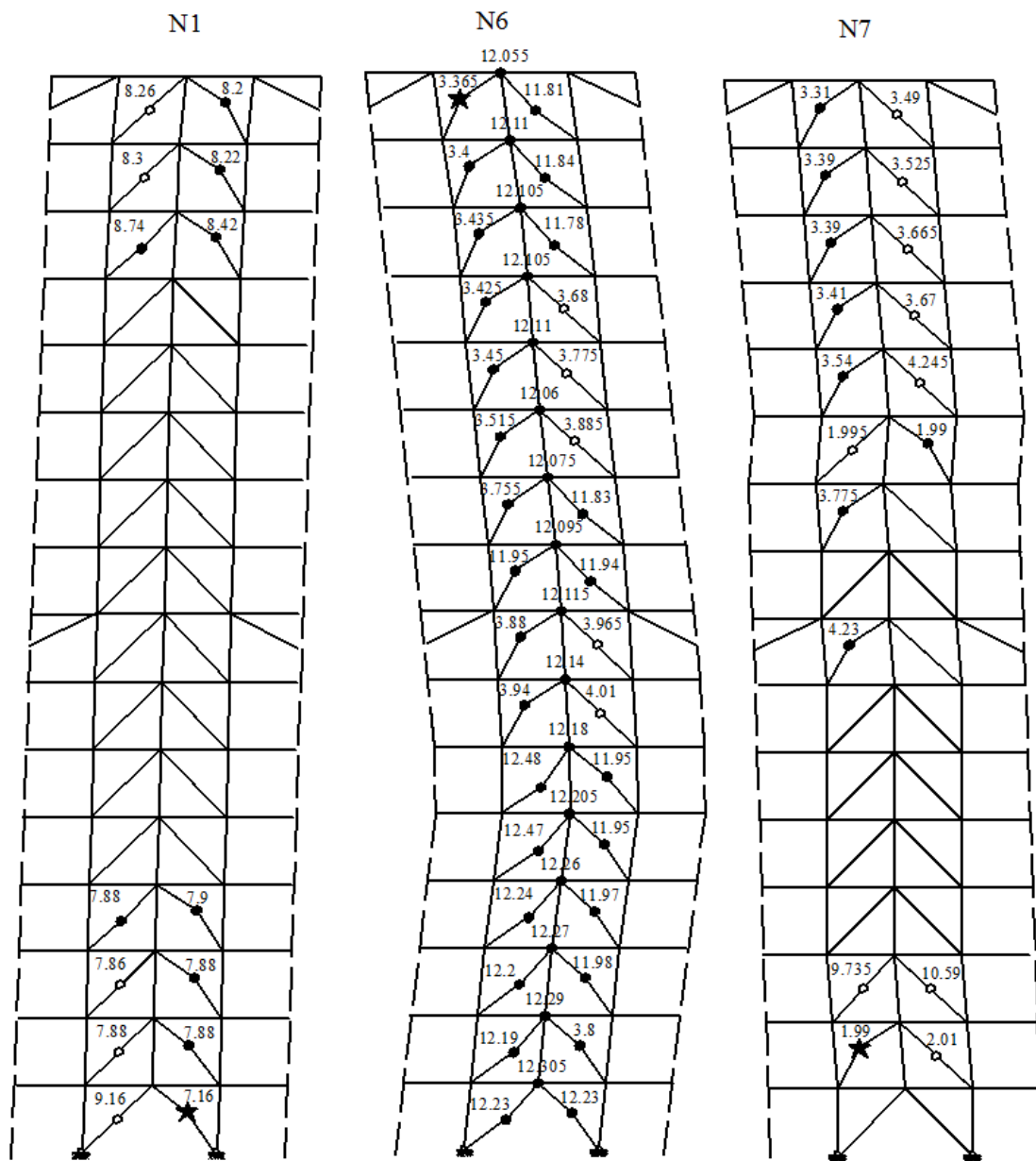


Figure 5.22 Time-history response of brace buckling and beam hinging for 16-storey building with two outrigger trusses under N1, N6, and N7 (★ the first buckled brace; ● subsequently buckled brace and beam hinging; ○ yielding of brace)

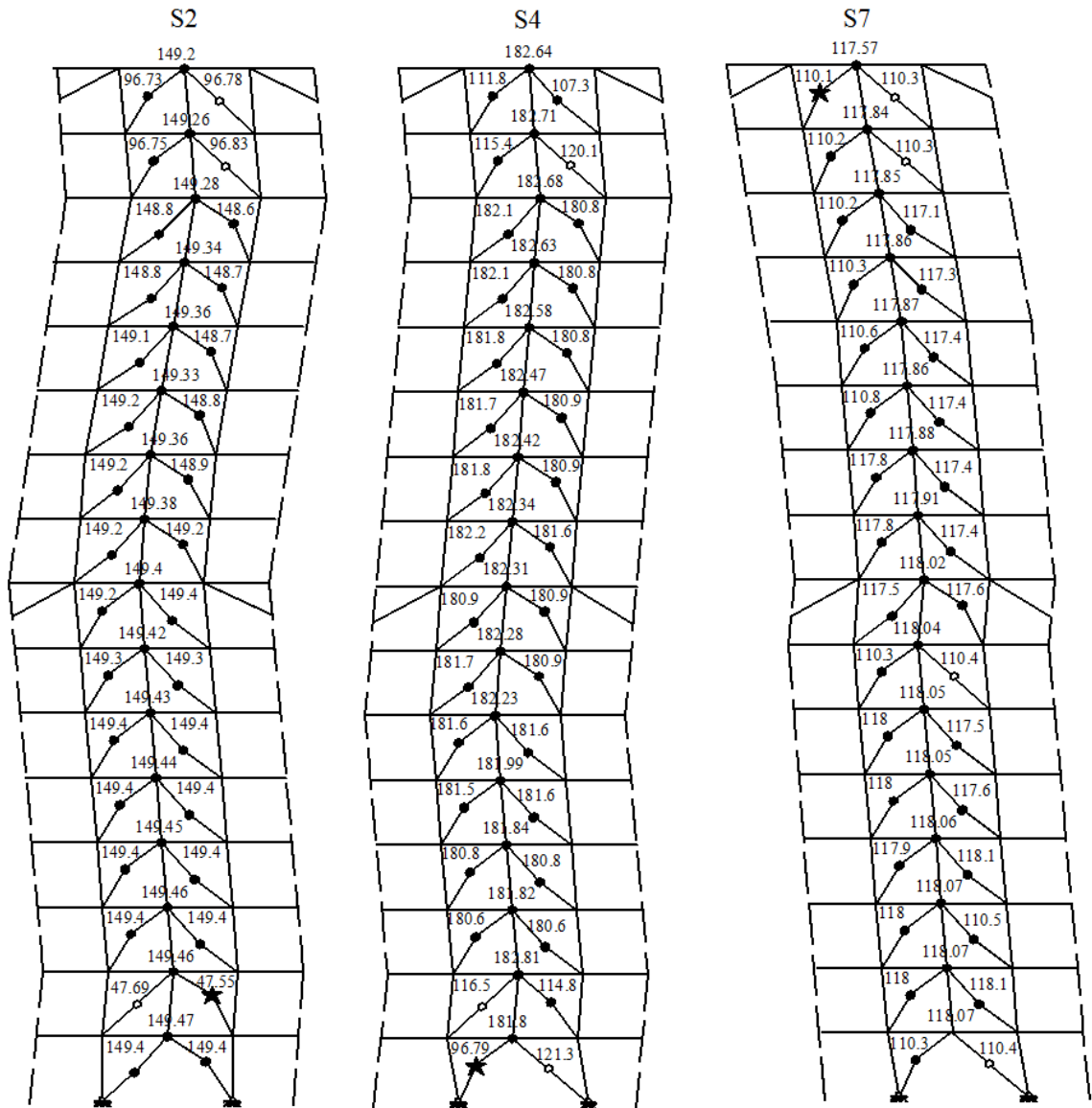


Figure 5.23 Time-history response of brace buckling and beam hinging for 16-storey building with two outrigger trusses under S2, S4, and S7 (★ the first buckled brace; ● subsequently buckled brace and beam hinging; ○ yielding of brace)

5.8 The behavior of outrigger trusses added to the roof and the 8th floor level of the 16-storey building

The time history of axial forces developed in the panel of the top outrigger trusses under the C2 ground motions is shown in Figure 5.24 and in the panels of mid-height outrigger truss is shown in Figure 5.25.

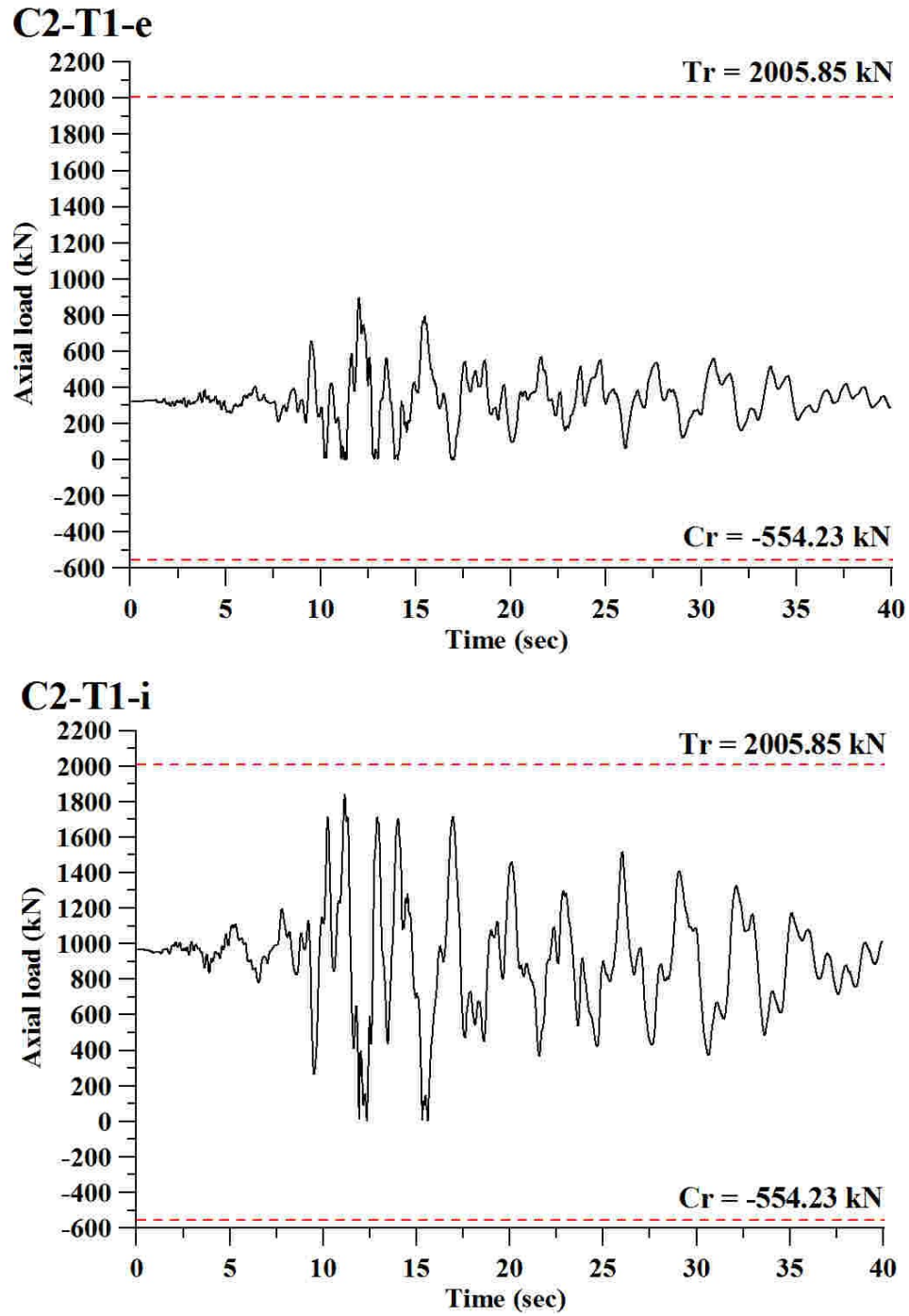


Figure 5.24 Time-history axial load in diagonals of roof outrigger under ground motion
C2: a) top exterior pane T1-e and b) top interior pane T1-i

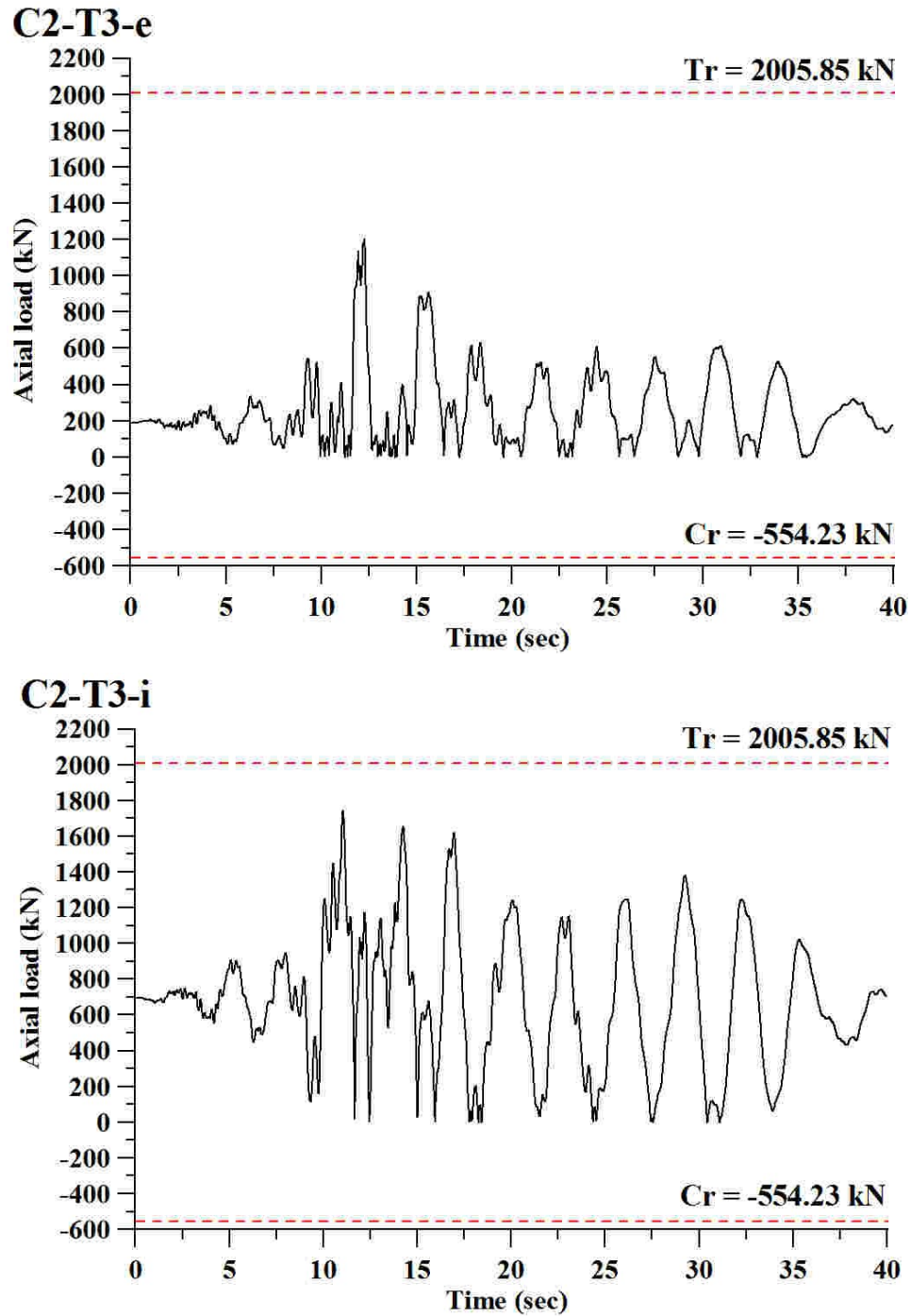


Figure 5.25 Time-history axial load in diagonals of mid-height outrigger under ground motion C2: a) mid-height exterior pane T3-e, and mid-height interior pane T3-i

5.9 Summary of comparative study of seismic response of ZBF with and without outrigger trusses

By conducting the non-linear dynamic analysis, the seismic performance of 12-storey and 16-storey zipper braced frame structure with and without outrigger trusses are studied. The analytical results are discussed based on the parameters which are forces in zippers and the interstorey drift.

The axial load in zipper columns is one of the primary indicators quantifying the seismic behavior of the studied building. As mentioned in Chapter two, the axial load in zipper columns result due to the unbalanced force caused due to buckling of braces. When large axial load is triggered in zipper columns, it means that a large input energy is absorbed into the ZBF structure. Referring to Figure 4.8, for the 12-storey building, the resulted axial demand in zipper columns are very close to the design envelopes. Comparing the values of axial load after adding outrigger trusses, the forces in zipper columns of ZBF with roof outriggers is larger than that developed in zipper columns of ZBF without outriggers. By adding two outrigger trusses, the period of the building decreases and a slightly larger base shear force is developed. In Figure 4.9, it is shown that for the 16-storey building, the design envelope of axial forces estimated to be triggered in zippers is slightly over estimated in the compression side, however, gives a good estimation in tension side. Similar to the 12-storey building, by adding outrigger trusses, the amount

of axial load developed in zipper columns increases, and by adding more outrigger trusses, the axial load demand increases as well.

Another quantified parameter is the interstorey drift. In Figures 4.10 and 4.11, the interstorey drift data of the 12-storey ZBF and 16-storey ZBF with and without outrigger trusses are summarized. To emphasize the interstorey drift parameter, in Figure 5.26 is shown that without outrigger trusses the mean values of interstorey drifts are below the code limit under the Crustal and Near-field ground motions ensembles. However, when applied strong ground motions like Subduction records, the interstorey drift become larger than the code limit, $2.5\%h_s$. By adding one outrigger truss at the roof floor level, under all three ground motion ensembles, the maximum interstorey drift satisfies the code limit. Under subduction ground motions, the peak mean value of the interstorey drift drops from $2.74\%h_s$ to $1.47\%h_s$. In Figure 5.27, it shows that for the 16-storey ZBF, the mean values of interstorey drift are not satisfying the code limit under the Crustal and Subduction ground motion ensembles. By adding one outrigger truss at the top floor level, the response is more stable. Under Crustal ground motions, the interstorey drift decreases from $2.92\%h_s$ to $1.85\%h_s$. Under Near-field ground motions, the mean value of drift ratio decreases from $2.16\%h_s$ to $1.7\%h_s$ and under Subduction ground motions, the mean value of interstorey drift drops from $3.13\%h_s$ to $2.19\%h_s$. Furthermore, after adding a second truss, the interstorey drift is lower than the code limit. Under Crustal motions, the peak mean value of interstorey drift is $1.36\%h_s$. Under Near-field motions, the result is similar,

and it is $1.32\%h_s$. Under Subduction motions, the peak interstorey drift parameter is $1.56\%h_s$. Thus, after adding outrigger trusses, the structure became stiffer and can support the loads developed under the scaled ground motions. However, it seems that the scale factor is slightly larger for long periods and the design UHS should be revised for periods larger than 3s.

Considering the aforementioned two parameters and also the history of brace buckling and beam hinging presented in this chapter, it is concluded that the 16-storey zipper braced frame structures shows the activation of higher modes.

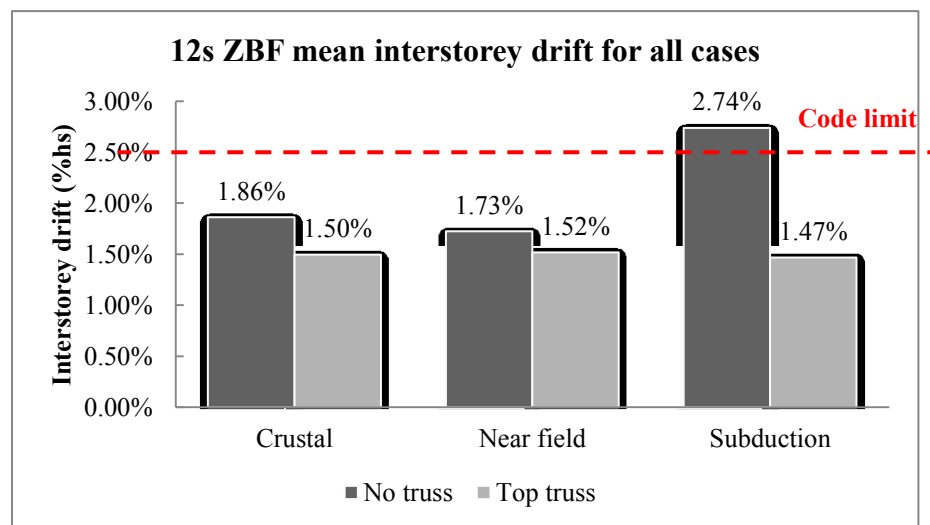


Figure 5.26 Summary of interstorey drifts in 12-storey ZBF under all considered ground motions

Future research should be carrying out in order to find the optimum location of added outrigger trusses in ZBF structure. In addition incremental dynamic analysis

should be conducted in order to obtain the Incremental Dynamic Analysis (IDA) curves that are able to emphasize the reserve capacity of the building below the design demand.

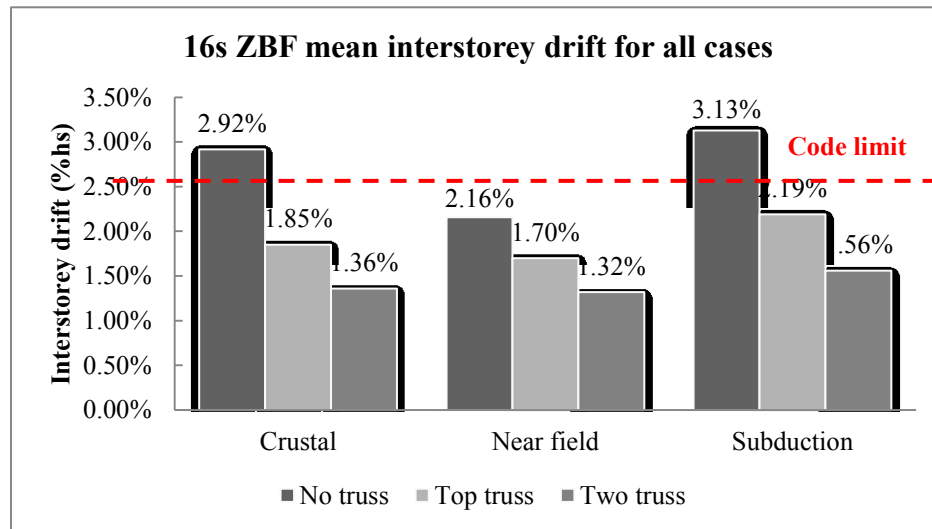


Figure 5.27 Summary of interstorey drifts in the 16-storey ZBF under all considered ground motions

CHAPTER SIX

Conclusions and Future Work

6.1 Conclusions

As one of the widely used seismic force resisting systems in North America, chevron braced frame provides high stiffness and moderate ductility. However, under strong ground motion excitations, the structure is prone to storey mechanism formation and reduced energy dissipation capacity due to the concentration of damage within one floor. To overcome this drawback, an innovative system is to add a zipper column at the brace to beam intersection points with the aim of carrying the unbalanced force resulted from brace buckling. Nevertheless, based on the previous work carried out by Tremblay and Tirca (2003), Chen (2011) and Tirca and Chen (2012), the dynamic instability effect may be triggered when the higher modes effect is activated. To improve the lateral capacity of zipper braced frame in taller building, in this study, it is proposed to add outrigger trusses and/or belt trusses to the zipper braced frame structure.

This study is the first conducted with the aim to understand the behavior of high-rise zipper braced frame systems (16-storey) located in a high risk seismic zone, as Victoria, BC. In order to overcome instability due to the activation of higher modes effect, in this

study it was proposed to add outrigger trusses at the roof floor level and at the roof and building mid-height.

The design method employed for zipper columns is the method proposed by Tremblay and Tirca (2003) and refined by Tirca and Chen (2012). The axial force envelope triggered in zipper column in tension and compression is validated against time-history analyses. Thus, by designing zippers in compression, the LP-ST load pattern was considered and by designing zipper columns to act in tension, the LP-P pattern load is considered. The maximum forces developed in zippers under time-history analysis are lower than the design envelope even for the 16-storey building.

In order to overcome large values of interstorey drift especially at the uppermost floors of the ZBF system, in this study, outrigger trusses are proposed to be added to the SFRS located in the external gridline. Based on steel beams configuration belonging to the floor or roof system, for example in the study, in one direction (N-S) larger axial forces are transfer in the diagonals of outriggers than those located in the E-W direction.

In this research, the design of the outrigger truss elements follows the concept of displacement compatibility method proposed by Stafford & Salim (1981) and the graphic method developed by Hoenderkamp & Bakker (2003). In addition, to optimize the size of outrigger truss diagonals, two outrigger trusses configurations were considered. It was found that the optimal configuration of outrigger truss diagonals is that when the diagonal are loaded in tension under the gravity load component. Thus, diagonals work as pre-stress

members and are designed to respond mostly in tension under all ground motions considered.

The results of the nonlinear dynamic analyses presented in Chapter 4 and 5 have shown that for the 12-storey building, the interstorey drift ratio is well controlled when the studied buildings were subjected to Crustal and Near-field ground motions. However, when the strong excitations like Subduction ground motions is applied, the building cannot carry 100% the load resulted from scaled ground motions and large interstorey drift is observed.

For the 16-storey ZBF with roof outrigger trusses building, the seismic response is more stable when outrigger trusses are added and is uniformly distributed along the building height.

Regarding scaling ground motions, it is found that matching the minimum base shear force for high-rise building is too conservative. In addition, the design spectrum ordinate corresponding to 4.0 s is half that that corresponding to 2.0s. It seems that a ratio of 2 is too conservative in design. However the UHS should be revised for periods larger than 3s. Meanwhile, a new hazard spectrum curve should be proposed for subduction ground motions.

6.2 Future work

As was mentioned in Chapter 4, future work should be done in finding the optimum location of outrigger trusses added in zipper braced frame structure. In addition, it is required to compute the optimum number of outrigger trusses required for a cost-efficient design. In this study, it was shown the impact of outrigger trusses on the seismic response of ZBF structures. Although, previous researchers investigated the optimum location of belt truss in concentrically braced frame, this work was mostly based on wind loading than on earthquake loading. However, the complexity of zipper braced frame system with outrigger trusses should be investigated in detail in order to achieve stable seismic response under different types of ground motions.

Regarding the structural system efficiency, a relationship between the building height and the required number of outrigger trusses must be determined.

Furthermore, incremental dynamic analysis curves should be computed toward an effective performance base design approach.

REFERENCE

Ali, M. M., & Moon, K. S. (2007, June 13). Structural Developments in Tall Buildings: Current Trends and Future Prospects. *Architectural Science Review*, 50(3), 205-223.

American Society of Civil Engineers (ASCE). (2000). *Prestandard and Commentary for the Seismic Rehabilitation of Buildings* (FEMA-356 ed.). Washington, D.C.: Federal Emergency Management Agency.

Baker, J. (2010). The conditional mean spectrum: A tool for ground motion selection. *Journal of Structural Engineering*, 137(3), 322-331.

Bruneau, M., Anagnostopoulou, M., MacRae, G., Clifton, C., & Fussell, A. (2010). Preliminary report on steel building damage from the darfield earthquake of september 4,2010. *Bulletin of the New Zealand Society for earthquake engineering*, 43(4), 351-359.

Bruneau, M., Engelhardt, M., Filiatrault, A., Goel, S. C., Itani, A., Hajjar, J., . . . Uang, C. M. (2005). Review of selected recent research on US seismic design and retrofit strategies for steel structures. *Progress in Structural Engineering and Materials*, 7(3), 103-114.

Bryan Stafford Smith, A. (1991). *Tall building structures: Analysis and Design*. New York: John Wiley & Sons, Inc.

Buyukozturk, O., & Gunes, O. (2004). High-Rise Buildings: Evolution and Innovations. *CIB2004 World Building Congress*. Toronto: Massachusetts Institute of Technology.

Canadian Standard Association. (2009). *CAN/CSA-S16-09 Limit State Design of Steel Structures*. Toronto, ON: Canadian Standard Association.

Chen, L. (2011). *Master Thesis: Innovative brace system for earthquake resistant concentrically braced frame structures*. Montreal: Department of Building, Civil & Environmental Engineering, Concordia University.

Hoenderkamp, J., & Bakker, M. (2003). Analysis of high-rise braced frames with outriggers. *The Structural Design of Tall and Special Buildings*, 335-350.

Hoenderkamp, J., & Snijder, H. (2000). Simplified analysis of facade rigger braced high-rise structures. *The Structural Design of Tall Buildings*, 12, 309-319.

Hoenderkamp, J., & Snijder, H. (2003). Preliminary analysis of high-rise braced frames with facade riggers. *Journal of Structural Engineering*, 129(5), 640-647.

Kalkan, E., & Chopra, A. (2011). Modal-pushover-based ground motion scaling procedure. *Journal of Structural Engineering*, 137(2), 298-310.

Kalkan, E., & Chopra, A. (2010). *Practical guidelines to select and scale Earthquake records for nonlinear response history analysis of structures*. Earthquake Engineering Research Institute.

Khatib, I., Mahim, S., & Pister, K. (1988). *Seismic behavior of concentrically braced steel frames*. University of California: Berkeley: Earthquake Engineering Research Center.

Leon, R., & Yang, C. (2003). Special inverted-v-braced frames with suspended zipper struts. *International workshop on steel and concrete composite construction*, (pp. 89-96). Taipei (Taiwan) National Center for Research on Earthquake.

Lignos, D., Ricles, J., Love, J., Okazaki, T., & Midorikawa, M. (2011). *Effects of the 2011 Tohoku Japan Earthquake on Steel Structures*. Earthquake Engineering Research Institute.

National Research Council of Canada. (2005). *National Building Code of Canada* (2005 ed.). Ottawa, ON: National Research Council of Canada.

Nouri, G. R., Imani Kalesar, H., & Ameli, Z. (2009). The applicability of the zipper strut to seismic rehabilitation of steel structure. *World Academy of Science*, (pp. 402-405).

R.S.Nair. (1998). Belt Trusses and Basements as "Virtual" Outriggers for Tall Buildings. *Engineering Journal*, 35(4), 140-146.

Reyes, J., & Kalkan, E. (2011). *Required number of records of ASCE/SEI-7 ground motion scaling procedure*. U.S. Geological Survey Open File Report 2011 - 1083.

Rutenberg, A., & Tal, D. (1987). Lateral load response of belted tall building structures. *Engineering structure*, 9, 53-67.

Sabelli, R. (2001). *Research on improving the design and analysis of earthquake resistant steel braced frames*. Oakland: Earthquake Engineering Research Institute .

Shaback, B., & Brown, T. (2003). Behaviour of Square Hollow Structural Steel Braces with End Connections under Reversed Cyclic Axial Loading. *Canadian Journal of Civil Engineering*, 30(4), 745-753.

Smith, B., & Coull, A. (1991). *Tall building Structures: Analysis and Design* (1 ed.). New York: John Wiley & Sons Inc.

Smith, B., & Salim, I. (1981). Paramter study of outrigger-braced tall building stuctures. *Journal of the Structural Division*, 2001-2013.

Smith, B., Cruvellier, M., & Nollet, M. (1996). Offset Outrigger Concept for Tall Buildings. In C. o. Habitat, *Tall Building Structures—A World View* (pp. 73-80). New York.

Taranath, B. (1974). Optimum belt truss location for high rise structures. *Engineering Journal*, 18-21.

Taranath, B. (1975). Optimum belt truss locations for high rise structures. *The structural engineer*, 345-348.

Taranath, B. (2010). *Reinforced Concrete Design of Tall Building*. New York: CRC Press.

Tirca, L., & Chen, L. (2012). The Influence of Lateral Load Patterns on the Seismic Design of Zipper Braced Frames (Accepted). *Journal of Structural Engineering*.

Tirca, L., & Tremblay, R. (2003). Behaviour and Design of Multi-Storey Zipper Concentrically Braced Steel Frames for the Mitigation of Soft-Storey Response. *Stessa 2003: Behaviour of Steel Structures in Seismic Areas*, (pp. 471-477). Lisse.

Tirca, L., & Tremblay, R. (2004). Influence of Building Height and Ground Motion Type on the Seismic Behaviour of Zipper Concentrically Braced Steel Frames. *13th World Conference on Earthquake Engineering*. Vancouver.

Tremblay, R., Bruneau, M., & Wilson, J. (1996). Performance of Steel Bridges During the 1995 Hyogo-Ken Nanbu (Kobe, Japan) Earthquake. *Canadian Journal of Civil Engineering*, 23(3), 678-713.

Yang, C.-S., Leon, R., & DesRoches, R. (2008). Design and behavior of zipper-braced frames. *Engineering Structures*, 30(4), 1092-1100.